

Holistic Star Formation

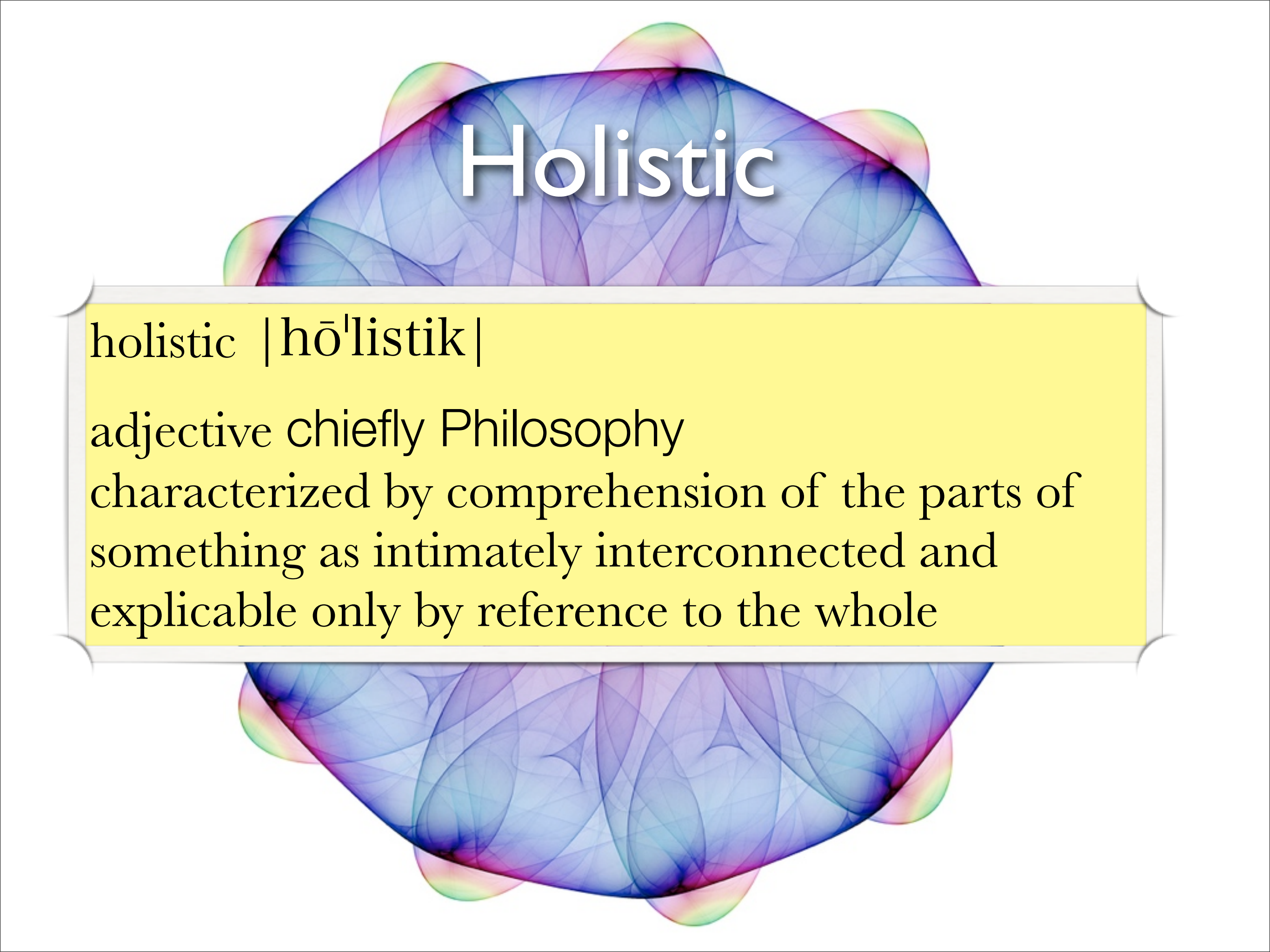
Alyssa A. Goodman (Harvard-Smithsonian Center for Astrophysics)

with

*João Alves, Héctor Arce, Frank Bertoldi, **Michelle Borkin**, Paola Caselli, David Collins, **Jonathan Foster**, Katherine Guenthner, Michael Halle, **Jens Kauffmann**, Elizabeth Lada, Phil Myers, **Jaime Pineda**, Naomi Ridge, Carlos Román-Zúñiga, **Erik Rosolowsky**, Sana Sharma, Scott Schnee, & **Rahul Shetty***

& thanks to Douglas Alan, Kevin Covey, Nick Holliman, Doug Johnstone, Helen Kirk, Kaisey Mandel, Gus Muench, Stella Offner, Paolo Padoan, & Tom Robitaille





Holistic

holistic | hō'listik |

adjective chiefly Philosophy
characterized by comprehension of the parts of
something as intimately interconnected and
explicable only by reference to the whole

Magnetic
Fields

Gravity

Chemical & Phase
Transformations

~ 1 pc

“Holistic Physics”

Radiation

Thermal
Pressure

“Turbulence”
(Random Kinetic Energy)

Outflows
& Winds

...from 0.1 pc to 100 pc

Massive Star-Forming Regions

warm dust cold dust

HII regions(+SNR)

radio SNR

20 cm VLA from MAGPIS (Helfand et al. 2006) & MIR from Spitzer GLIMPSE (see Churchwell et al.)

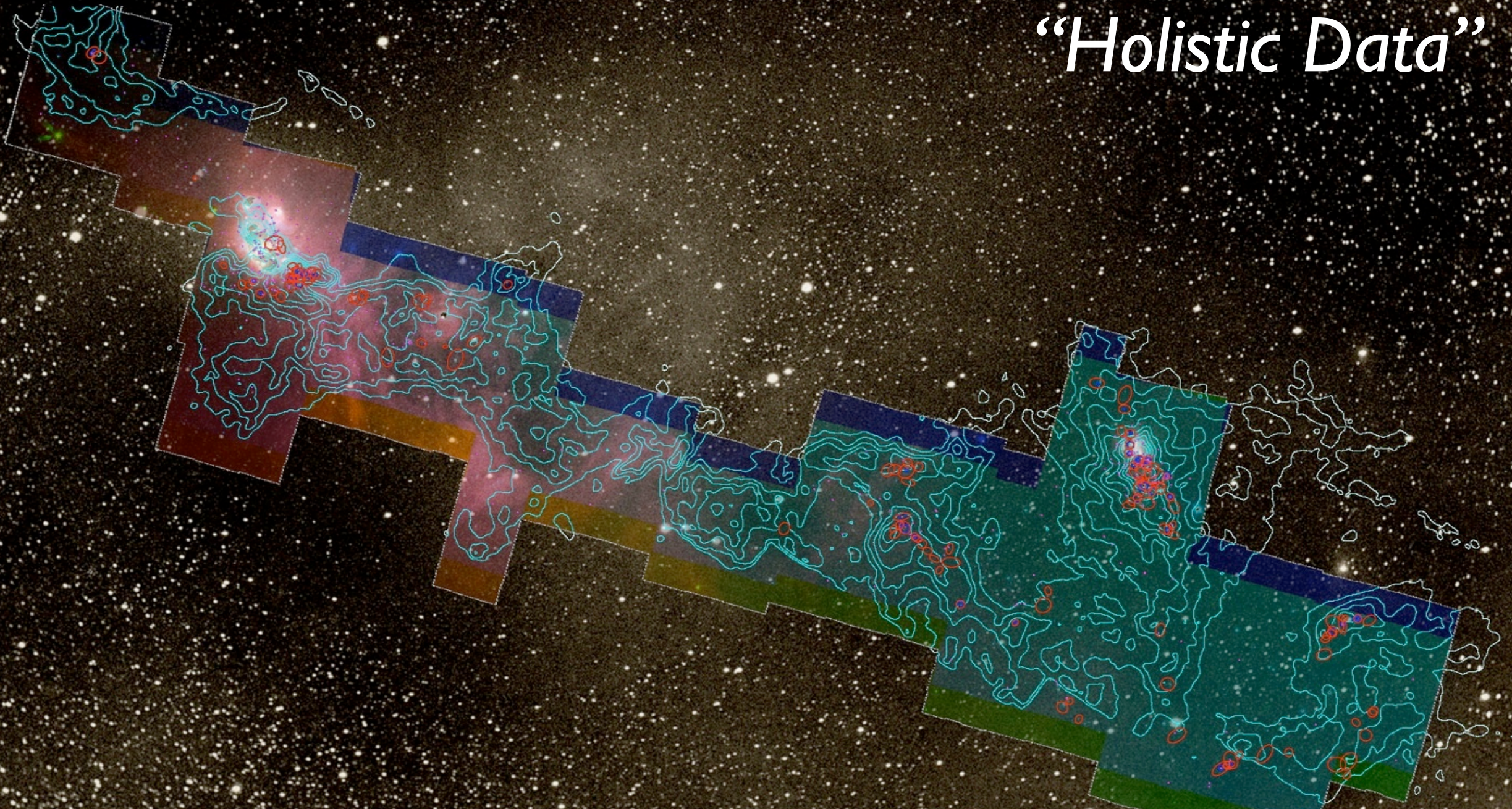
3.6, 4.5, 8.0, 20cm (Luptonized, see Lupton et al. 2004)

image "height" is 1.6 degrees (e.g. 140 pc at 5 kpc)

COMPLETE =

COordinated MOlecular PRobe Line EXtinction Thermal
Emission Survey of Star-Forming Regions

“Holistic Data”



COMPLETE Collaborators,
2009:

Alyssa A. Goodman (CfA/IIC)

João Alves (Calar Alto, Spain)

Héctor Arce (Yale)

Michelle Borkin (Harvard SEAS/IIC)

Paola Caselli (Leeds, UK)

James DiFrancesco (HIA, Canada)

Jonathan Foster (B.U.)

Mark Heyer (UMASS/FCRAO)

Doug Johnstone (HIA, Canada)

Jens Kauffmann (JPL/Caltech)

Helen Kirk (CfA)

Di Li (JPL/Caltech)

Stella Offner (CfA)

Jaime Pineda (CfA, PhD Student)

Thomas Robitaille (CfA)

Erik Rosolowsky (UBC Okanagan)

Rahul Shetty (ITA Heidelberg)

Scott Schnee (HIA Victoria)

Mario Tafalla (OAN, Spain)

The West-End of Perseus

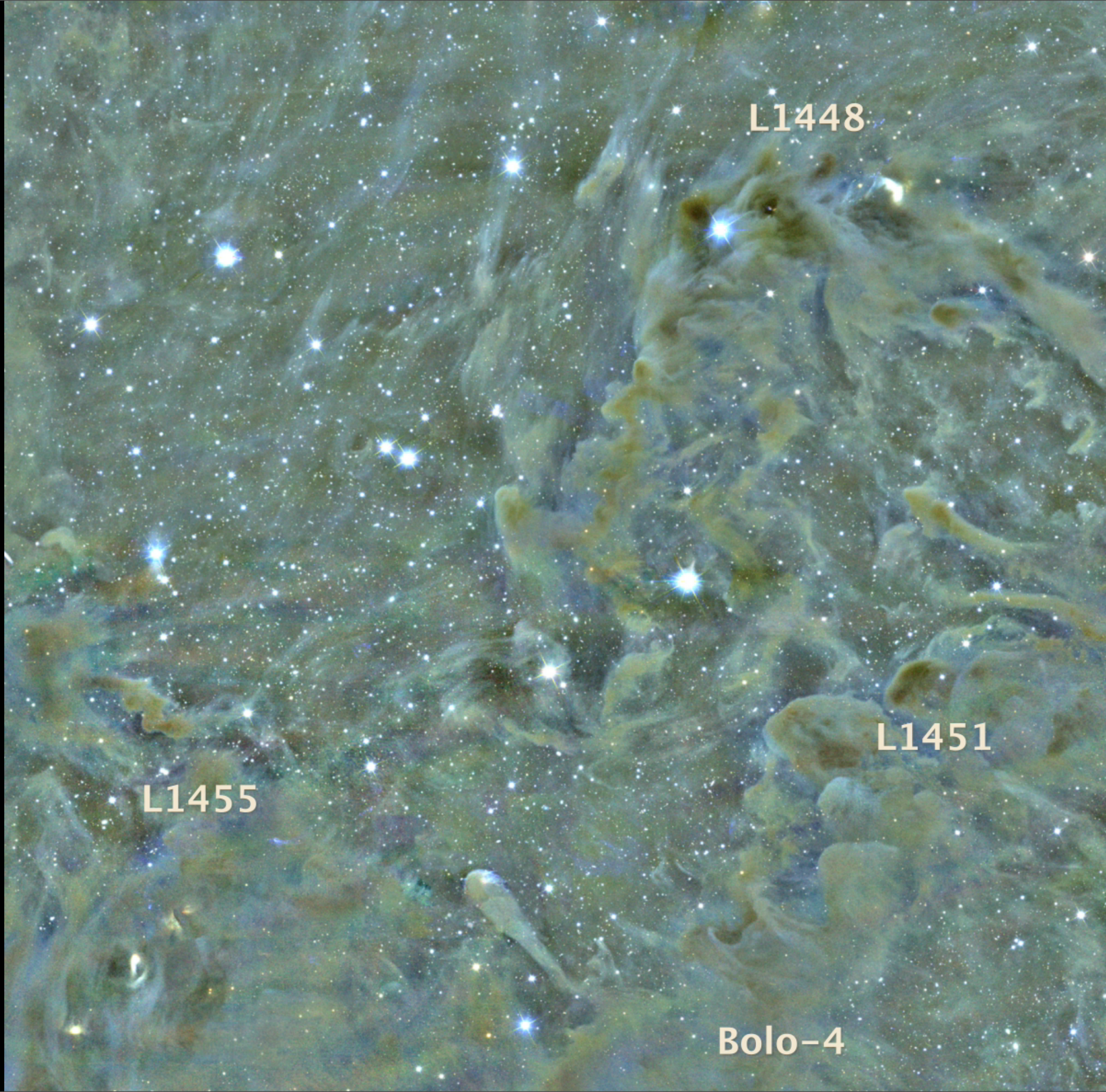
A journey through star-formation in reverse, by Jonthathan Foster.

Main Image:

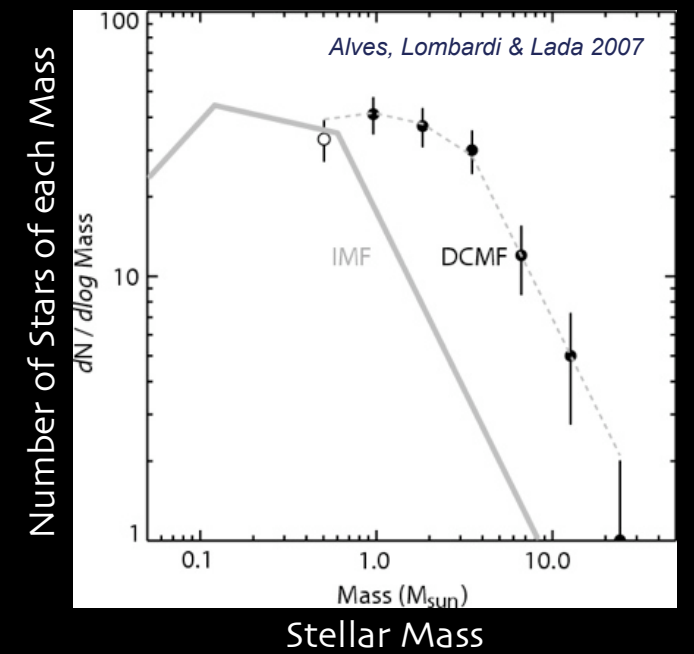
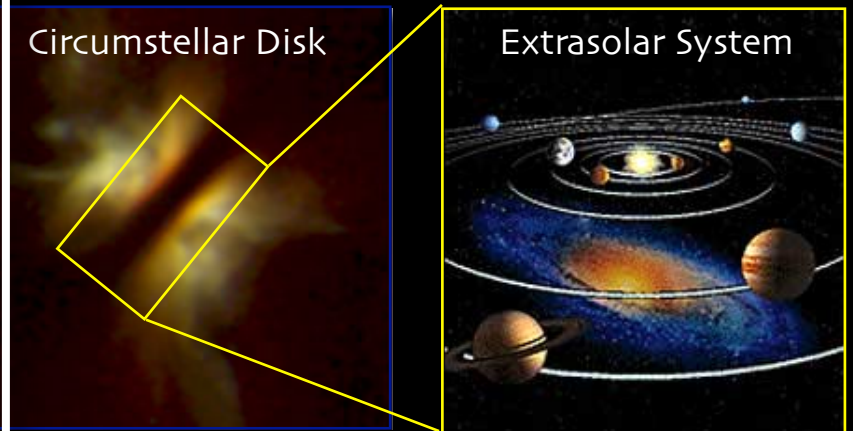
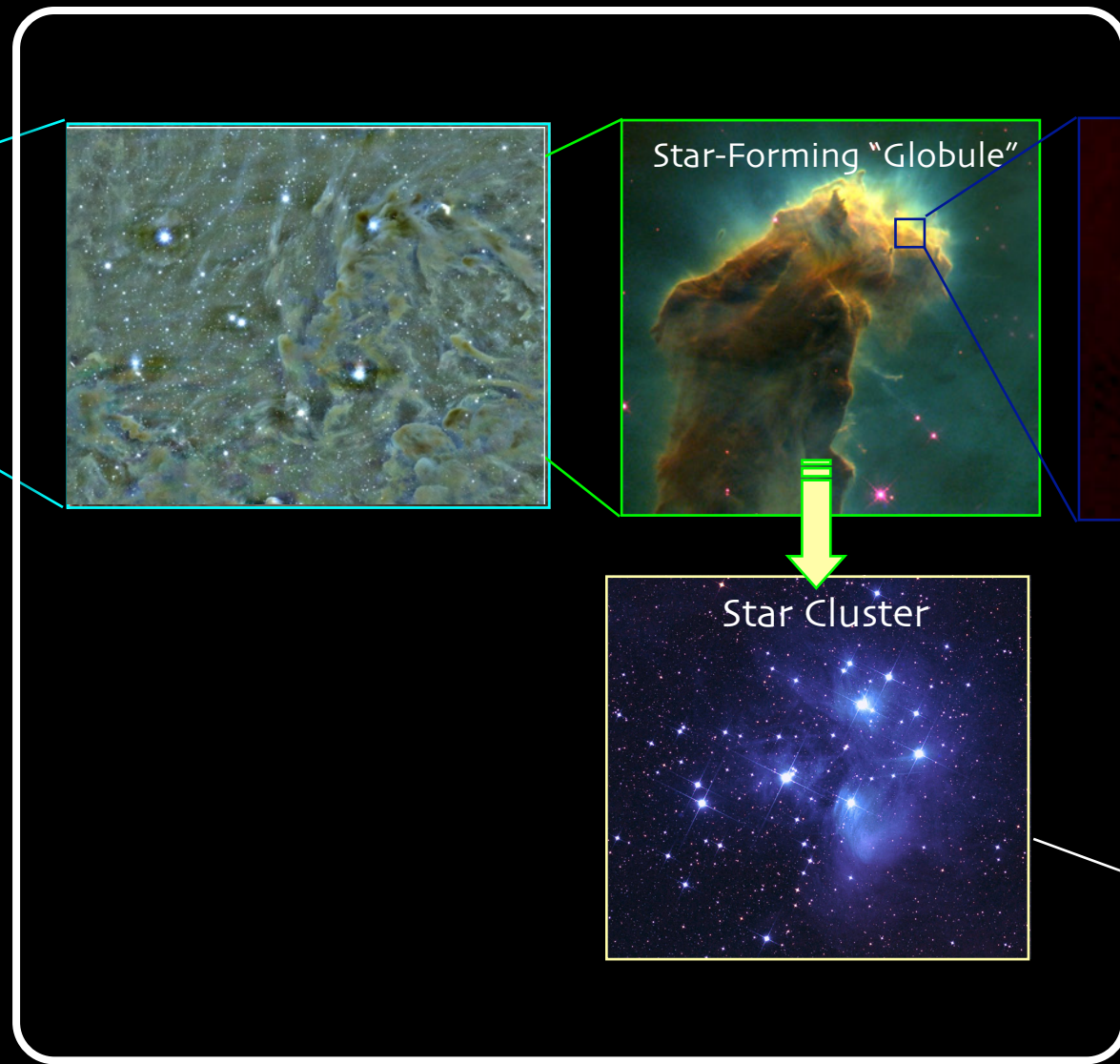
MMT/
Megacam
r,i,z

Zooms/fades:

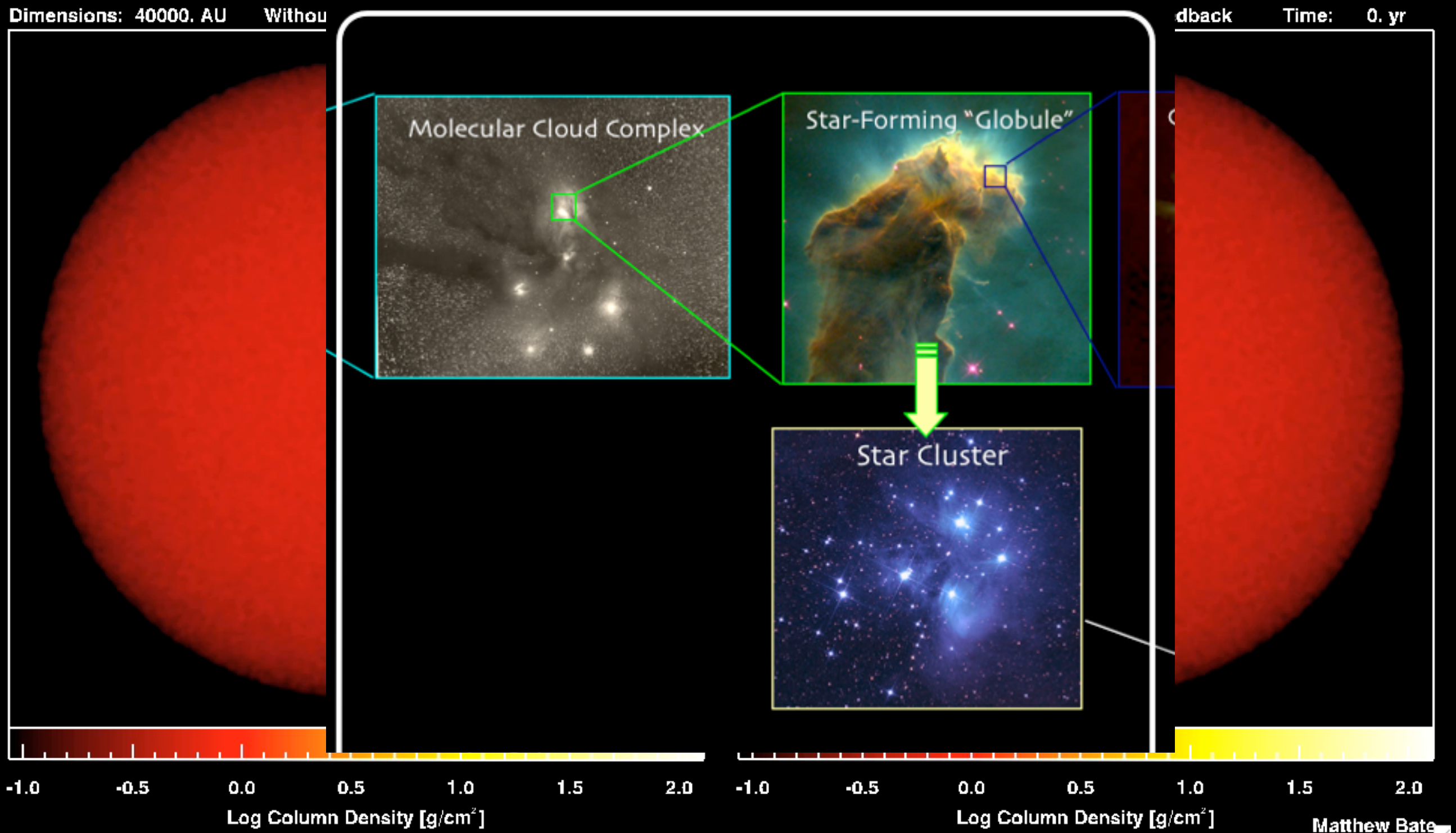
Calar Alto/
OMEGA2000
J,H,K_s



Star (and Planet, and Moon) Formation 30 I



Our Goal is to “Taste” Star Formation



Simulations of Bate 2009

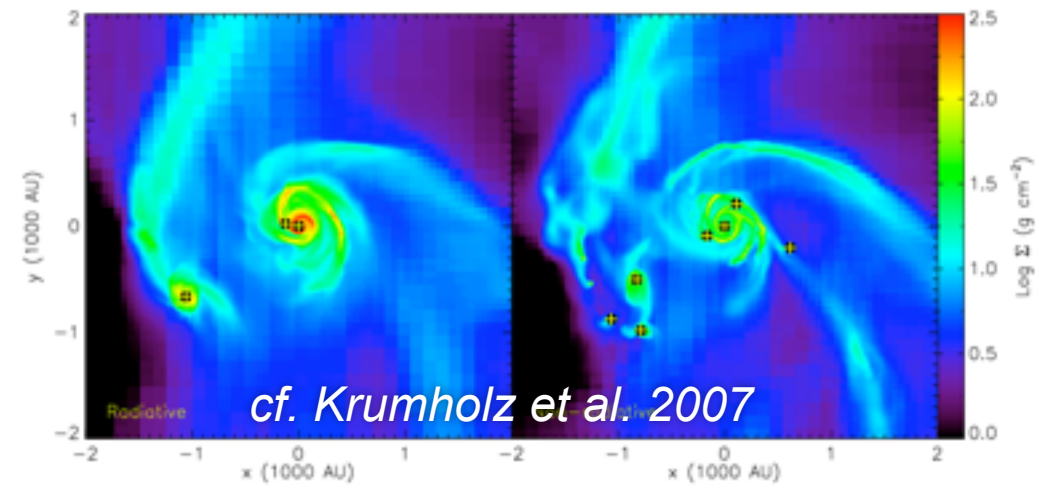


FIG. 9 A comparison of two simulations with identical initial conditions and evolution times, one including radiative transfer (*left panel*) and one done without it (*right panel*). Stars are indicated by plus signs. The simulation without radiative transfer forms a factor of ~ 4 more stars than the one including it, and has significantly less mass in its gaseous disk. (*Images adapted from Krumholz et al. (2007a)*).

Today's Dissection

LETTERS

A role for self-gravity at multiple length scales in the process of star formation

Alyssa A. Goodman¹, Erik W. Rosolowsky¹, Michelle A. Barkin¹, Jonathan S. Foster¹, Michael Halle¹, Ivan Kaffmann² & Jaime E. Pineda¹

Self-gravity plays a decisive role in the final stages of star formation, where dense cores (size ~ 0.1 parsecs) of molecular clouds collapse to form star-formation regions. But self-gravity's role at earlier times (and on larger length scales, such as ~ 1 parsec) in shaping some molecular cloud configurations that do not include self-gravity suggest that turbulent fragmentation alone is insufficient to create a mass distribution of dense cores that resembles, and sets, the stellar initial mass function. Here we report a new algorithm (hierarchical tree-diagram) analysis that reveals that self-gravity plays a significant role over the full range of possible scales tested by CO observations in the L1448 molecular cloud, but not everywhere in the observed region. In particular, more than 80 per cent of the compact (pre-stellar cores) traced by peaks of dust emission are projected on the fly within one of the dendrogram's self-gravitating 'cores'. As these peaks mark the base of already-forming stars, or of those probably about to form, self-gravitating cores create a critical condition for their evolution. Turbulent fragmentation creates without self-gravity a core of non-gravitating (non-stellar) material — one that does not self-gravitate and produces very similar to what is observed in clouds like L1448. But a dendrogram of such a simulation shows that nearly all the gas in it (much more than in the observations) appears to be self-gravitating. A potentially significant role for gravity in how self-gravitating, a potentially significant role for gravity in how self-gravitating, and that it is essential to include self-gravity in any realistic simulation of the star-formation process in galactic cores.

Spectral line mapping shows molecular clouds (especially near to hundreds of parsecs across, and surrounded by atomic gas) to be highly self-gravitating, which means that their internal structure is dominated by self-gravity. This is in contrast to the observations, where self-gravitating structures are often found on relatively small scales (less than a few parsecs) and are often surrounded by non-gravitating material. This is a function of scale and conditions, within an individual region.

Star-formation identification in molecular clouds has been highly successful, which makes it difficult to quantify the physical conditions on multiple scales using a single data set. A solution, for example, the widely used algorithm CLUMPFIND, is to use dimensionally reduced data cubes (CLUMPFIND) to represent a multi-dimensional data cube, identifying local maxima in the position-position-velocity (p-p-v) cube and assigning relative masses to each maximum. Figure 1 shows a visualization of the L1448 region using CLUMPFIND, and Figure 2 shows a visualization of the L1448 region using the new algorithm, which is able to identify self-gravitating structures on multiple scales. The new algorithm, which is able to identify self-gravitating structures on multiple scales, is able to identify self-gravitating structures on multiple scales. The new algorithm, which is able to identify self-gravitating structures on multiple scales, is able to identify self-gravitating structures on multiple scales.

Figure 1. Hierarchical images of the L1448 star-forming region with contours of column density. The dendrogram shows the hierarchical structure of the data cube, with nodes representing local maxima and branches representing connections between them. The dendrogram is color-coded by mass, with larger masses in red and smaller masses in blue.

LETTERS

Comparison of the 'dendrogram' and CLUMPFIND feature-identification algorithms as applied to CO emission from the L1448 region of Perseus

Figure 1 shows a visualization of the surfaces indicated by contours in the dendrogram shown in a 3D perspective view. The dendrogram shows a complex, hierarchical structure of the data cube, with nodes representing local maxima and branches representing connections between them. The dendrogram is color-coded by mass, with larger masses in red and smaller masses in blue.

Figure 2 shows a visualization of the surfaces indicated by contours in the dendrogram shown in a 3D perspective view. The dendrogram shows a complex, hierarchical structure of the data cube, with nodes representing local maxima and branches representing connections between them. The dendrogram is color-coded by mass, with larger masses in red and smaller masses in blue.

Figure 3 shows a visualization of the surfaces indicated by contours in the dendrogram shown in a 3D perspective view. The dendrogram shows a complex, hierarchical structure of the data cube, with nodes representing local maxima and branches representing connections between them. The dendrogram is color-coded by mass, with larger masses in red and smaller masses in blue.

Figure 4 shows a visualization of the surfaces indicated by contours in the dendrogram shown in a 3D perspective view. The dendrogram shows a complex, hierarchical structure of the data cube, with nodes representing local maxima and branches representing connections between them. The dendrogram is color-coded by mass, with larger masses in red and smaller masses in blue.

Figure 5 shows a visualization of the surfaces indicated by contours in the dendrogram shown in a 3D perspective view. The dendrogram shows a complex, hierarchical structure of the data cube, with nodes representing local maxima and branches representing connections between them. The dendrogram is color-coded by mass, with larger masses in red and smaller masses in blue.

LETTERS

Comparison of the 'dendrogram' and CLUMPFIND feature-identification algorithms as applied to CO emission from the L1448 region of Perseus

Figure 1 shows a visualization of the surfaces indicated by contours in the dendrogram shown in a 3D perspective view. The dendrogram shows a complex, hierarchical structure of the data cube, with nodes representing local maxima and branches representing connections between them. The dendrogram is color-coded by mass, with larger masses in red and smaller masses in blue.

Figure 2 shows a visualization of the surfaces indicated by contours in the dendrogram shown in a 3D perspective view. The dendrogram shows a complex, hierarchical structure of the data cube, with nodes representing local maxima and branches representing connections between them. The dendrogram is color-coded by mass, with larger masses in red and smaller masses in blue.

Figure 3 shows a visualization of the surfaces indicated by contours in the dendrogram shown in a 3D perspective view. The dendrogram shows a complex, hierarchical structure of the data cube, with nodes representing local maxima and branches representing connections between them. The dendrogram is color-coded by mass, with larger masses in red and smaller masses in blue.

Figure 4 shows a visualization of the surfaces indicated by contours in the dendrogram shown in a 3D perspective view. The dendrogram shows a complex, hierarchical structure of the data cube, with nodes representing local maxima and branches representing connections between them. The dendrogram is color-coded by mass, with larger masses in red and smaller masses in blue.

Figure 5 shows a visualization of the surfaces indicated by contours in the dendrogram shown in a 3D perspective view. The dendrogram shows a complex, hierarchical structure of the data cube, with nodes representing local maxima and branches representing connections between them. The dendrogram is color-coded by mass, with larger masses in red and smaller masses in blue.

LETTERS

Comparison of the 'dendrogram' and CLUMPFIND feature-identification algorithms as applied to CO emission from the L1448 region of Perseus

Figure 1 shows a visualization of the surfaces indicated by contours in the dendrogram shown in a 3D perspective view. The dendrogram shows a complex, hierarchical structure of the data cube, with nodes representing local maxima and branches representing connections between them. The dendrogram is color-coded by mass, with larger masses in red and smaller masses in blue.

Figure 2 shows a visualization of the surfaces indicated by contours in the dendrogram shown in a 3D perspective view. The dendrogram shows a complex, hierarchical structure of the data cube, with nodes representing local maxima and branches representing connections between them. The dendrogram is color-coded by mass, with larger masses in red and smaller masses in blue.

Figure 3 shows a visualization of the surfaces indicated by contours in the dendrogram shown in a 3D perspective view. The dendrogram shows a complex, hierarchical structure of the data cube, with nodes representing local maxima and branches representing connections between them. The dendrogram is color-coded by mass, with larger masses in red and smaller masses in blue.

Figure 4 shows a visualization of the surfaces indicated by contours in the dendrogram shown in a 3D perspective view. The dendrogram shows a complex, hierarchical structure of the data cube, with nodes representing local maxima and branches representing connections between them. The dendrogram is color-coded by mass, with larger masses in red and smaller masses in blue.

Figure 5 shows a visualization of the surfaces indicated by contours in the dendrogram shown in a 3D perspective view. The dendrogram shows a complex, hierarchical structure of the data cube, with nodes representing local maxima and branches representing connections between them. The dendrogram is color-coded by mass, with larger masses in red and smaller masses in blue.

TASTE TEST

Goodman, Rosolowsky, Barkin, Foster, Halle, Kaffmann & Pineda 2009, Nature, 457, 63.

“turbulent fragmentation” “LI 448” “(magneto-)hydrodynamic simulation”

“Cloudshine”

“bi-jection”

“pre-stellar core”

“virial parameter”

“protostar”

“column density”

“integrated intensity”

“turbulent power spectrum”

“p-p-v cube”

“synthetic observation”

“segmentation”

“depletion, opacity”

“CLUMPFIND”

“taste-test”

“Dendrogram”

caveats

LETTERS

A role for self-gravity at multiple length scales in the process of star formation

Alyssa A. Goodman^{1,2}, Erik W. Rosolowsky^{1,2}, Michelle A. Barkin¹, Jonathan S. Foster¹, Michael Hebb^{1,2}, Tom Kaufman^{1,2} & James I. Probst¹

Figure 1: Near-infrared image of the L1448 star-forming region with dendrogram overlaid. The dendrogram shows hierarchical clustering of the region's features.

Figure 2: Comparison of the 'Dendrogram' and 'CLUMPFIND' feature-identification algorithms as applied to "CO emission from the L1448 region of Perseus. A 3D visualization of the surface indicated by volume in the dendrogram is shown in a. Purple illustrates the smallest scale self-gravitating structures in the region corresponding to the leaves of the dendrogram; pink shows the smallest surfaces that contain distinct self-gravitating leaves within them, and green corresponds to the surface of the data cube containing all the significant emission. Dendrogram branches corresponding to self-gravitating objects have been highlighted in yellow over the range of T_{mb} (main beam temperature) (unit: mJy beam^{-1}) for which the virial parameter is less than 2. The x and y locations of the four 'self-gravitating' leaves marked with yellow balls are the same as those shown in Fig. 1. The 3D visualization shows position-position-velocity (p - p - v) space. In a, right ascension, declination. For comparison with the ability of dendrograms to track hierarchical structure, d shows a pseudo-dendrogram of the CLUMPFIND segmentation (b), with the same four labels used in Fig. 1 and in a. As 'leaves' are not allowed to belong to larger structures, each pseudo-branch in d is simply a series of lines connecting the maximum emission value in each clump to the threshold value. A very large number of clumps appear in b because of the sensitivity of CLUMPFIND to noise and small-scale structure in the data. In the online PCC version, the 3D cubes in (a) and (b) can be rotated to any orientation, and surfaces can be traced as cut-off intersections (see also Kaufman et al. 2018 for details). In the printed version, the front face of each 3D cube (the 'best' view in the interactive online version) corresponds exactly to the pink of (a) shown in Fig. 1, and velocity with respect to the Local Standard of Rest increases from front (-0.5 km s^{-1}) to back (0 km s^{-1}).

Figure 3: Schematic illustration of the dendrogram process. Shown is the construction of a dendrogram from a hypothetical one-dimensional emission profile (black). The dendrogram (blue) can be constructed by 'flopping' a test constant emission level (purple) from above in five steps (contaginated in the text; right-hand side of the illustration) and merges are found, and connected to nodes. The intersection of a test level with the emission is a set of points (the yellow dots); in one dimension, a cluster exists in two dimensions, and so intersects in three dimensions. The dendrogram of 3D data shown in Fig. 2, is the direct analogue of the one shown here, only constructed from 'isomeric' rather than 'real' interactions. It has been sorted and flattened for representation as a flat page, a fully representing dendrogram for 3D data cubes would require four dimensions.

LETTERS

Using 2D maps of column density. With this early 2D work as inspiration, we have developed a structure-identification algorithm that extracts the hierarchical structure of a 2D (p - p) data cube into an easily visualized representation called a 'dendrogram'.

Figure 3 and its legend explain the construction of dendrograms schematically. The dendrogram quantifies how and where local masses of emission merge with each other, and its implementation is explained in Supplementary Methods. Critically, the dendrogram is determined almost entirely by the data itself, and it has negligible sensitivity to algorithm parameters. To make graphical presentation possible on paper and 2D screens, we 'flatten' the dendrograms of 3D data (see Fig. 3 and its legend), by setting their 'branches' to rest cross, which discards dimensional information on the z axis while preserving all information about connectivity and hierarchy. Numbers 'behind' ball labels in the figure let the reader match features between a 2D map (Fig. 1), an interactive 3D map (Fig. 2a online) and a sorted dendrogram (Fig. 3c).

A dendrogram of a spectral line data cube allows for the estimation of key physical properties associated with volumes bounded by isosurfaces, such as radius (R), velocity dispersion (σ), and luminosity (L). The volumes can have any shape, and in other work^{1,2} we focus on the significance of the especially elongated features seen in L1448 (Fig. 2a). The luminosity is an approximate proxy for mass, such that $M_{\text{gas}} \approx X_{\text{CO}} \rho_{\text{CO}} V$, where $X_{\text{CO}} \approx 0.07$ on K km^{-1} (ref. 1); see Supplementary Methods and Supplementary Fig. 2). The derived values for size, mass and velocity dispersion can then be used to estimate the role of self-gravity at each point in the hierarchy, via calculation of an 'observed' virial parameter, $\alpha_{\text{obs}} = \frac{L}{M_{\text{gas}} \sigma^2}$. In principle, extended portions of the tree (Fig. 3c, yellow highlighting) where $\alpha_{\text{obs}} < 2$ (where gravitational energy is comparable to or larger than kinetic energy) correspond to regions of p - p space where self-gravity is significant. As α_{obs} only represents the ratio of kinetic energy to gravitational energy at one point in time, and does not explicitly capture external over pressure and/or magnetic fields, its measured value should only be used as a guide to the longevity (boundariness) of any particular feature.

Figure 3: Schematic illustration of the dendrogram process. It shows a 1D emission profile (black line) and its corresponding hierarchical tree structure (blue lines). The tree is constructed by 'flopping' a test constant emission level (purple) from above in five steps. The intersection of a test level with the emission is a set of points (yellow dots). In one dimension, a cluster exists in two dimensions, and so intersects in three dimensions. The dendrogram of 3D data shown in Fig. 2, is the direct analogue of the one shown here, only constructed from 'isomeric' rather than 'real' interactions. It has been sorted and flattened for representation as a flat page, a fully representing dendrogram for 3D data cubes would require four dimensions.

LETTERS

The formation of self-gravitating volumes as a function of scale in L1448 and a comparison to simulations.

Figure 4: Plot of virial parameter vs. scale for L1448 and simulations. The plot shows the virial parameter α_{obs} as a function of scale for the L1448 region (black line) and for simulations (red line). The L1448 region shows a virial parameter that is generally less than 2, indicating self-gravity is significant.

Figure 5: Plot of column density vs. scale for L1448 and simulations.

Figure 5: Plot of column density vs. scale for L1448 and simulations. The plot shows the column density N_{H_2} as a function of scale for the L1448 region (black line) and for simulations (red line). The L1448 region shows a column density that is generally higher than the simulations, indicating self-gravity is significant.

LETTERS

Consideration of the region associated with a self-gravitating leaf in the test associated with a millimetre-wave peak, suggesting it is a more robust source of CO than the associated region of the self-gravitating leaves is critical to the surface phases of star formation.

Figure 6: Plot of virial parameter vs. scale for L1448 and simulations, showing a different set of parameters.

Figure 6: Plot of virial parameter vs. scale for L1448 and simulations, showing a different set of parameters. The plot shows the virial parameter α_{obs} as a function of scale for the L1448 region (black line) and for simulations (red line). The L1448 region shows a virial parameter that is generally less than 2, indicating self-gravity is significant.

“COMPLETE”

“3D PDF”

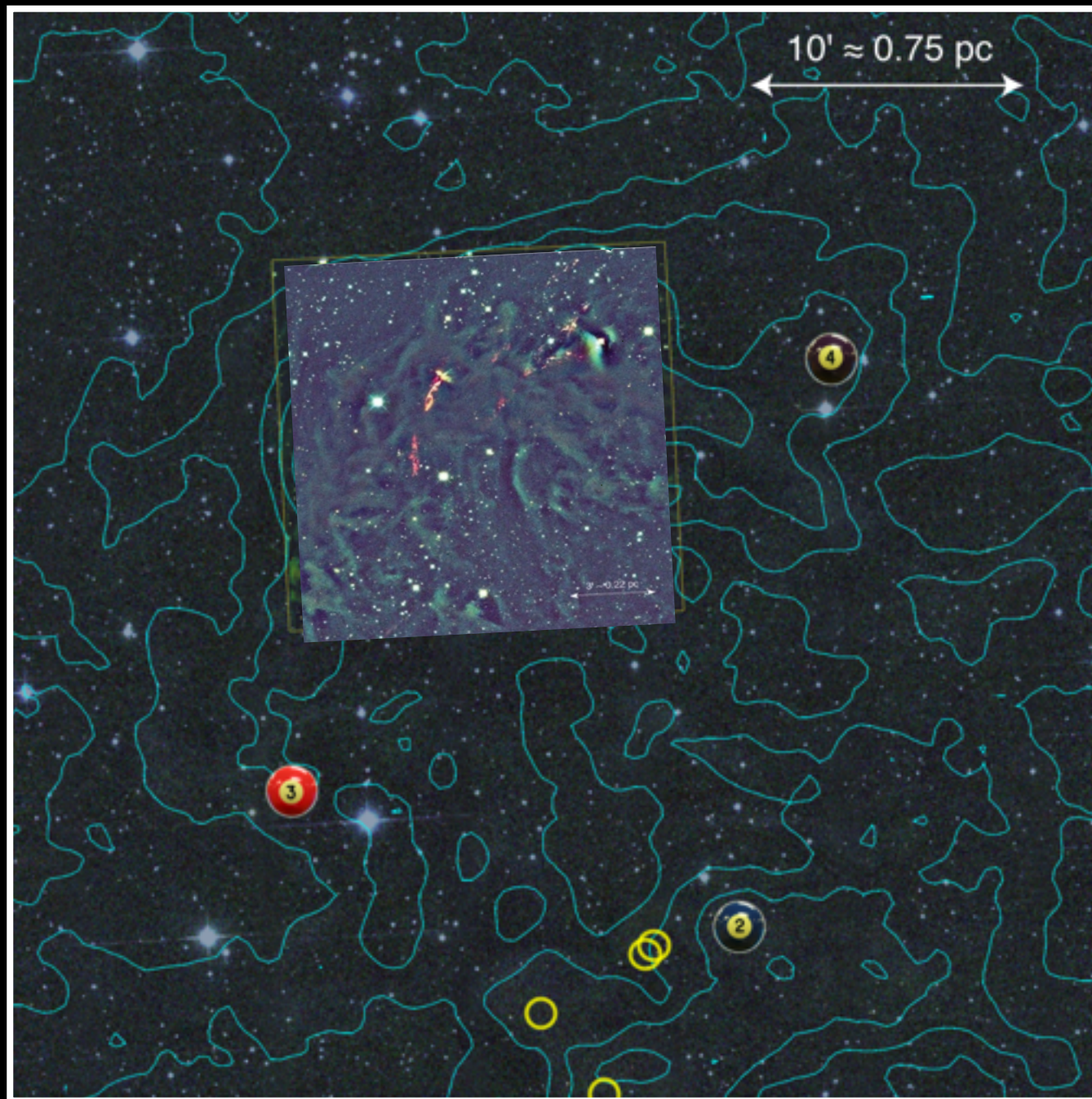
“L1448”

“Cloudshine”

“pre-stellar core”

“protostar”

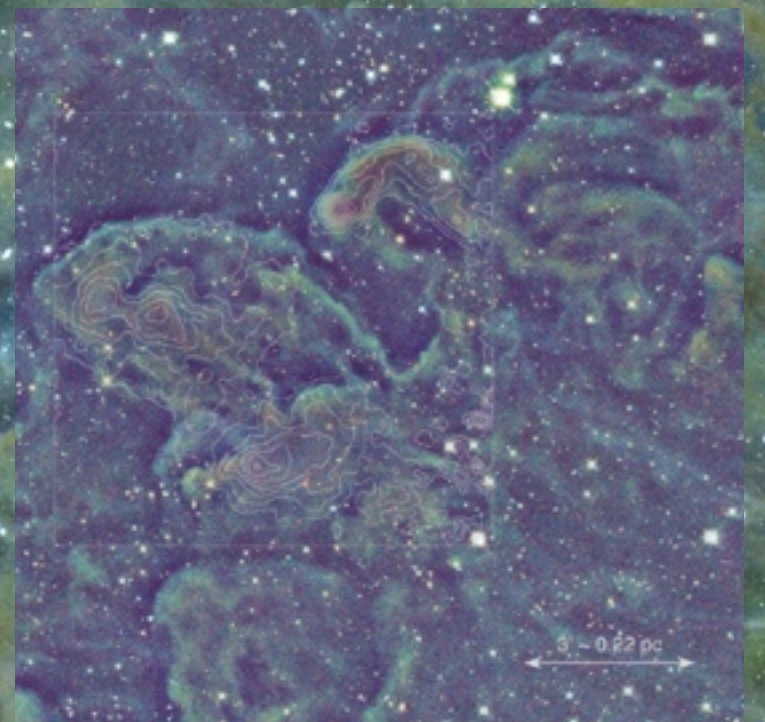
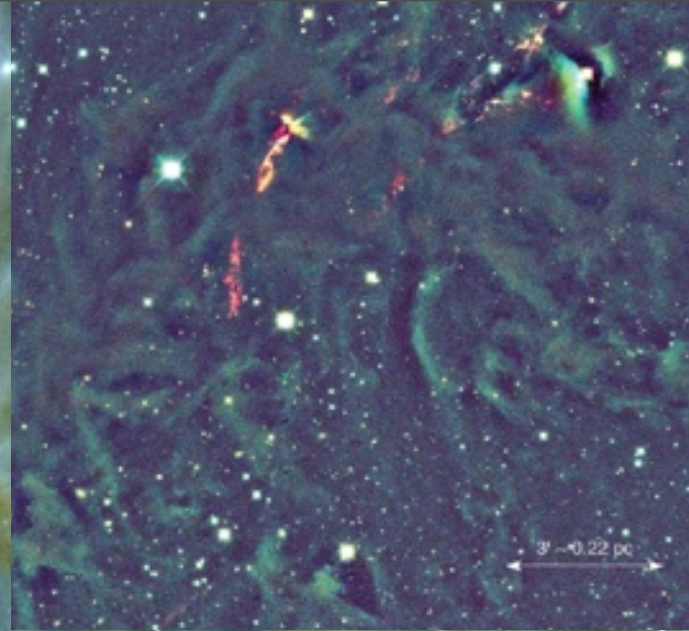
“integrated intensity”



“column density”

“COMPLETE”

“Cloudshine”



Background: to appear in Foster, Mandel, Pineda, Covey & Goodman 2009
Insets: Foster & Goodman 2006, Calar Alto JHK

✓ “L1448”

“Cloudshine” ✓

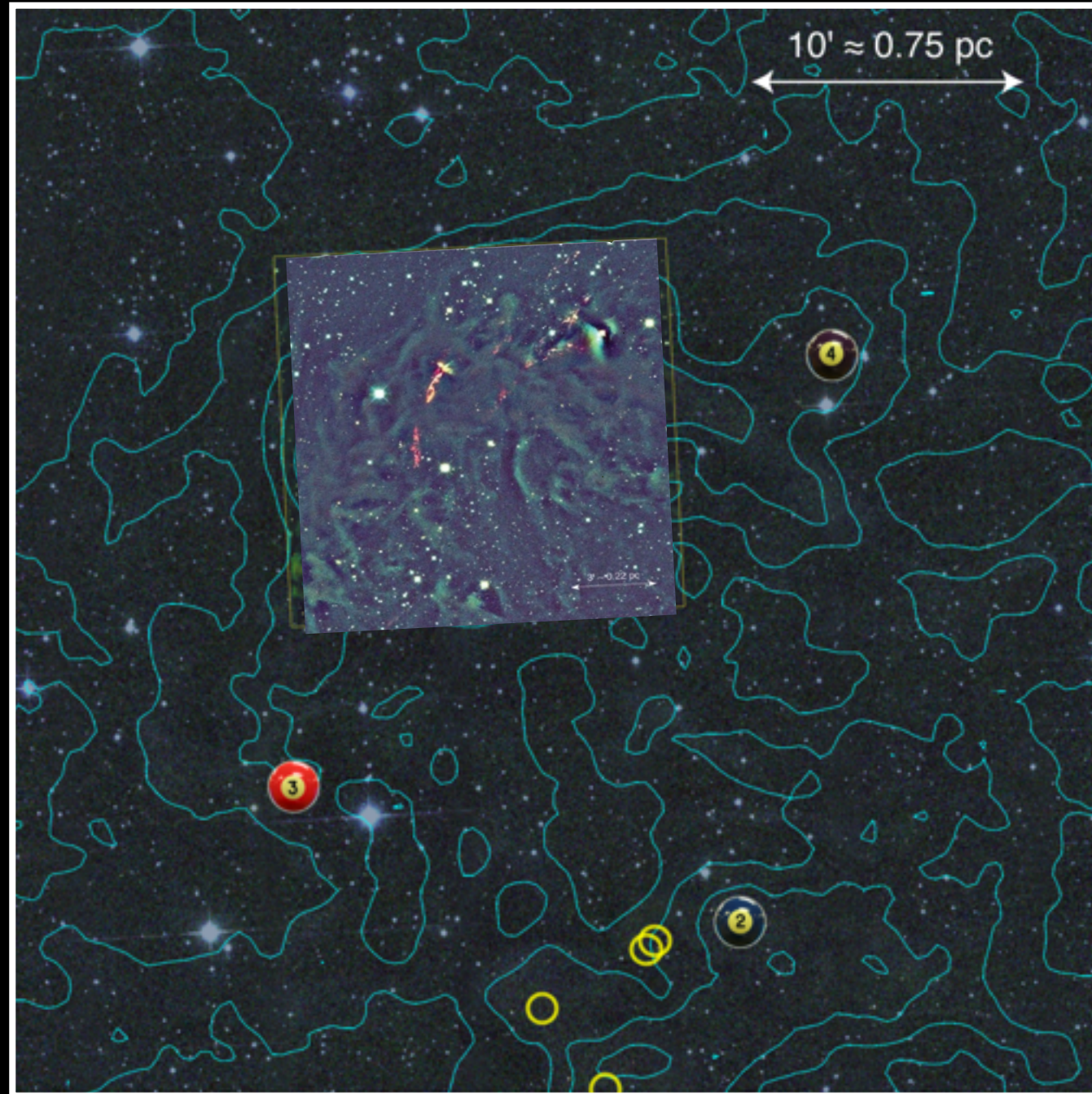
○ “pre-stellar core”

...compact
thermal dust peak ✓

* “protostar” ✓

...Spitzer c2d (MIR) point
source with “right” SED

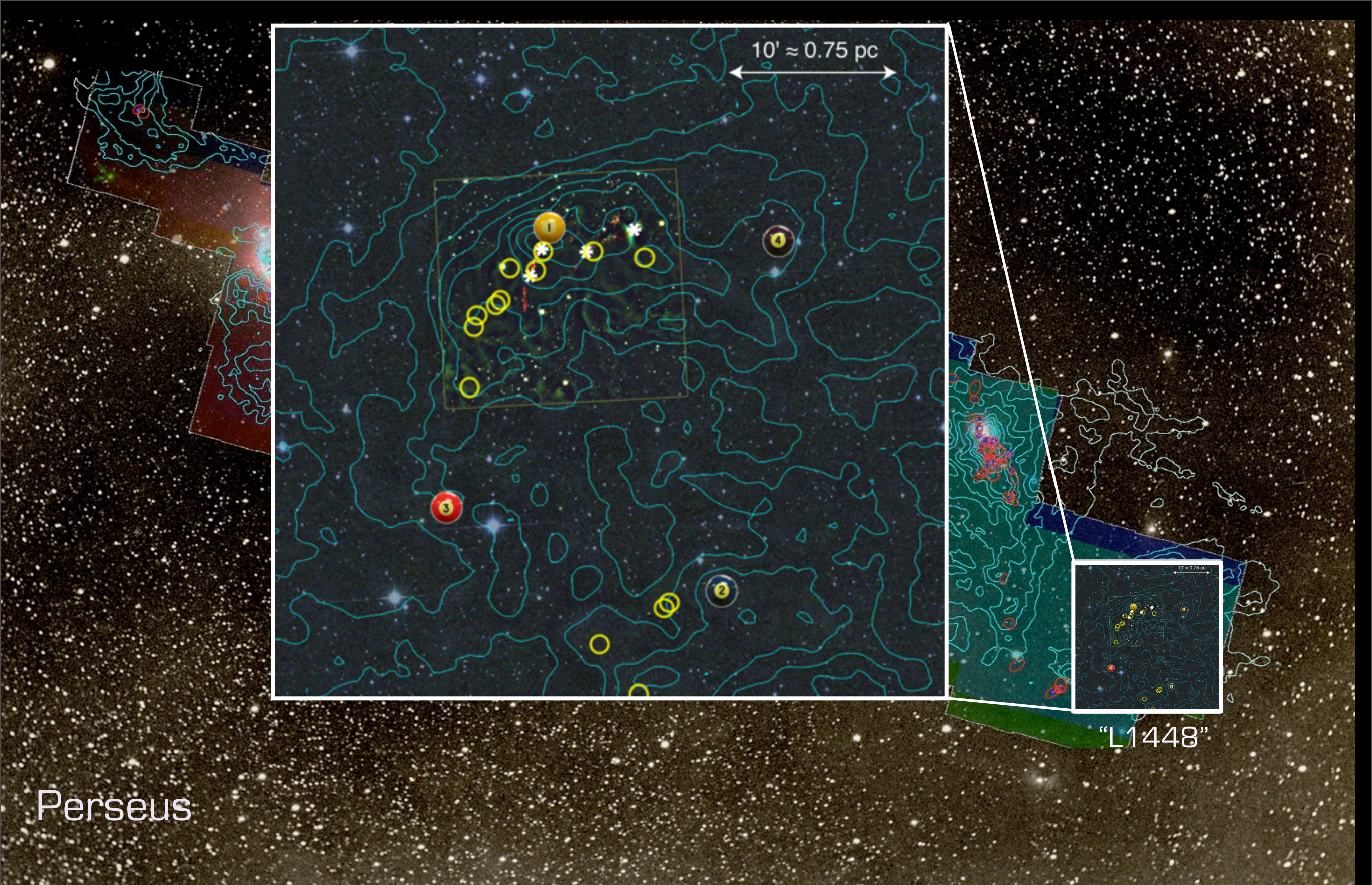
“integrated
intensity”



“column
density”

“COMPLETE”

(3 ...later)



Perseus

"L1448"



"integrated intensity"

"column density"

COMPLETE

COMPLETE Data Coverage Tool

http://www.worldwidetelescope.org/COMPLETE/WWTCoverageTool.htm#

COMPLETE



COMPLETE Data Available

Center on Perseus | Center on Ophiuchus | Center on Serpens

Full-Cloud Data (Phase I, All Data Available)

Dataset	Show	Perseus	Ophiuchus	Serpens	Link
GBT: HI Data Cube	<input checked="" type="checkbox"/>	✓	✓	∅	Data
IRAS: Av/Temp Maps	<input checked="" type="checkbox"/>	✓	✓	✓	Data
FCRAO: 12CO	<input checked="" type="checkbox"/>	✓	✓	✓	Data
FCRAO: 13CO	<input checked="" type="checkbox"/>	✓	✓	✓	Data
JCMT: 850 microns	<input checked="" type="checkbox"/>	✓	✓	∅	Data
Spitzer c2d: IRAC 1,3 (3.6,5.8 μm)	<input checked="" type="checkbox"/>	✓	✓	✓	Data
Spitzer c2d: IRAC 2,4 (4.5,8 μm)	<input checked="" type="checkbox"/>	✓	✓	✓	Data
CSO/Bolocam: 1.2-mm	<input checked="" type="checkbox"/>	✓	∅	∅	Data
Spitzer MIPS: Derived Dust Map	<input checked="" type="checkbox"/>	✓	∅	∅	Data

Targeted Regions (Phase II, Some Data Not Yet Available)

CTIO/Calar Alto: NIR (J,H,Ks)	<input checked="" type="checkbox"/>	✓	✓	∅	Data
IRAM 30-m: N2H+ and C18O	<input checked="" type="checkbox"/>	✓	∅	∅	Data
IRAM 30-m: 1.1-mm continuum	<input checked="" type="checkbox"/>	✓	∅	∅	Data
Megacam/MMT: r,i,z images	<input checked="" type="checkbox"/>	✓	∅	∅	Data

Catalogs & Pointed Surveys

NH3 Pointed Survey	<input type="checkbox"/>	✓	∅	∅	Data
YSO Candidate list (c2d)	<input type="checkbox"/>	✓	✓	✓	Data

Microsoft Research
WorldWide Telescope

Done

To explore on your own, go to <http://www.cfa.harvard.edu/COMPLETE/>, then click on

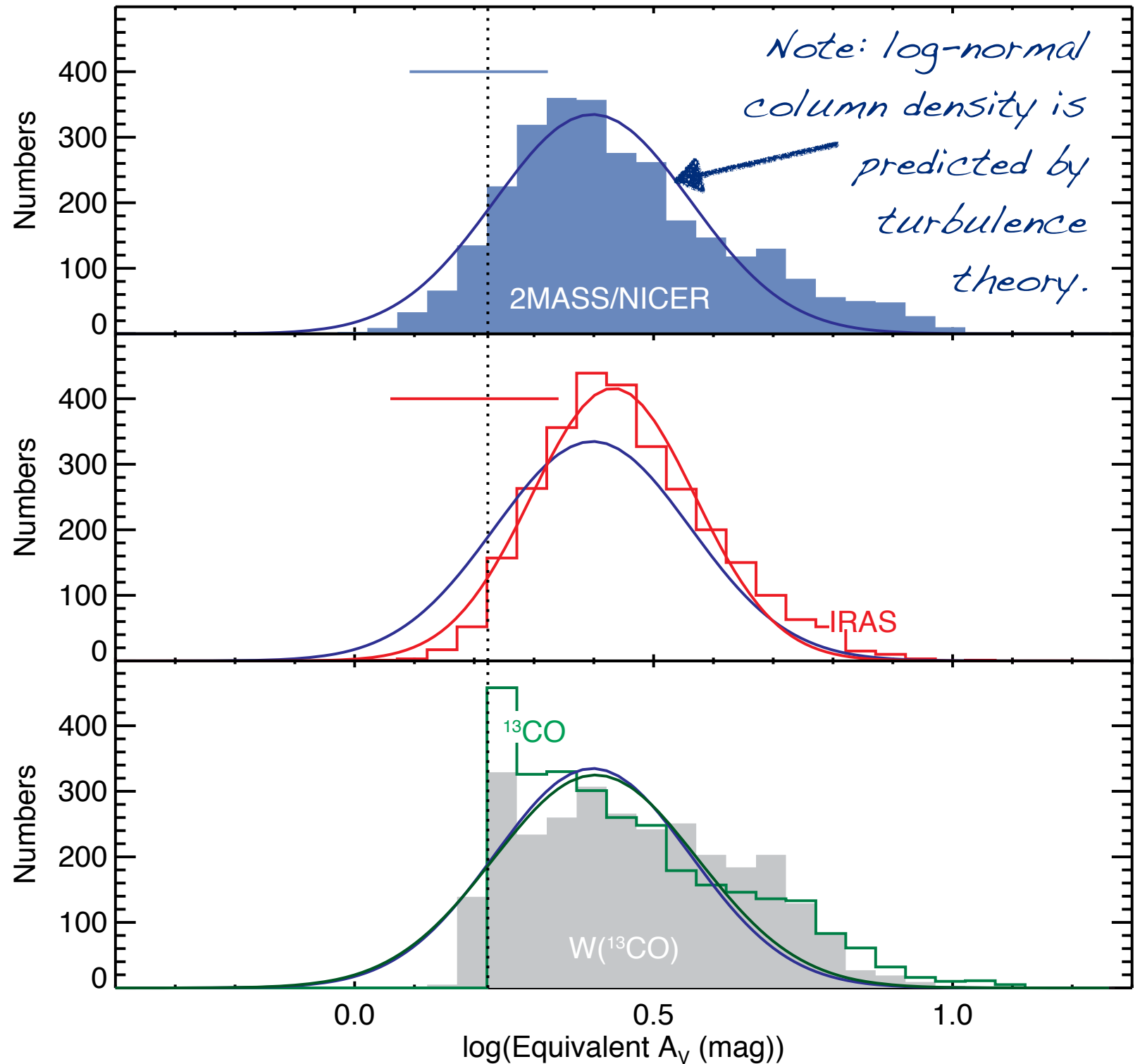
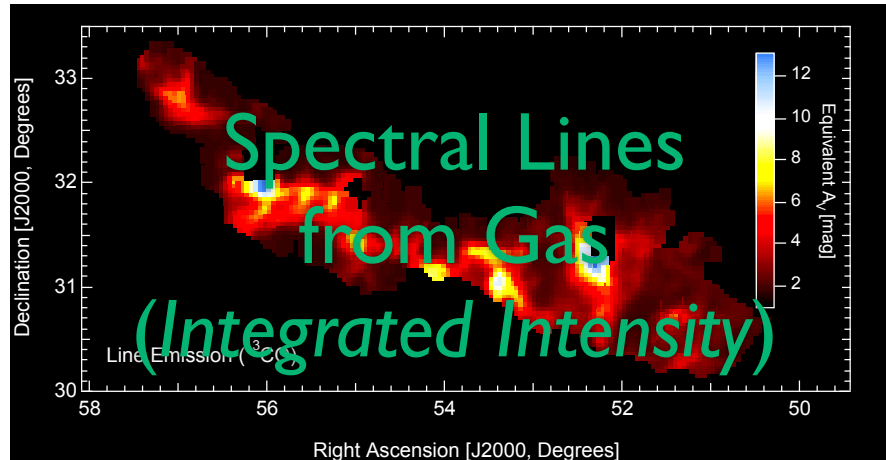
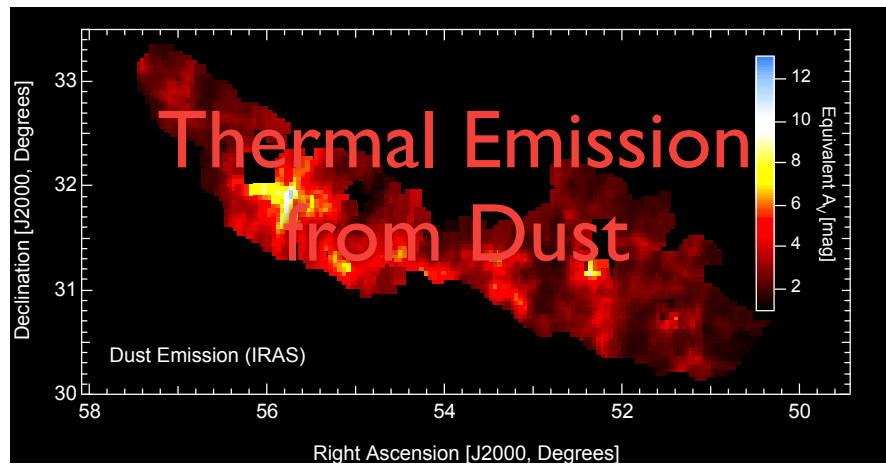
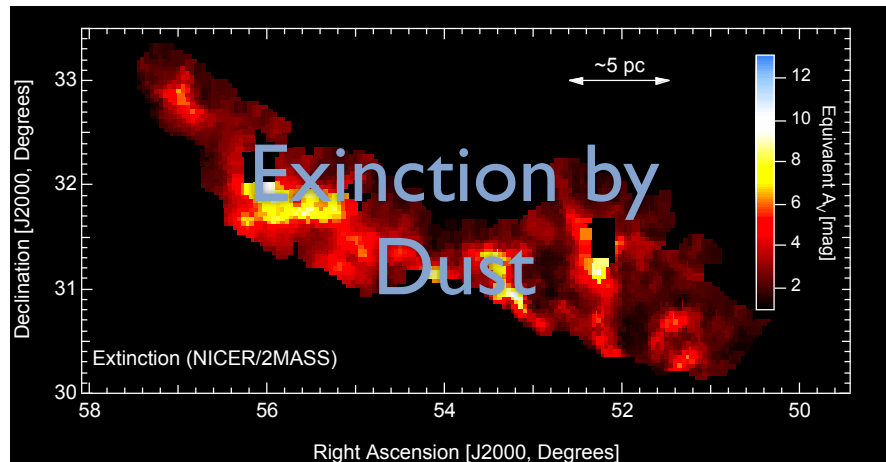


and choose to see the Interactive Coverage Tool in either Google Sky or WorldWide Telescope.

Many thanks to Jonathan Foster, Gus Muench & Jonathan Fay (MSR/WWT team) for these tools!

Column Density in Perseus, Measured 3 Ways

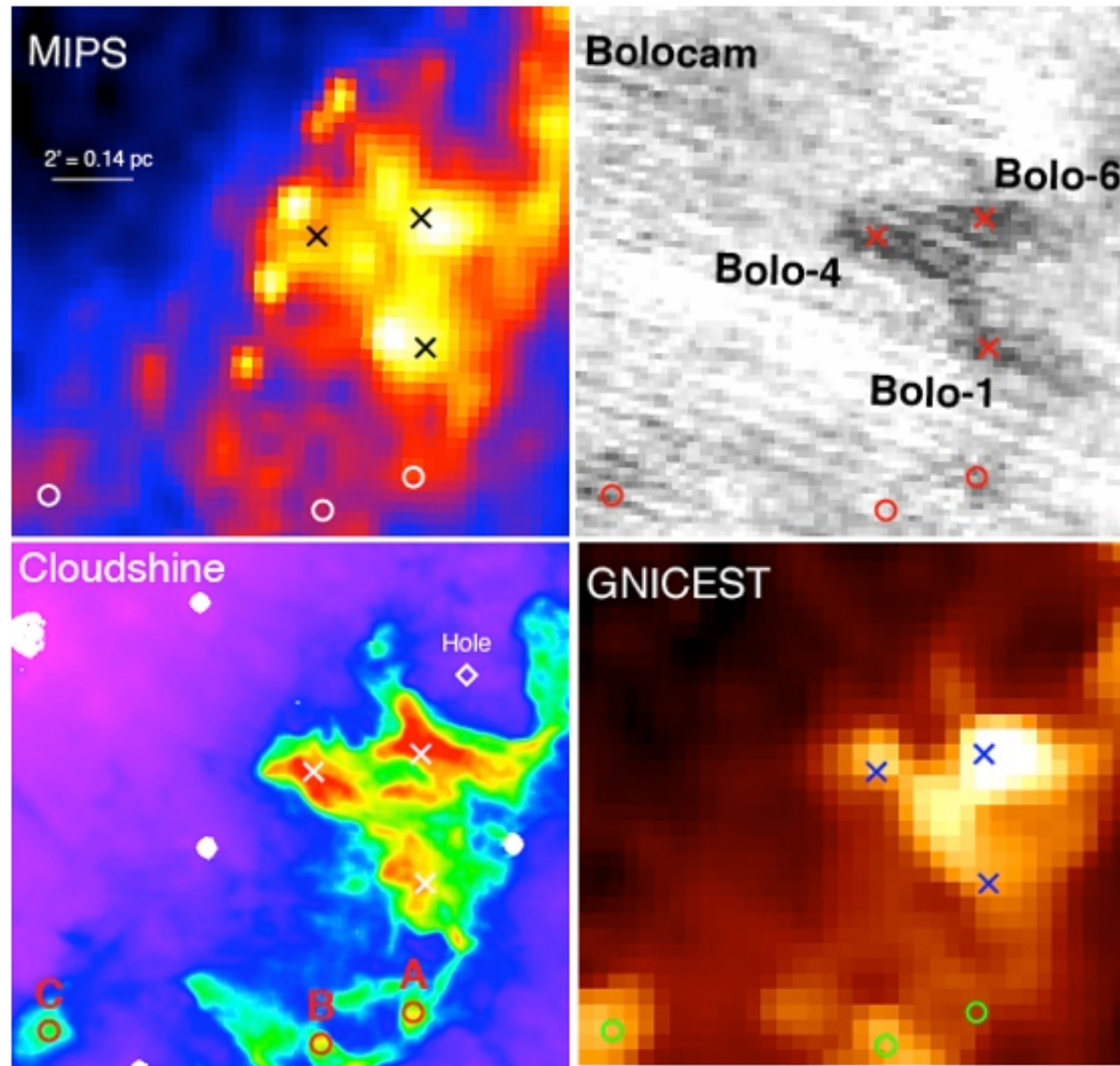
TASTE TEST



COMMERCIAL BREAK:

“Foster’s Showdown, v.2009”

...talk with Foster, Pineda, Offner, Draine and/or me later...



“turbulent fragmentation” “LI 448” “(magneto-)hydrodynamic simulation”

“Cloudshine”

“pre-stellar core”

“protostar”

“integrated intensity*”

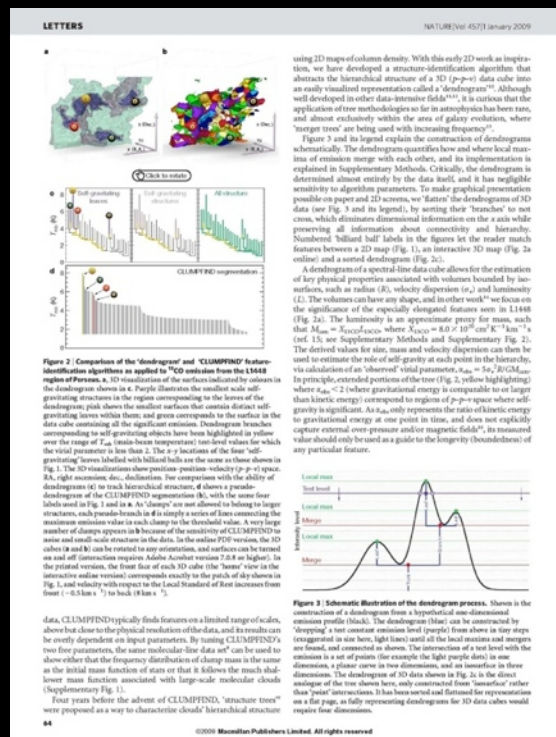
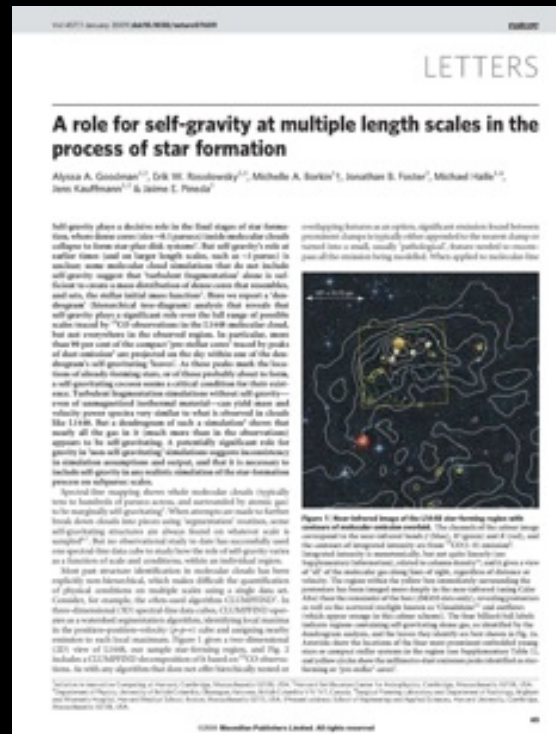
“p-p-v cube”

“segmentation”

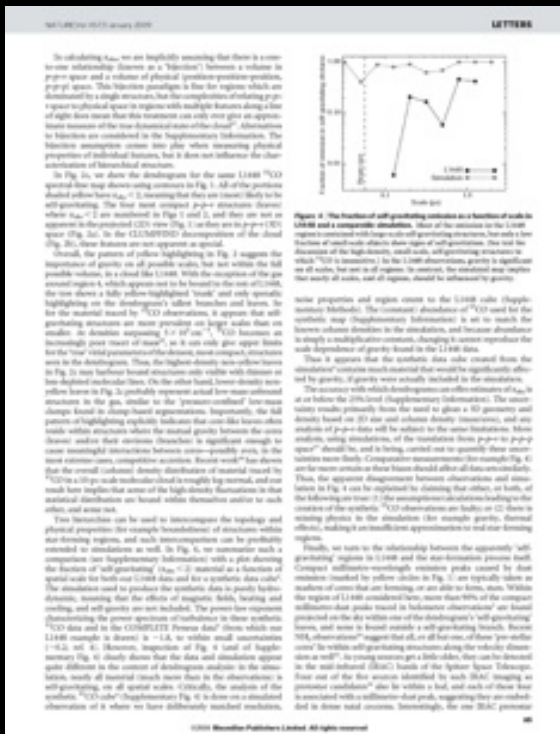
“CLUMPFIND”

“Dendrogram”

*...more to come



“COMPLETE”



“3D PDF”

“bi-jection”

“virial parameter”

“column density”

“turbulent power spectrum”

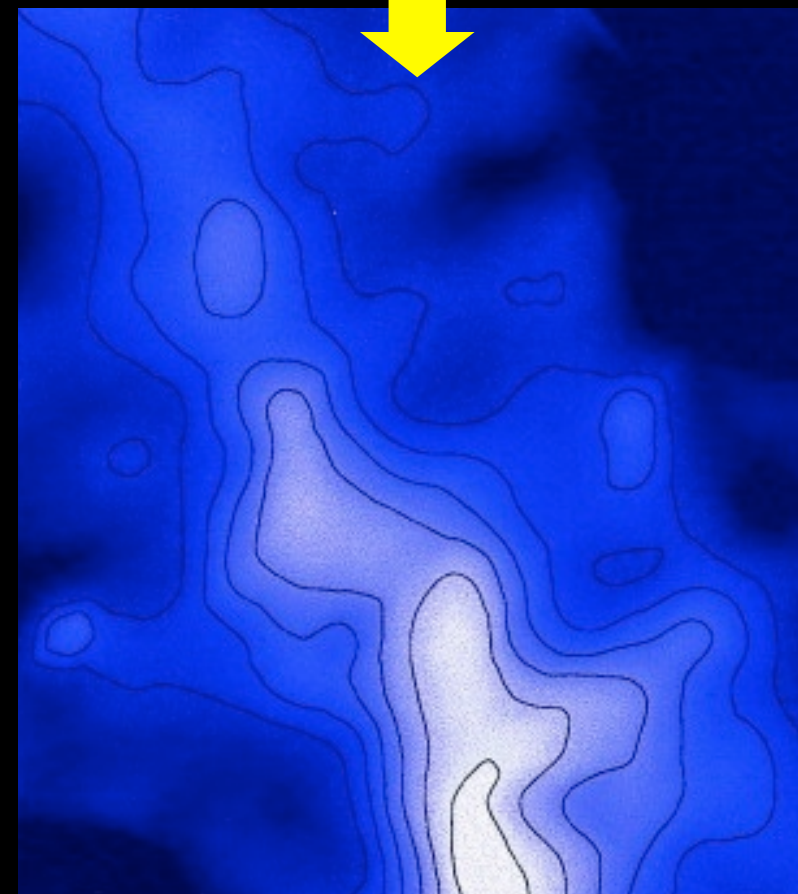
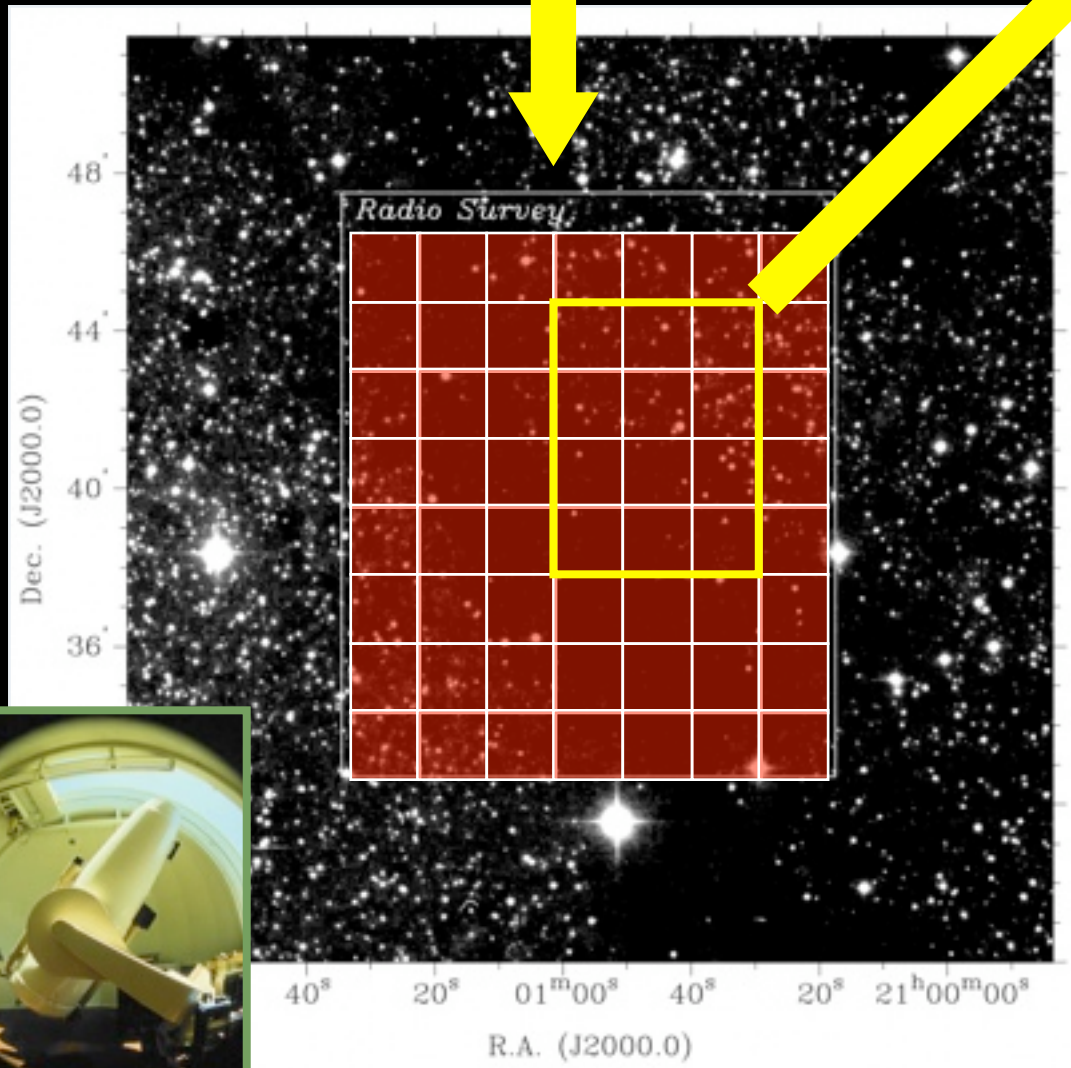
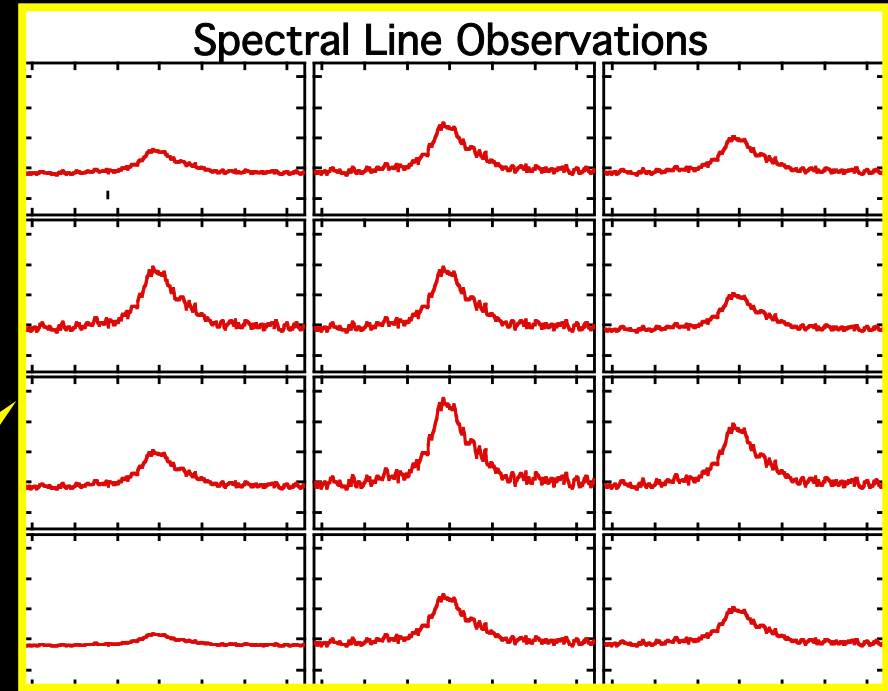
“synthetic observation”

“depletion, opacity”

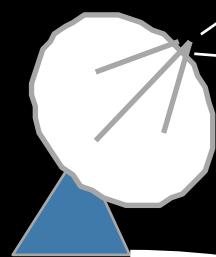
“taste-test”

caveats

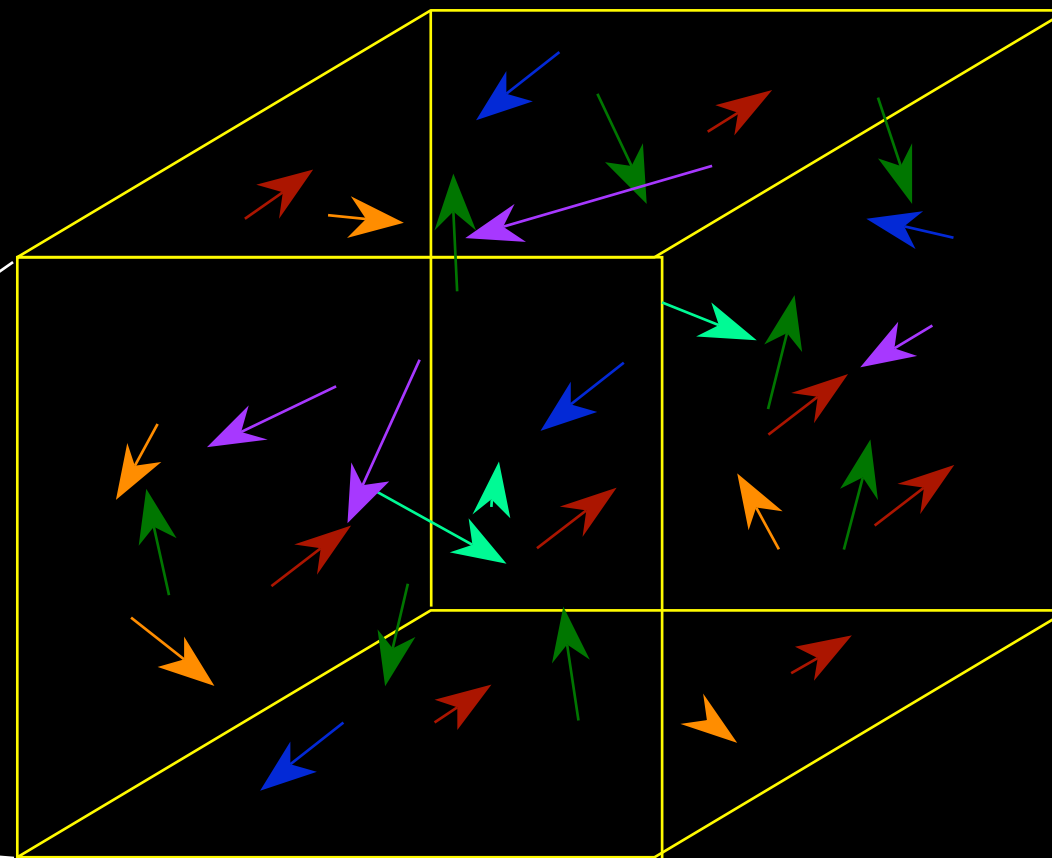
Radio Spectral-line Observations of Interstellar Clouds



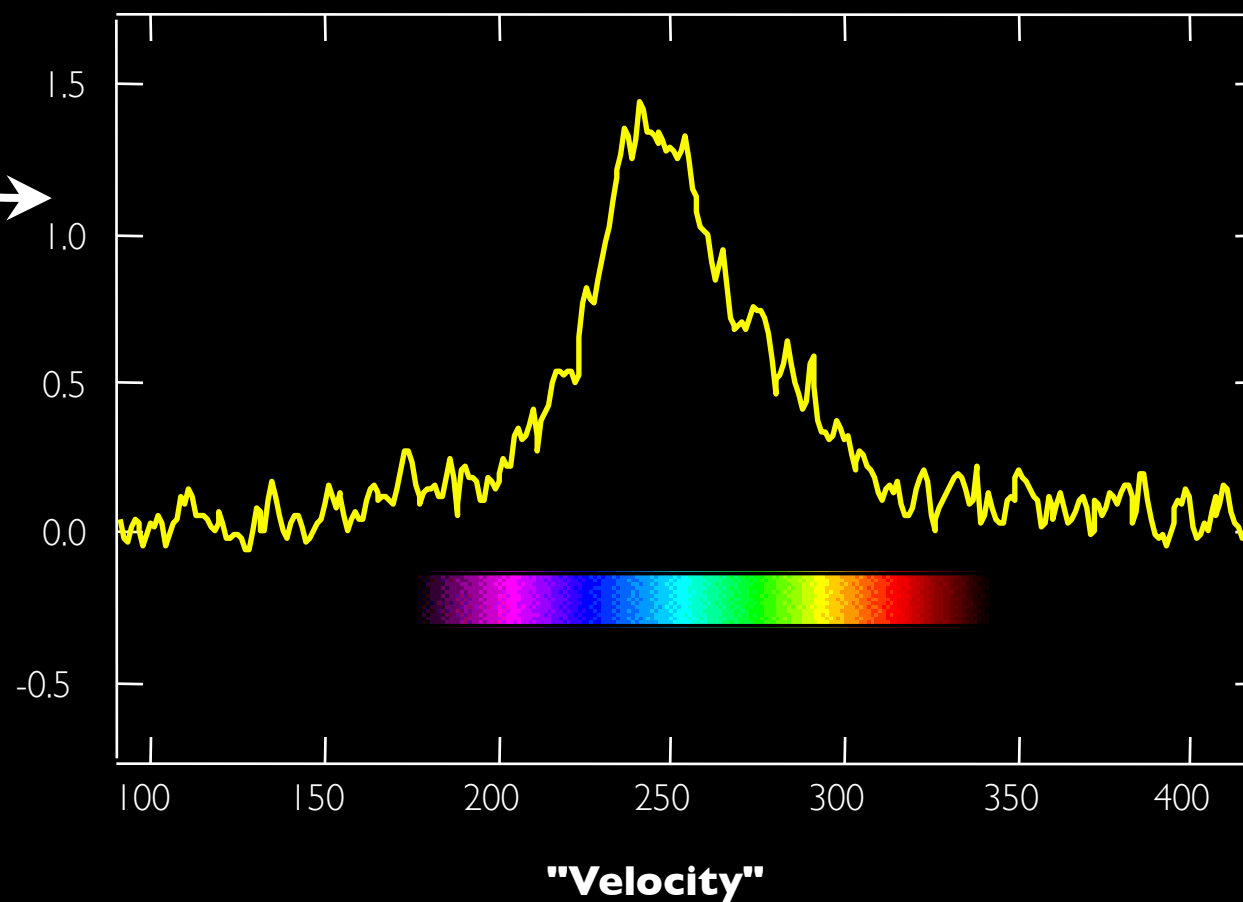
Velocity from Spectroscopy



Telescope +
Spectrometer



Observed Spectrum

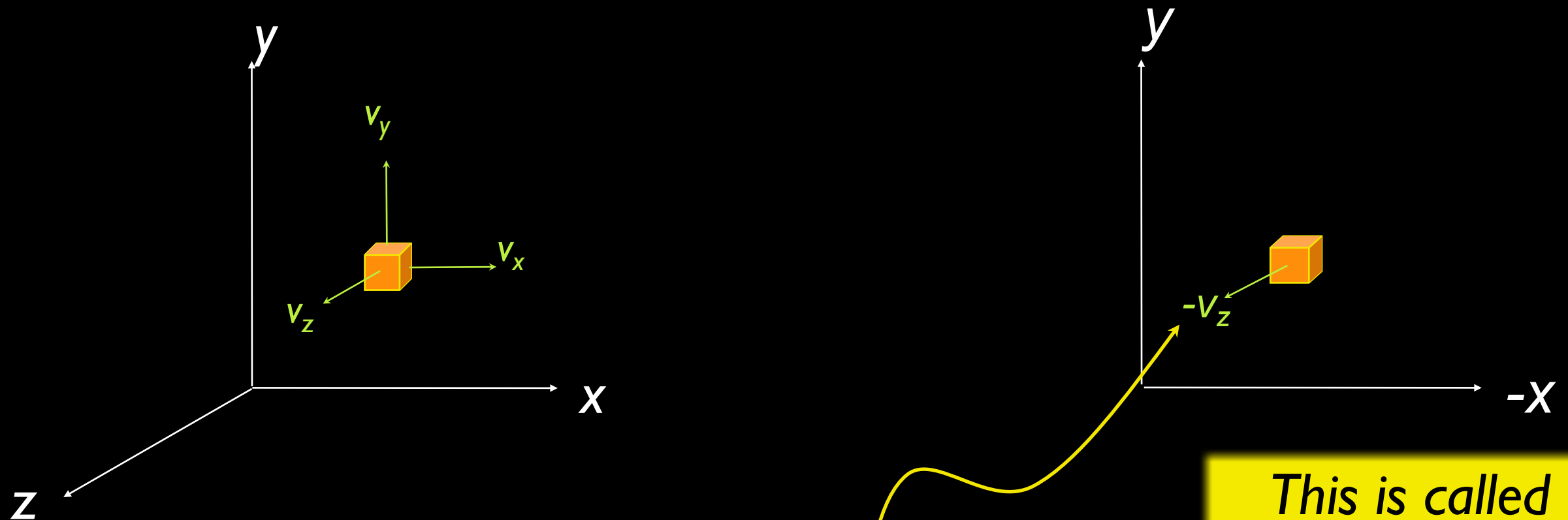


All thanks to Doppler

“Three” Dimensions: Spectral-Line Mapping

We wish we could measure...

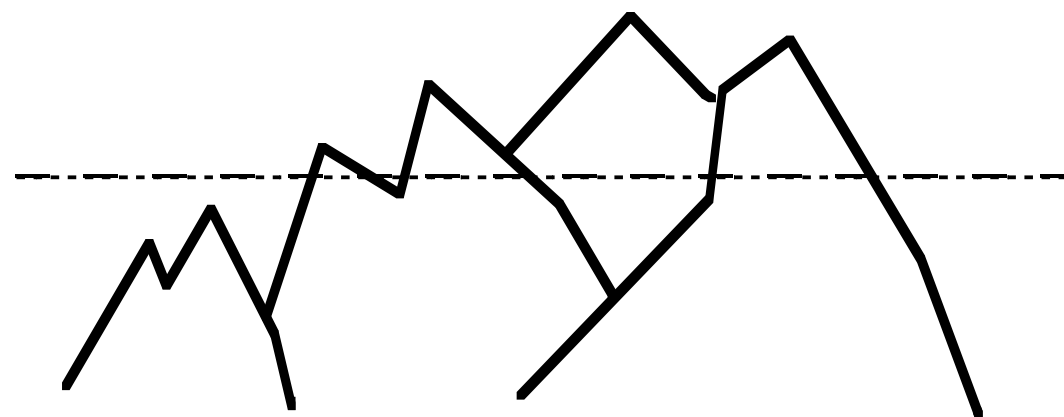
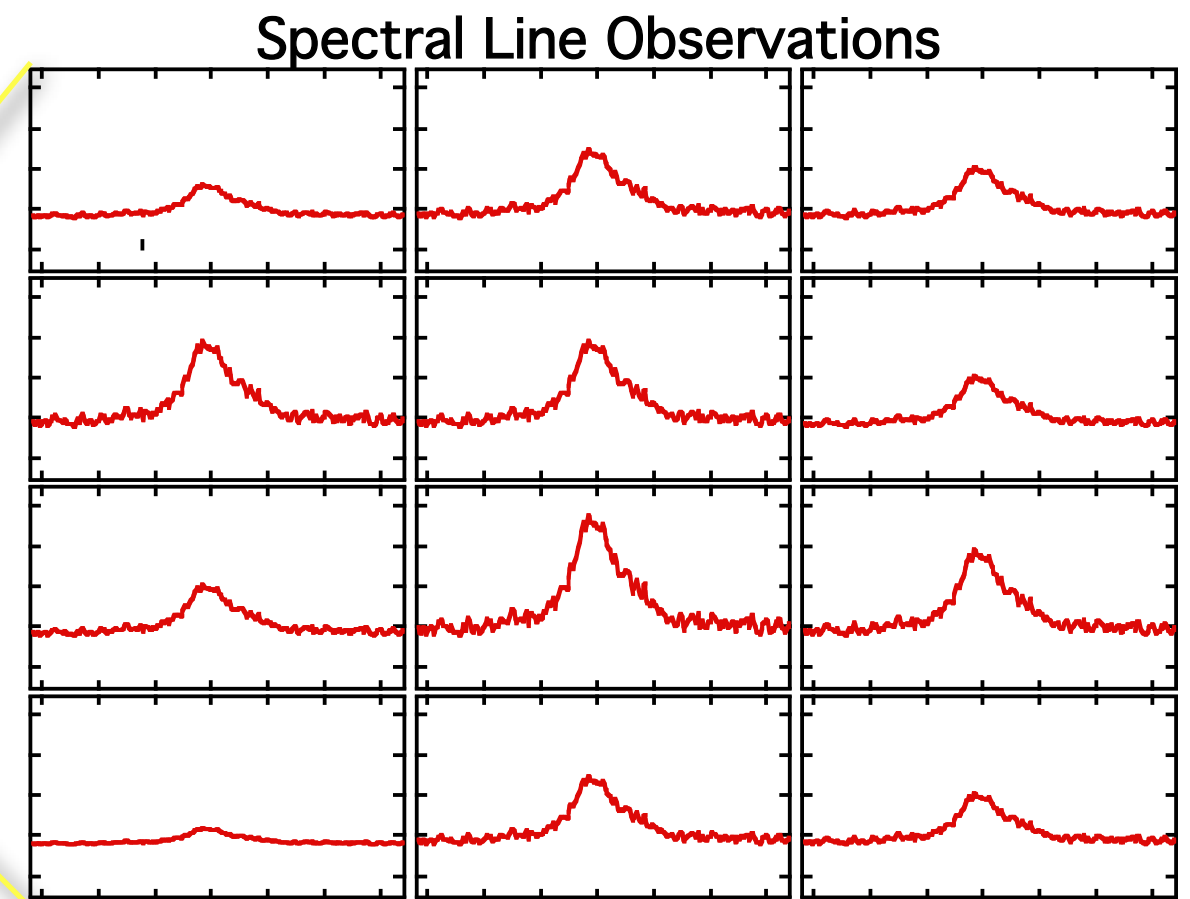
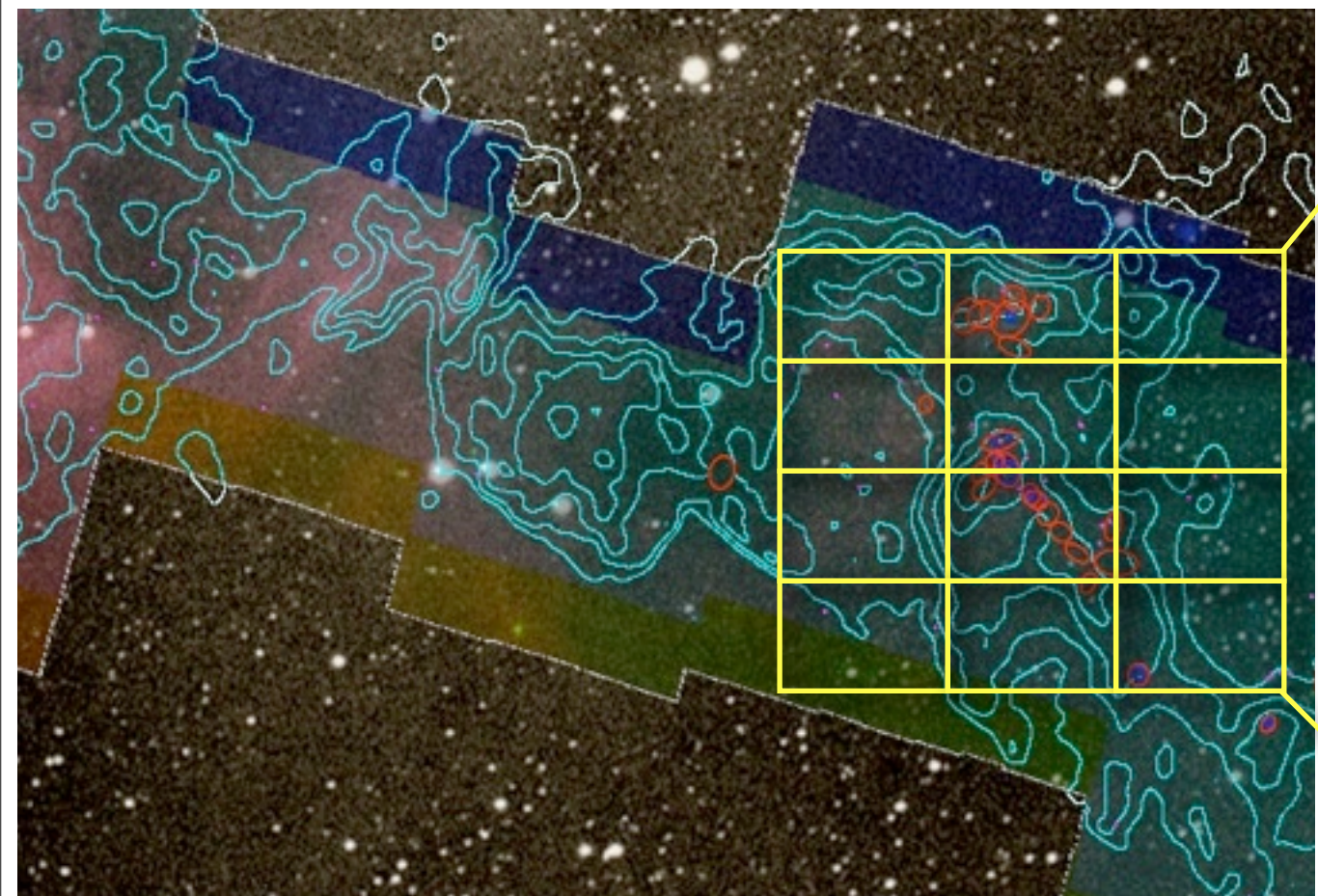
But we can measure...



v_z *only* from
“spectral-line
maps”

This is called
“ **$p-p-v$** ” or
“position-
position-velocity”
space.

There's much more to life than "integrated intensity"



Mountain Range



No loss of information



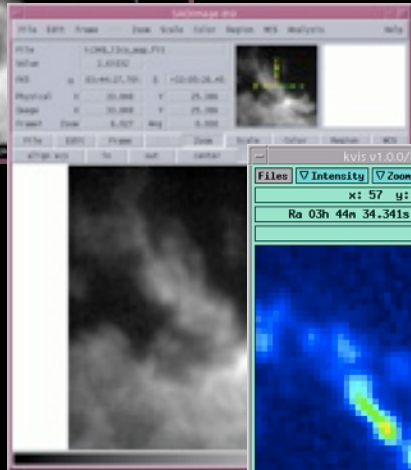
Loss of
1 dimension

Astronomical Visualization Tools are Traditionally 2D

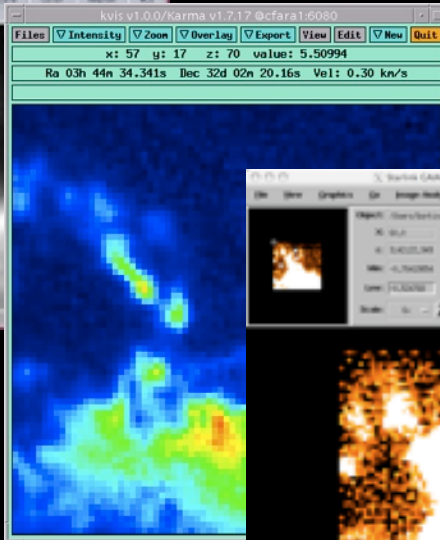
IDL



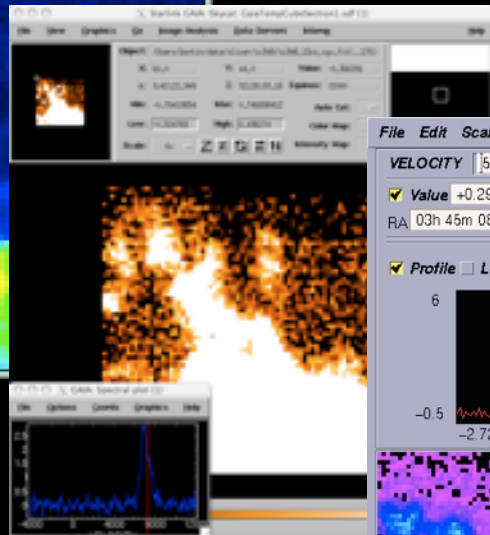
DS9



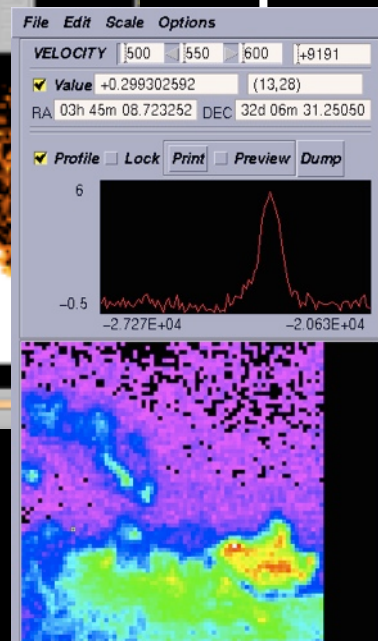
Karma*



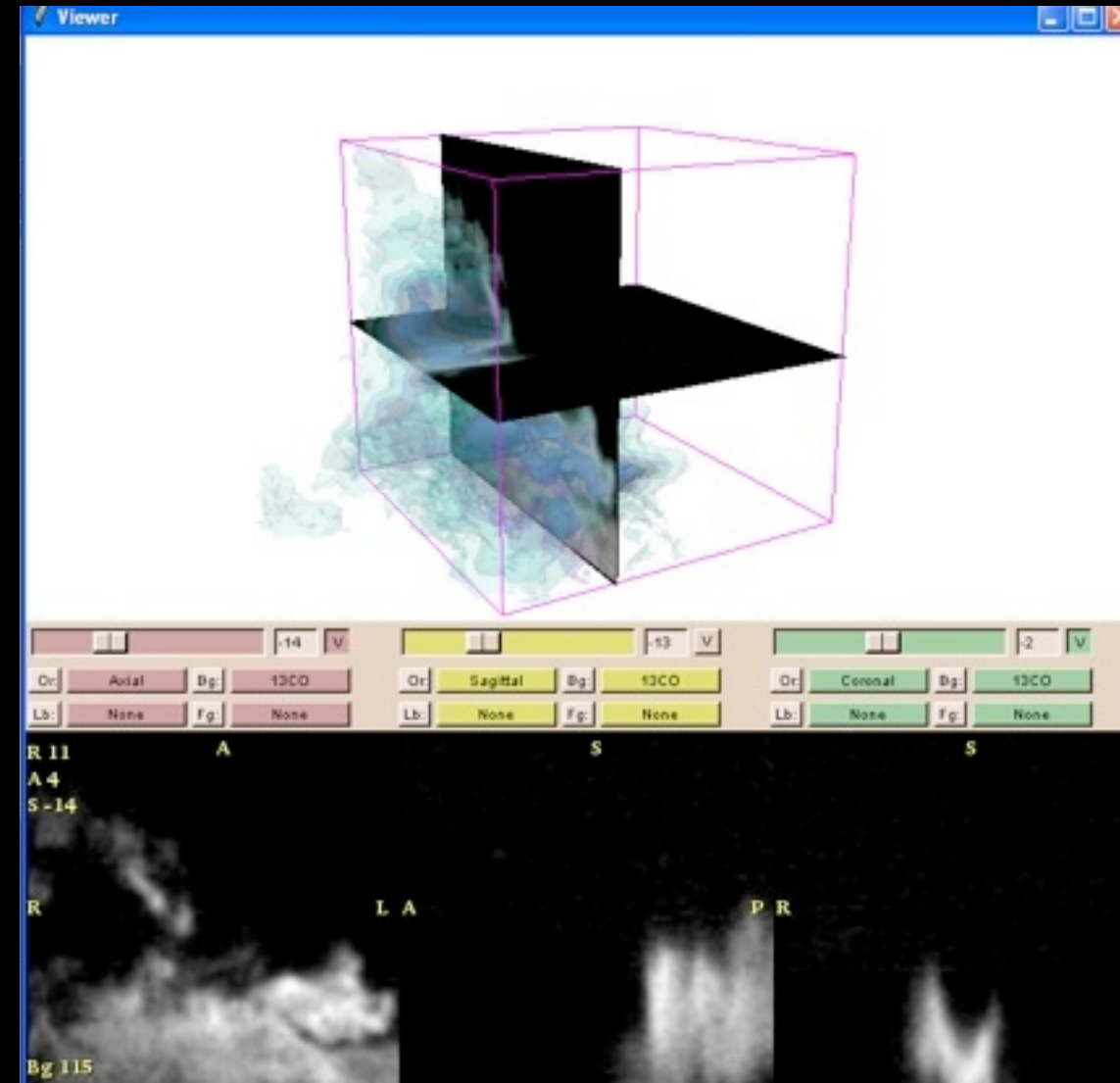
GAIA



Aipsview



3D Slicer

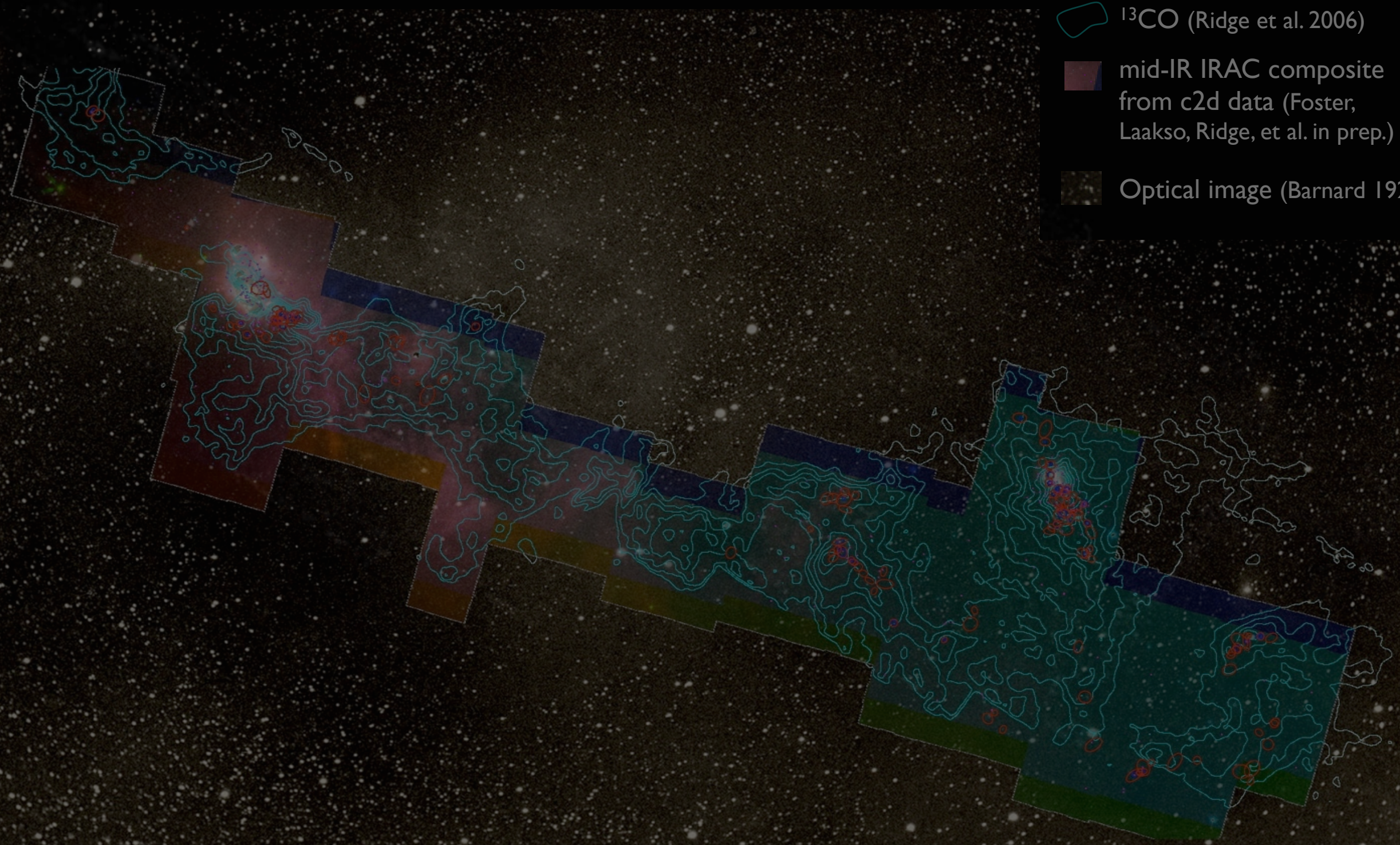


“3D”=movies

COMPLETE Perseus

Image size: 1305 x 733
VL: 63 WW: 127

-  mm peak (Enoch et al. 2006)
-  sub-mm peak (Hatchell et al. 2005, Kirk et al. 2006)
-  ^{13}CO (Ridge et al. 2006)
-  mid-IR IRAC composite from c2d data (Foster, Laakso, Ridge, et al. in prep.)
-  Optical image (Barnard 1927)

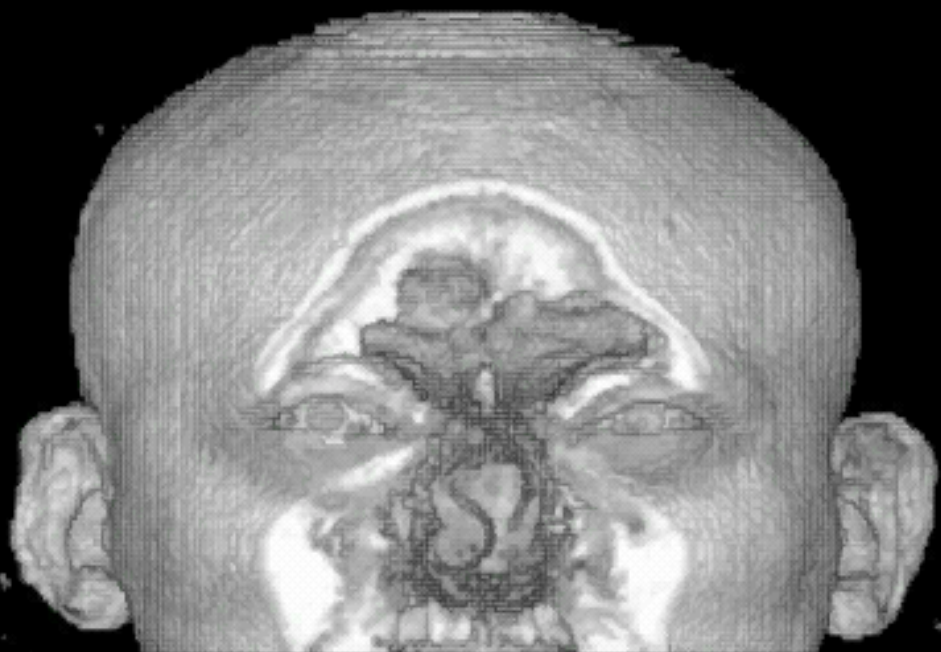


m: 17249
Zoom: 227% Angle: 0



“Astronomical Medicine”

“KEITH”



“z” is depth into head

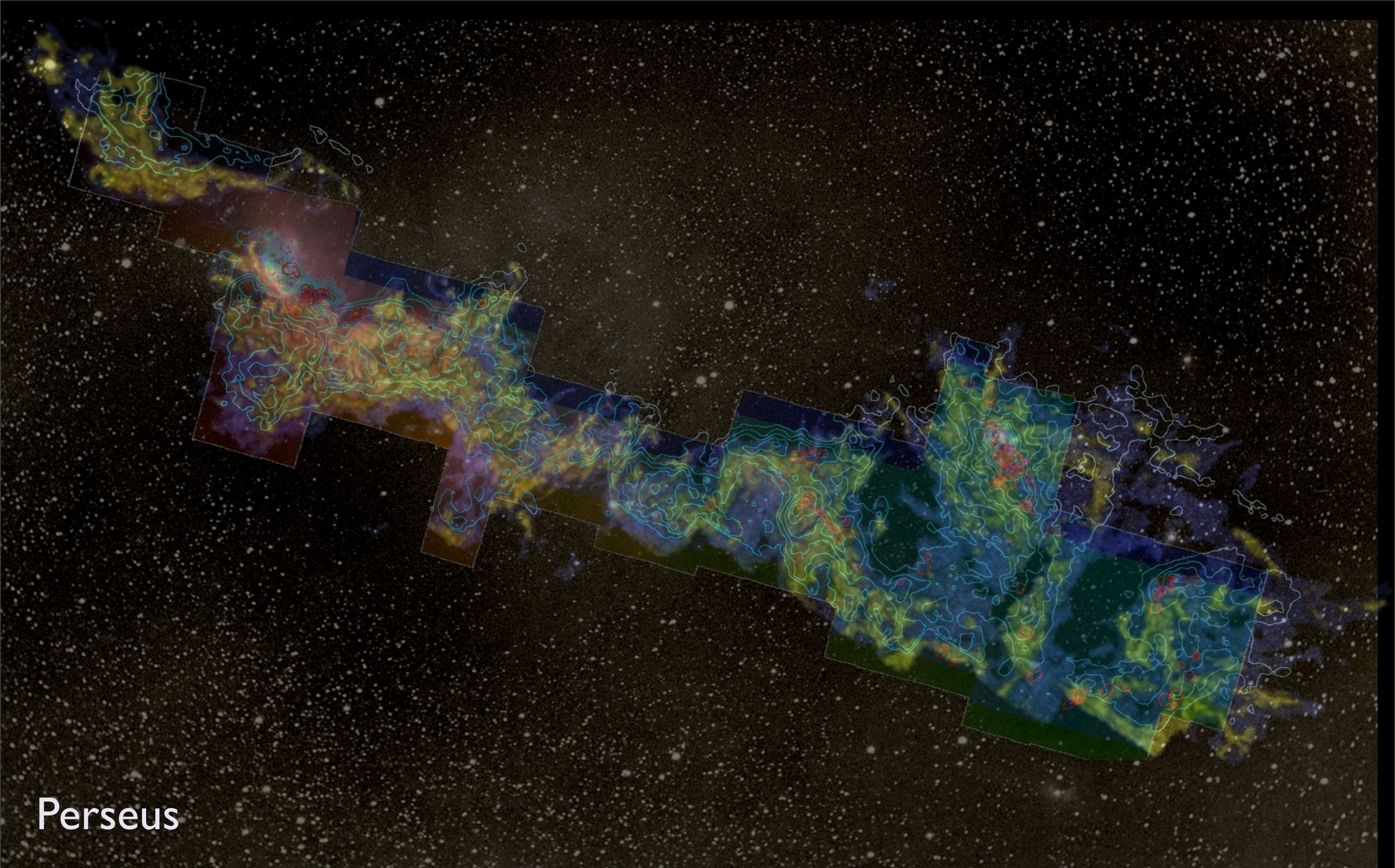
“PERSEUS”



“z” is line-of-sight velocity

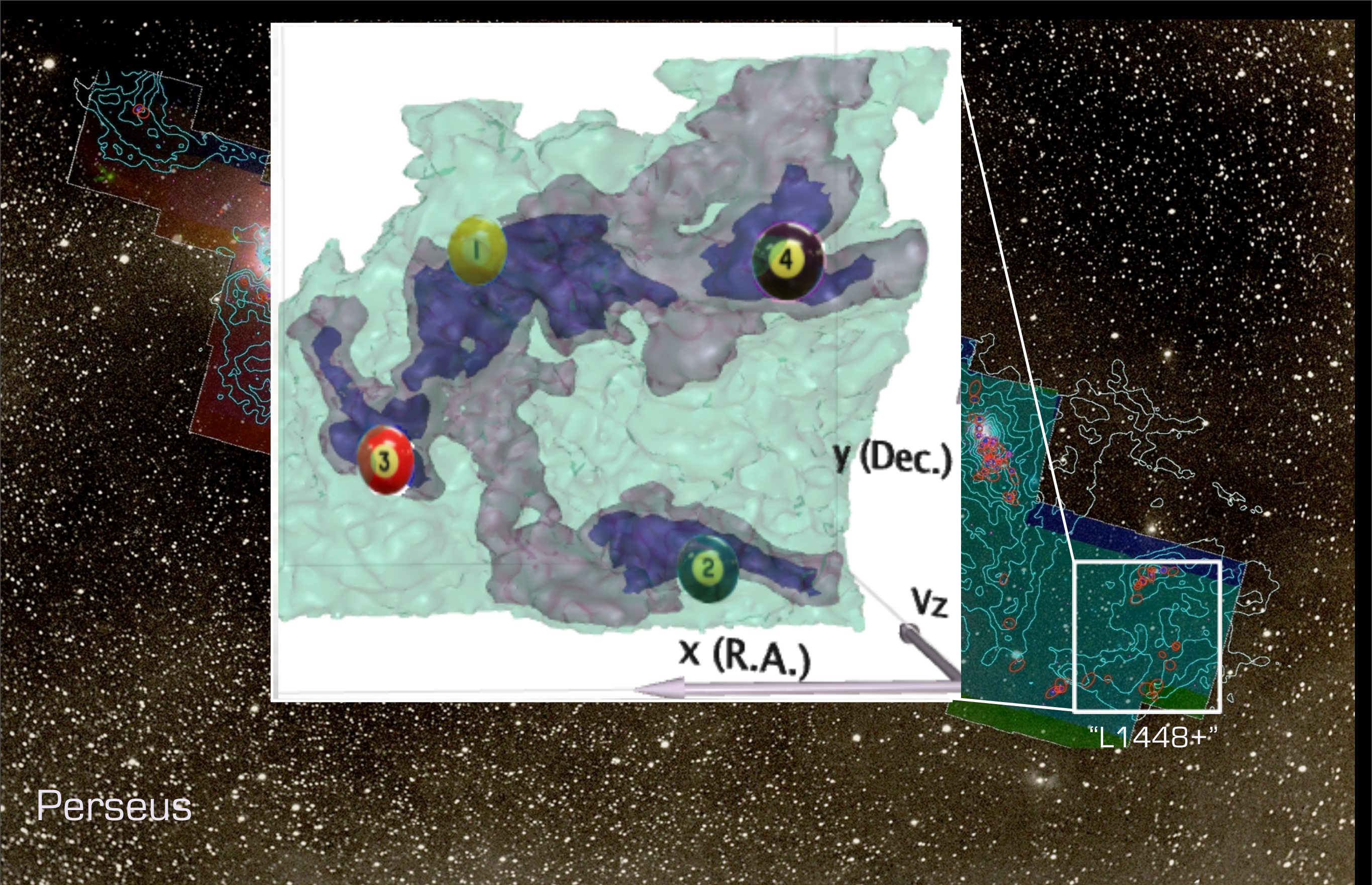
(This kind of “series of 2D slices view” is known in the Viz as “the grand tour”)





Perseus

3D Viz made with VolView



Perseus

“turbulent fragmentation”

“(magneto-)hydrodynamic simulation”

“bi-jection”

“virial parameter”

“virial parameter”

“turbulent power spectrum”

“synthetic observation”

“depletion, opacity”

“taste-test”
caveats

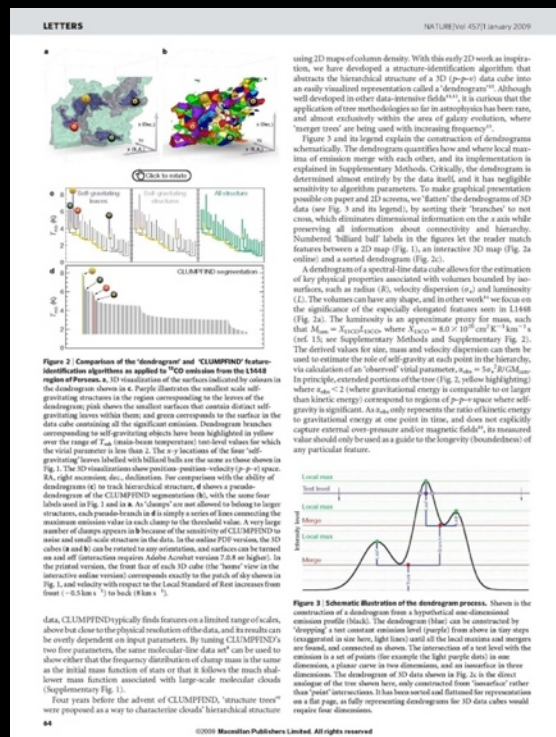
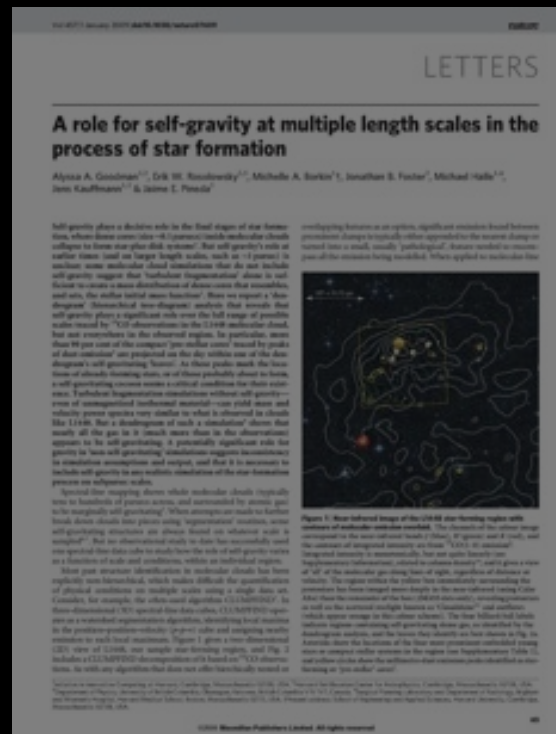
✓ “integrated intensity*”

✓ “p-p-v cube”

“segmentation”

“CLUMPFIND”

“Dendrogram”



“3D PDF”

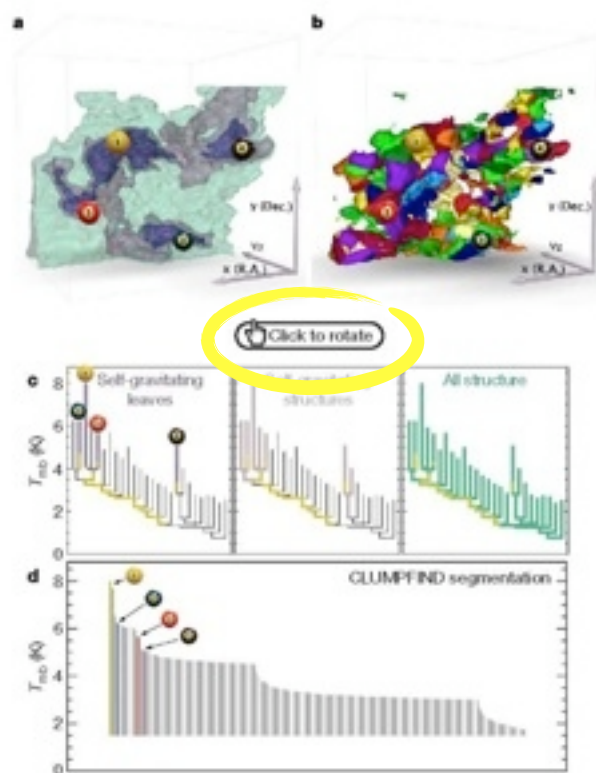


Figure 2 | Comparison of the 'dendrogram' and 'CLUMPFIND' feature-identification algorithms as applied to ^{13}CO emission from the L1448 region of Perseus. **a, 3D visualization of the surfaces indicated by colours in the dendrogram shown in **c**. Purple illustrates the smallest scale self-gravitating structures in the region corresponding to the leaves of the dendrogram; pink shows the smallest surfaces that contain distinct self-gravitating leaves within them; and green corresponds to the surface in the data cube containing all the significant emission. Dendrogram branches corresponding to self-gravitating objects have been highlighted in yellow over the range of T_{sub} (main-beam temperature) test-level values for which the virial parameter is less than 2. The x - y locations of the four 'self-gravitating' leaves labelled with billiard balls are the same as those shown in Fig. 1. The 3D visualizations show position-position-velocity (p - p - v) space. RA, right ascension; dec., declination. For comparison with the ability of dendrograms (**c**) to track hierarchical structure, **d** shows a pseudo-dendrogram of the CLUMPFIND segmentation (**b**), with the same four labels used in Fig. 1 and in **a**. As 'dumps' are not allowed to belong to larger structures, each pseudo-branch in **d** is simply a series of lines connecting the maximum emission value in each clump to the threshold value. A very large number of dumps appears in **b** because of the sensitivity of CLUMPFIND to noise and small-scale structure in the data. In the online PDF version, the 3D cubes (**a** and **b**) can be rotated to any orientation, and surfaces can be turned on and off (interaction requires Adobe Acrobat version 7.0.8 or higher). In the printed version, the front face of each 3D cube (the 'home' view in the interactive online version) corresponds exactly to the patch of sky shown in Fig. 1, and velocity with respect to the Local Standard of Rest increases from front (-0.5 km s^{-1}) to back (8 km s^{-1}).**

data, CLUMPFIND typically finds features on a limited range of scales, above but close to the physical resolution of the data, and its results can be overly dependent on input parameters. By tuning CLUMPFIND's two free parameters, the same molecular-line data set⁸ can be used to show either that the frequency distribution of clump mass is the same as the initial mass function of stars or that it follows the much shallower mass function associated with large-scale molecular clouds (Supplementary Fig. 1).

Four years before the advent of CLUMPFIND, 'structure trees'⁹ were proposed as a way to characterize clouds' hierarchical structure

using 2D maps of column density. With this early 2D work as inspiration, we have developed a structure-identification algorithm that abstracts the hierarchical structure of a 3D (p - p - v) data cube into an easily visualized representation called a 'dendrogram'¹⁰. Although well developed in other data-intensive fields^{11,12}, it is curious that the application of tree methodologies so far in astrophysics has been rare, and almost exclusively within the area of galaxy evolution, where 'merger trees' are being used with increasing frequency¹³.

Figure 3 and its legend explain the construction of dendrograms schematically. The dendrogram quantifies how and where local maxima of emission merge with each other, and its implementation is explained in Supplementary Methods. Critically, the dendrogram is determined almost entirely by the data itself, and it has negligible sensitivity to algorithm parameters. To make graphical presentation possible on paper and 2D screens, we 'flatten' the dendrograms of 3D data (see Fig. 3 and its legend), by sorting their 'branches' to not cross, which eliminates dimensional information on the x axis while preserving all information about connectivity and hierarchy. Numbered 'billiard ball' labels in the figures let the reader match features between a 2D map (Fig. 1), an interactive 3D map (Fig. 2a online) and a sorted dendrogram (Fig. 2c).

A dendrogram of a spectral-line data cube allows for the estimation of key physical properties associated with volumes bounded by isosurfaces, such as radius (R), velocity dispersion (σ_v) and luminosity (L). The volumes can have any shape, and in other work¹⁴ we focus on the significance of the especially elongated features seen in L1448 (Fig. 2a). The luminosity is an approximate proxy for mass, such that $M_{\text{gas}} = X_{13\text{CO}} L_{13\text{CO}}$ where $X_{13\text{CO}} = 8.0 \times 10^{26} \text{ cm}^2 \text{ K}^{-1} \text{ km}^{-1} \text{ s}$ (ref. 15; see Supplementary Methods and Supplementary Fig. 2). The derived values for size, mass and velocity dispersion can then be used to estimate the role of self-gravity at each point in the hierarchy, via calculation of an 'observed' virial parameter, $\alpha_{\text{obs}} = 5\sigma_v^2 R / GM_{\text{gas}}$. In principle, extended portions of the tree (Fig. 2, yellow highlighting) where $\alpha_{\text{obs}} < 2$ (where gravitational energy is comparable to or larger than kinetic energy) correspond to regions of p - p - v space where self-gravity is significant. As α_{obs} only represents the ratio of kinetic energy to gravitational energy at one point in time, and does not explicitly capture external over-pressure and/or magnetic fields¹⁶, its measured value should only be used as a guide to the longevity (boundedness) of any particular feature.

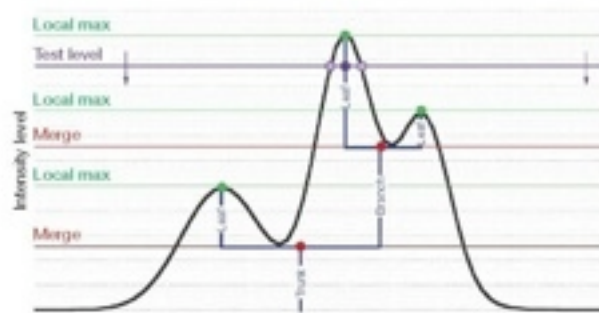


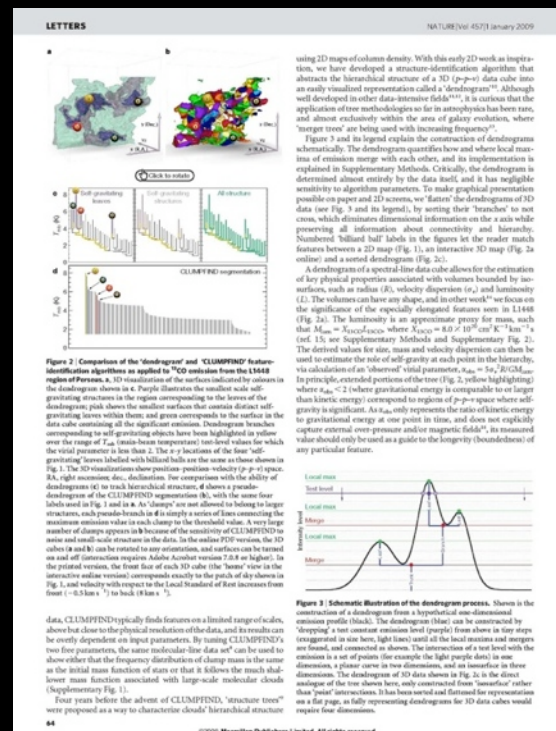
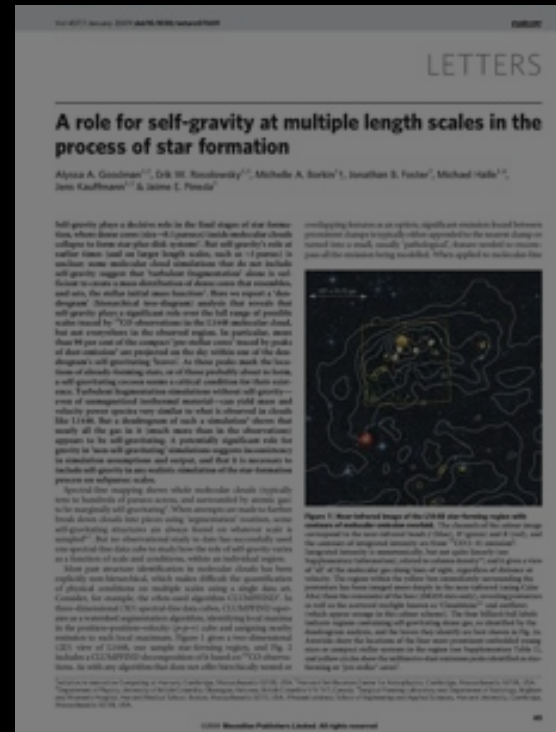
Figure 3 | Schematic illustration of the dendrogram process. Shown is the construction of a dendrogram from a hypothetical one-dimensional emission profile (black). The dendrogram (blue) can be constructed by 'dropping' a test constant emission level (purple) from above in tiny steps (exaggerated in size here, light lines) until all the local maxima and mergers are found, and connected as shown. The intersection of a test level with the emission is a set of points (for example the light purple dots) in one dimension, a planar curve in two dimensions, and an isosurface in three dimensions. The dendrogram of 3D data shown in Fig. 2c is the direct analogue of the tree shown here, only constructed from 'isosurface' rather than 'point' intersections. It has been sorted and flattened for representation on a flat page, as fully representing dendrograms for 3D data cubes would require four dimensions.

“turbulent fragmentation”

“(magneto-)hydrodynamic simulation”

“bi-jection”

“virial parameter”



“segmentation”

“CLUMPFIND”

“Dendrogram”

“turbulent power spectrum”

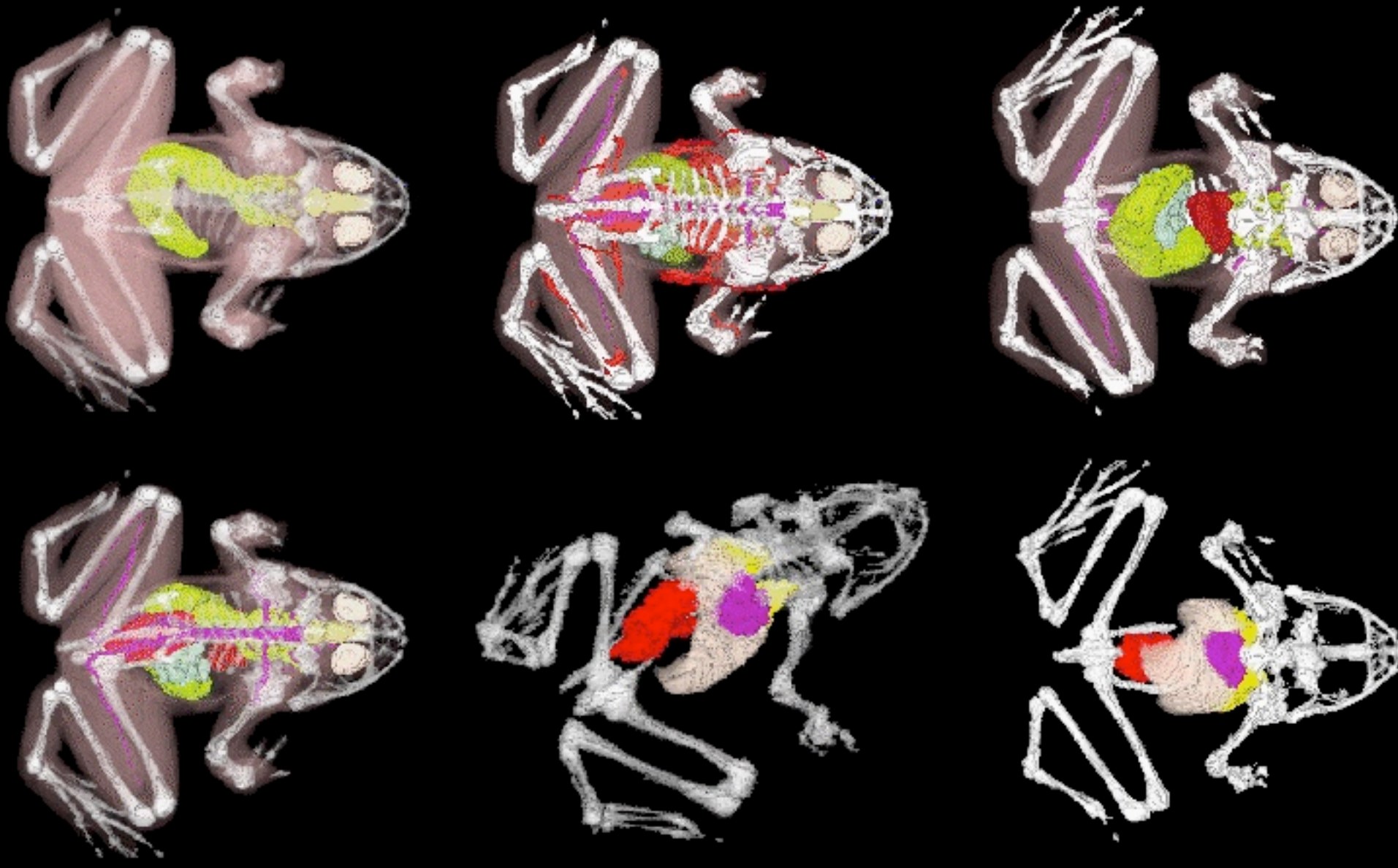
“synthetic observation”

“depletion, opacity”

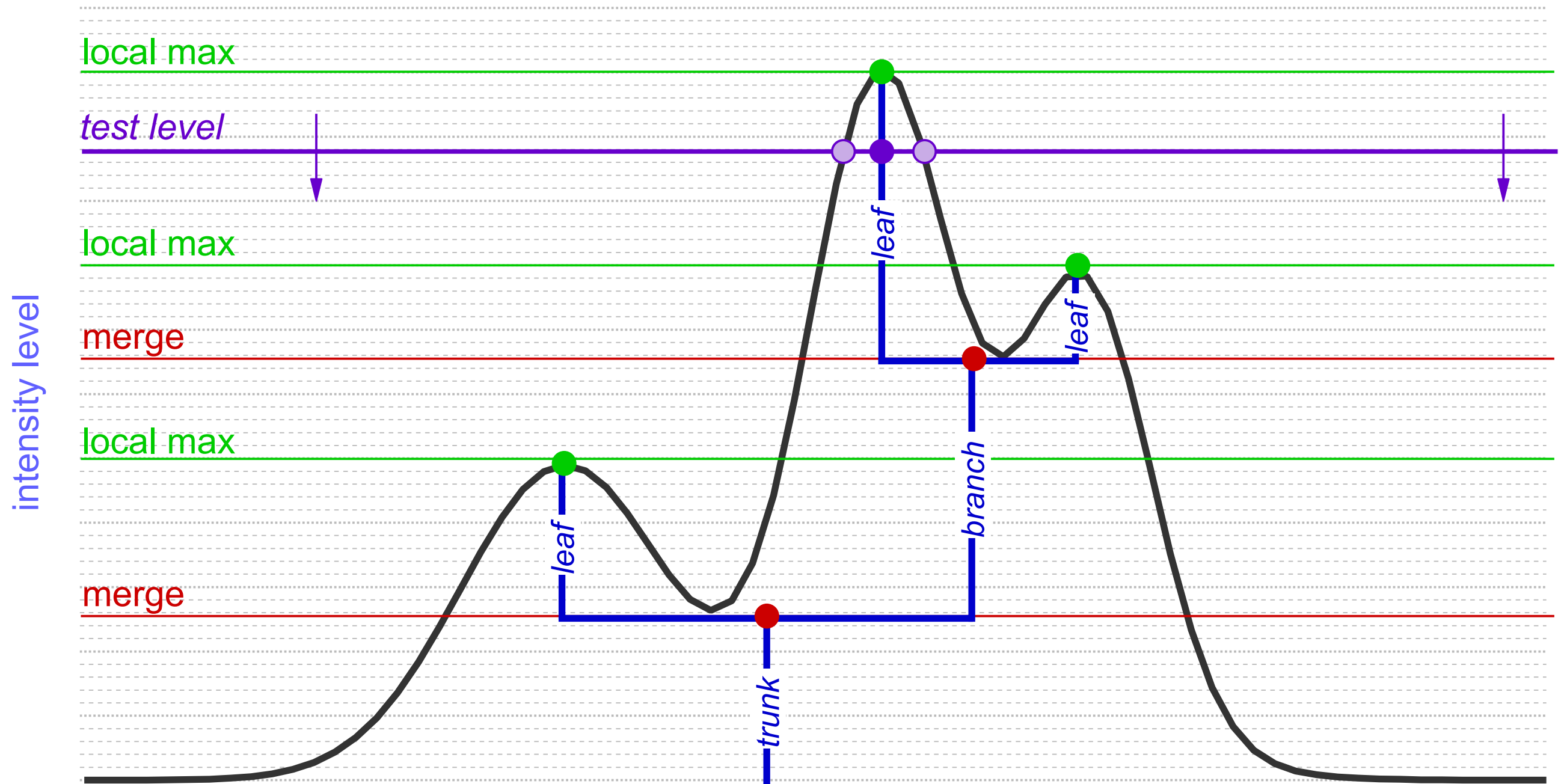
“taste-test”

caveats

“Segmentation”



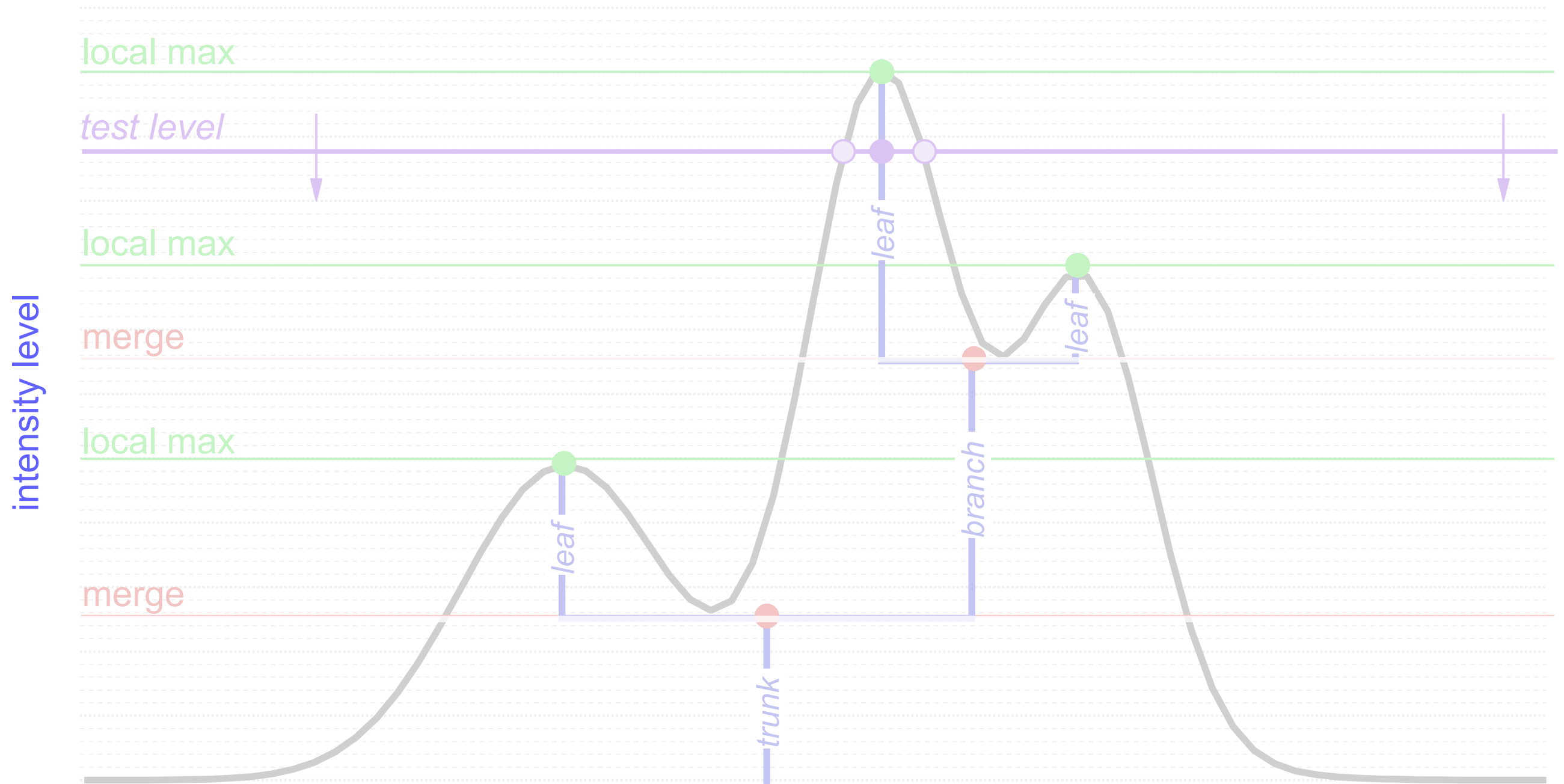
Dendrograms



Hierarchical "Segmentation"

Rosolowsky, Pineda, Kauffmann & Goodman 2008

Dendrograms



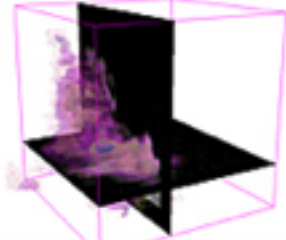
1-D: points; 2-D closed curves (contours); 3-D surfaces enclosing volumes

see 2D demo at <http://am.iic.harvard.edu/index.cgi/DendroStar/applet>

DendroStar/applet - IIC/AstroMed

http://am.iic.harvard.edu/index.cgi/DendroStar/applet

astronomical medicine




The Astronomical Medicine Project

Initiative In Innovative Computing at Harvard

The DendroStar Applet for L1448: Try me!

Harvard IIC Home

AM Project
 overview
 what's new?
 press
 about us
 contact us

Research
 background
 projects
 papers
 images
 movies

Software
 overview
 Slicer: getting started
 Slicer 3
 fits2itk
 OsiriX
 DendroStar

Links
 Center for Astrophysics
 COMPLETE Survey
 Surgical Planning Lab
 3D Slicer
 related projects

User
 Login

Search

Tint:

Suppress tint:

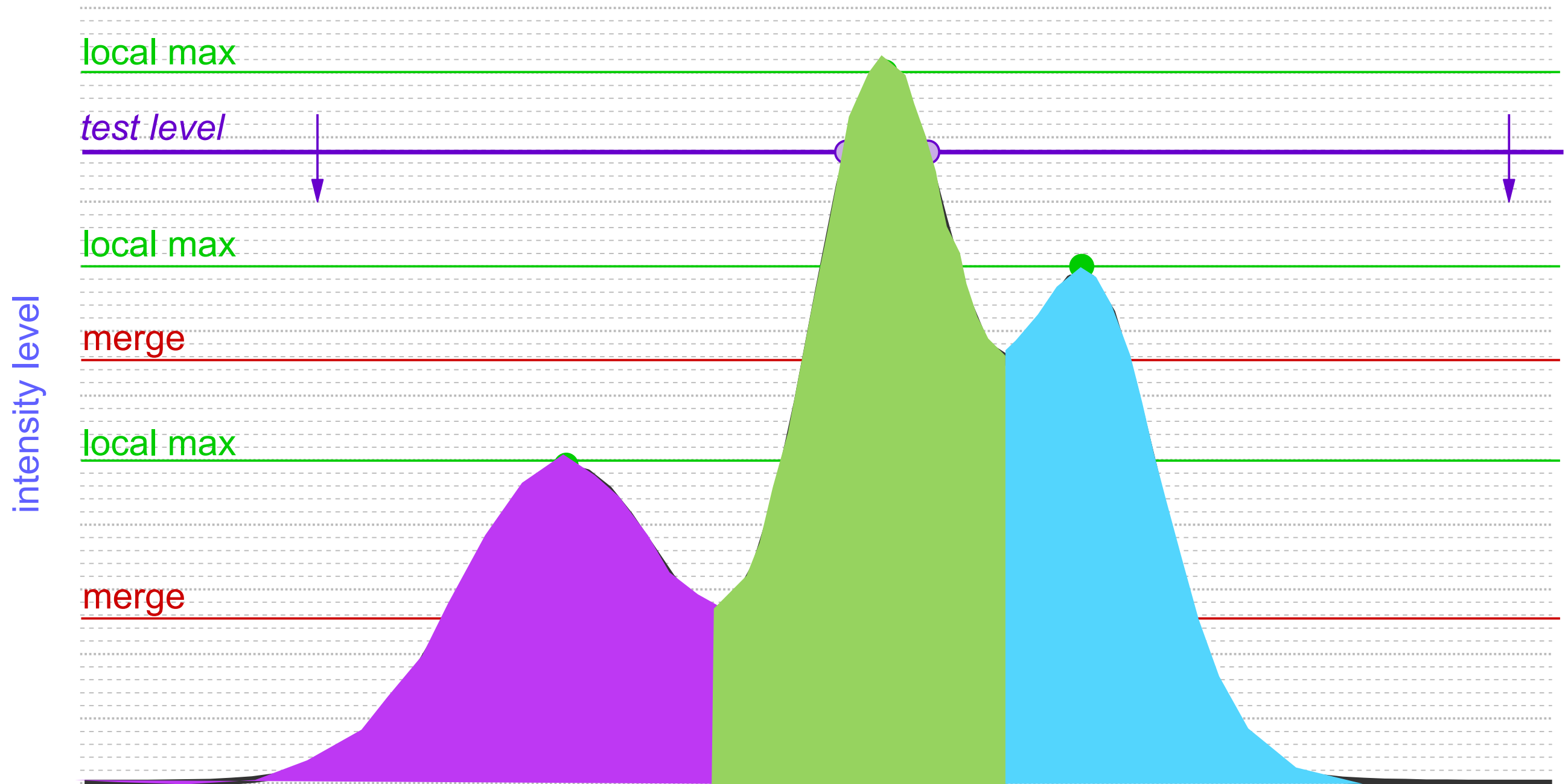
Reset:

Applet DendroStar started

<http://am.iic.harvard.edu/index.cgi/DendroStar/applet>
 Dendrogram Algorithm by Erik Rosolwosky; Applet by Douglas Alan

3D, see PDF...

What would *CLUMPFIND* do?



No hierarchy is allowed, all clumps go to the baseline.
(Williams, De Geus & Blitz 1994)



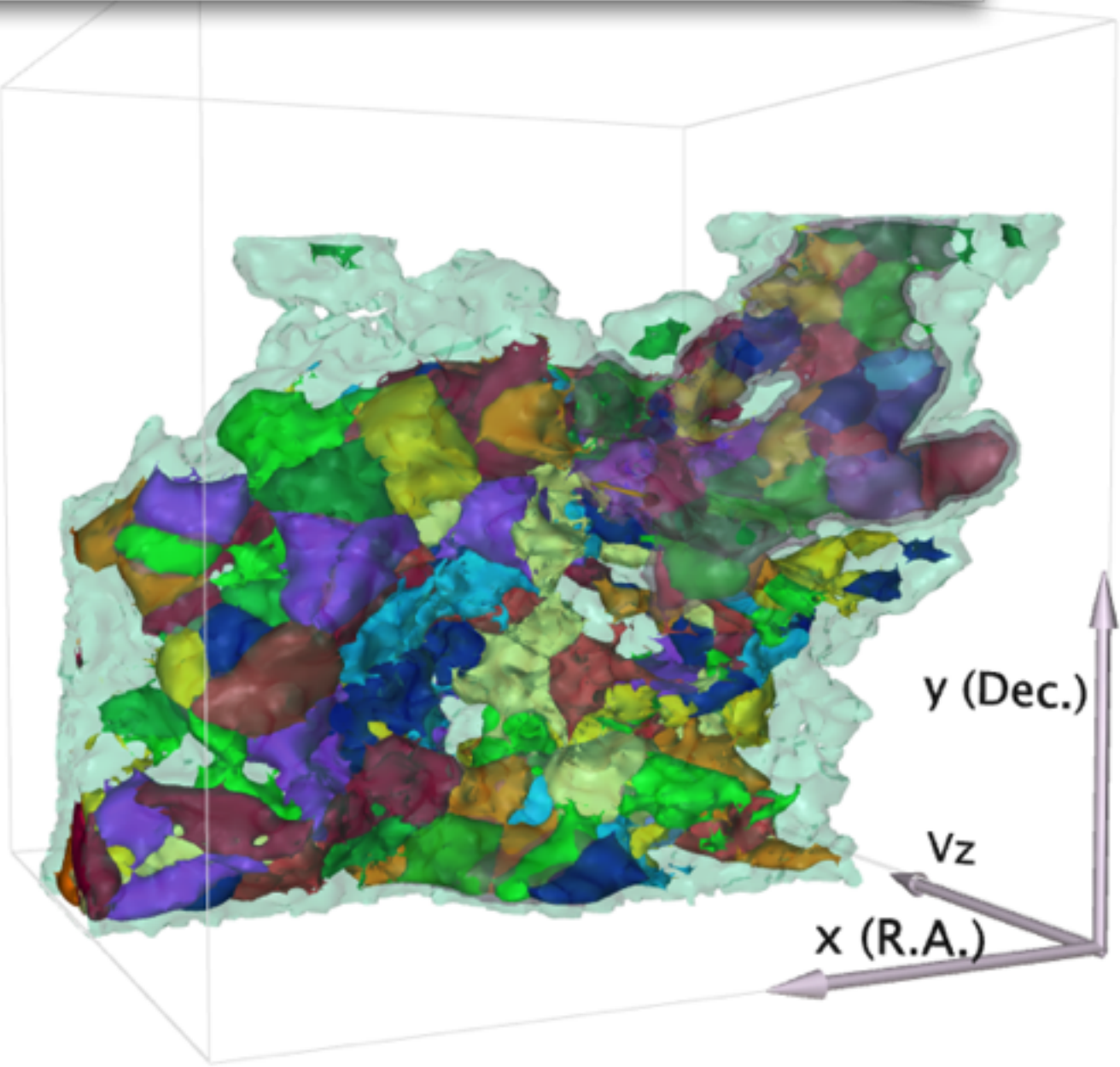
Model Tree

- Highlight Color
- model
 - Dendrogram decomposition
 - self-gravitating leaves
 - self-gravitating structures
 - all structure
 - CLUMPFIND decomposition
 - peaks within leaves
 - other clumps
 - billiard markers
 - axes

Options

- CLUMPFIND: peaks within leaves
- CLUMPFIND: R.A.-Dec.
- CLUMPFIND: R.A.-Vz
- CLUMPFIND: Vz-Dec.
- Combined: all structure
- Combined: self-grav. and peaks within le

Combined: all structure



This interactive 3D figure shows the result of the dendrogram hierarchical feature-identification algorithm applied to a data cube of ^{13}CO emission of the L1448 region of Perseus. Purple areas are the smallest scale self-gravitating structures in the region, pink shows the smallest regions that contain distinct self-gravitating sub-regions, and green depicts all regions with significant emission. Different views of the data cube can be selected from the Views menu. In addition, results of the alternative

<http://iic.harvard.edu/sites/all/files/interactive.pdf>

with many thanks to Mike Halle, Michelle Borkin, Jens Kauffmann & Douglas Alan

“Crowded” 3D data
(very dangerous)

“Sparse” 2D data
(OK)

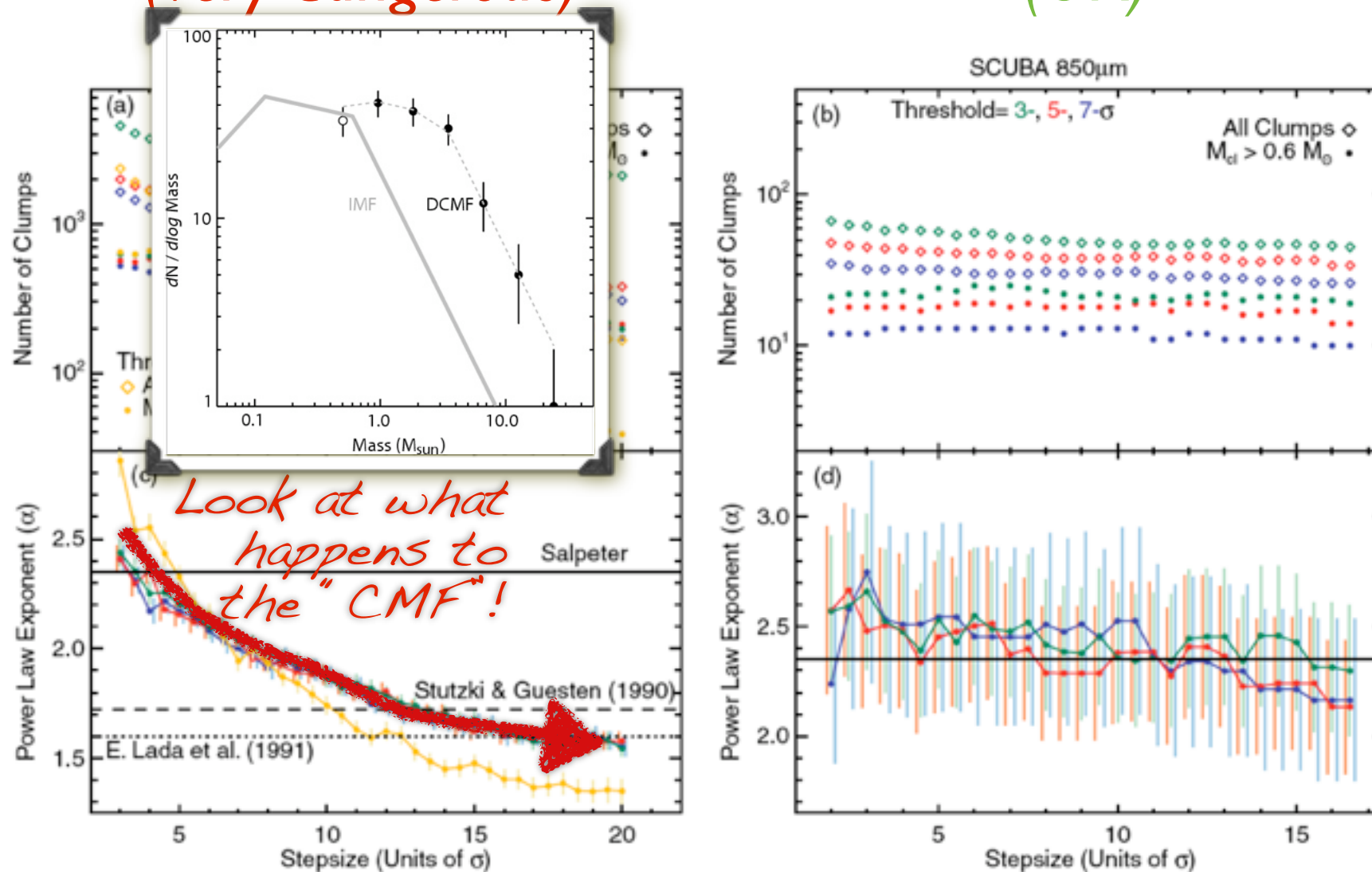


Figure 2. Summary of all Clumpfind runs as a function of stepsize. Color represent different thresholds: blue, red, and green for 3σ , 5σ , and 7σ , respectively; we also show in orange results with a threshold of 5σ for ^{13}CO data with added noise. Left and right columns show results for ^{13}CO and SCUBA data, respectively. Panels (a) and (b) show the number of clumps under a given category per model. Total number of clumps found, and total number of clumps with mass larger than the completeness limit are shown in open diamonds and filled circles, respectively. Panels (c) and (d) show the exponent of the fitted mass spectrum of clumps above the completeness limit, $dN/dM \propto M^{-\alpha}$, with error bars estimated from Equation (6). Horizontal black lines show some fiducial exponents for comparison. Average noise in ^{13}CO , ^{13}CO with added noise, and SCUBA data is 0.1 K , 0.2 K , and 0.06 Jy beam^{-1} , respectively. Completeness limit is estimated to be $4 M_{\odot}$, $3 M_{\odot}$, and $0.6 M_{\odot}$ for ^{13}CO , ^{13}CO with added noise, and SCUBA data. Panel (c) also shows that for different noise level in the data, if a threshold of $\sim 2\text{ K}$ (20σ and 10σ for original and noise-added data, respectively) is used, then the fitted power-law exponents are closer to previous works.

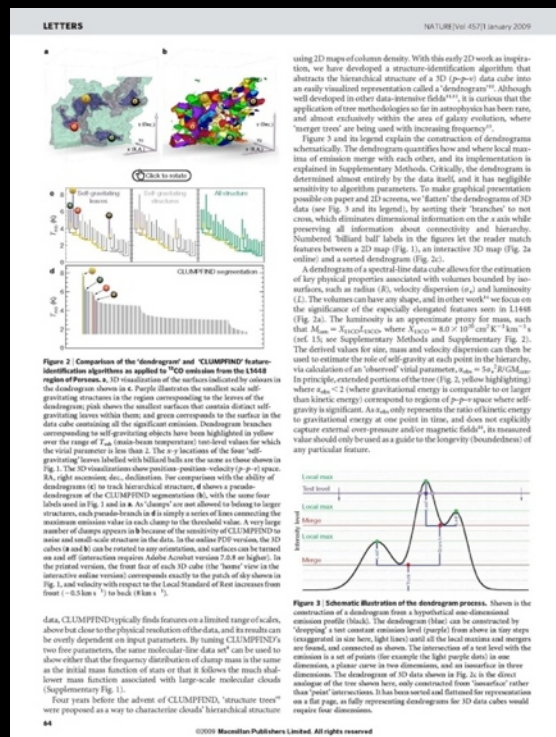
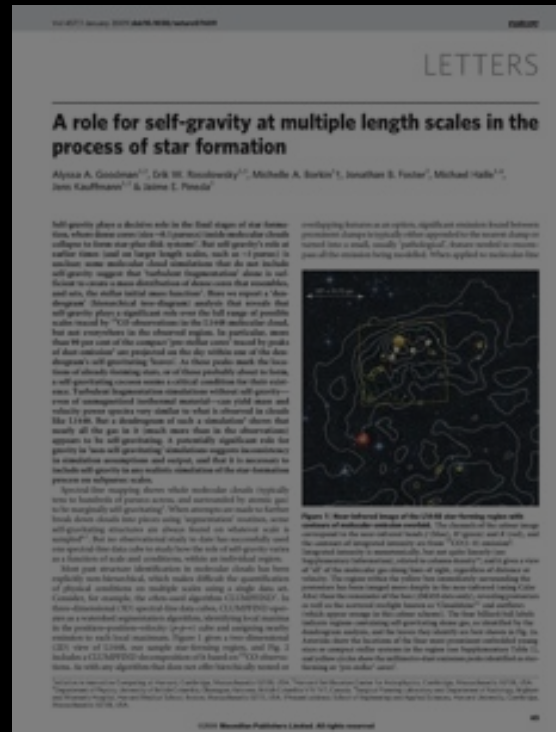
from “**The Perils of CLUMPFIND**” by Pineda, Rosolowsky & Goodman 2009

“turbulent fragmentation”

“(magneto-)hydrodynamic simulation”

“bi-jection”

“virial parameter”



✓ “segmentation”

✓ “CLUMPFIND”

✓ “Dendrogram”

“turbulent power spectrum”

“synthetic observation”

“depletion, opacity”

“taste-test”

caveats

“turbulent fragmentation”

“(magneto-)hydrodynamic simulation”

“bi-jection”

“virial parameter”

“turbulent power spectrum”

“synthetic observation”

“depletion, opacity”

“taste-test”

caveats

LETTERS

A role for self-gravity at multiple length scales in the process of star formation

Alyssa A. Goodman^{1,2}, Erik R. Rosenow^{1,2}, Michelle A. Barkin¹, Jonathan S. Foster¹, Michael Hebb^{1,2}, Jim Kaufman^{1,2} & James E. Pringle¹

Self-gravity plays a decisive role in the final stages of star formation, where dense cores (or self-gravitating molecular clouds) collapse to form star-planet disk systems. But self-gravity's role at earlier stages (and on larger length scales, such as 10³ parsecs) in turbulent molecular cloud simulations that do not include self-gravity suggests that turbulent fragmentation alone is insufficient to create a mass distribution of dense cores that resembles, and also, the stellar initial mass function. Here we report a “dendrogram” hierarchical tree-diagram analysis that reveals that self-gravity plays a significant role over the full range of possible scales (and in the observed region, the particular case that we use) in the formation of dense cores. In particular, more than 90 per cent of the compact “pre-stellar cores” found by peaks of their column density are produced on the day within one of the dendrogram’s self-gravitating “nodes”. As these peaks reach the final stage of already-forming stars, or of those gravitationally bound, a self-gravitating core reaches a critical condition: the dense core mass. Turbulent fragmentation conditions without self-gravity or unorganized turbulent material can yield more and thereby more objects very similar to what is observed in clouds like L1448. But a development of such a simulation shows that nearly all the gas in its clumps moves into the observations region by self-gravitating, a previously significant role that gravity plays in self-gravitating, simulation suggests inconsistency with simulation assumptions and suggest that it is necessary to include self-gravity in any realistic simulation of the star formation process on galactic scales.

Several key findings from this molecular cloud collapse study are: hierarchical fragmentation, and associated by-products, such as the magnitude of fragmentation, where fragmentation is defined as the ratio of the mass of a fragment to the mass of the parent cloud. Self-gravitating structures are shown to form at whatever scale is required. The low-dimensional study in this case is a study of the evolution of a turbulent medium, not a study of the evolution of a self-gravitating medium. The study shows that self-gravity is essential to the formation of dense cores, and that it is necessary to include self-gravity in any realistic simulation of the star formation process on galactic scales.

Figure 1: Mean infrared image of the L1448 star-forming region with dendrogram overlaid. The dendrogram is a hierarchical tree diagram that shows the fragmentation of the cloud into smaller and smaller structures. The root of the tree is the entire cloud, and the branches represent the fragmentation process. The leaves of the tree are the individual fragments. The dendrogram is overlaid on a mean infrared image of the L1448 star-forming region, showing the spatial distribution of the cloud and the locations of the fragments.

LETTERS

The formation of self-gravitating structures in a turbulent medium

Figure 2: A plot showing the relationship between the virial parameter and the turbulent power spectrum. The x-axis is labeled "Virial parameter" and the y-axis is labeled "Turbulent power spectrum". The plot shows a series of data points connected by lines, illustrating how the virial parameter varies with the turbulent power spectrum. The data points are scattered, showing a general trend of increasing virial parameter with increasing turbulent power spectrum.

LETTERS

Using 2D maps of column density to study star formation

Figure 3: Comparison of the dendrogram and CLUMPFIND algorithms as applied to CO emission from the L1448 region. The figure shows two panels: (a) the dendrogram and (b) the CLUMPFIND results. Panel (a) shows a hierarchical tree diagram representing the fragmentation of the cloud. Panel (b) shows the results of the CLUMPFIND algorithm, which identifies individual clumps and their properties. The dendrogram and CLUMPFIND results are compared to show their agreement in identifying clumps and their hierarchical structure.

LETTERS

Schematic illustration of the dendrogram process

Figure 4: Schematic illustration of the dendrogram process. The figure shows a hierarchical tree diagram representing the fragmentation of a cloud. The root of the tree is the entire cloud, and the branches represent the fragmentation process. The leaves of the tree are the individual fragments. The dendrogram is overlaid on a mean infrared image of the L1448 star-forming region, showing the spatial distribution of the cloud and the locations of the fragments.

(MHD) Simulations, Turbulent Fragmentation

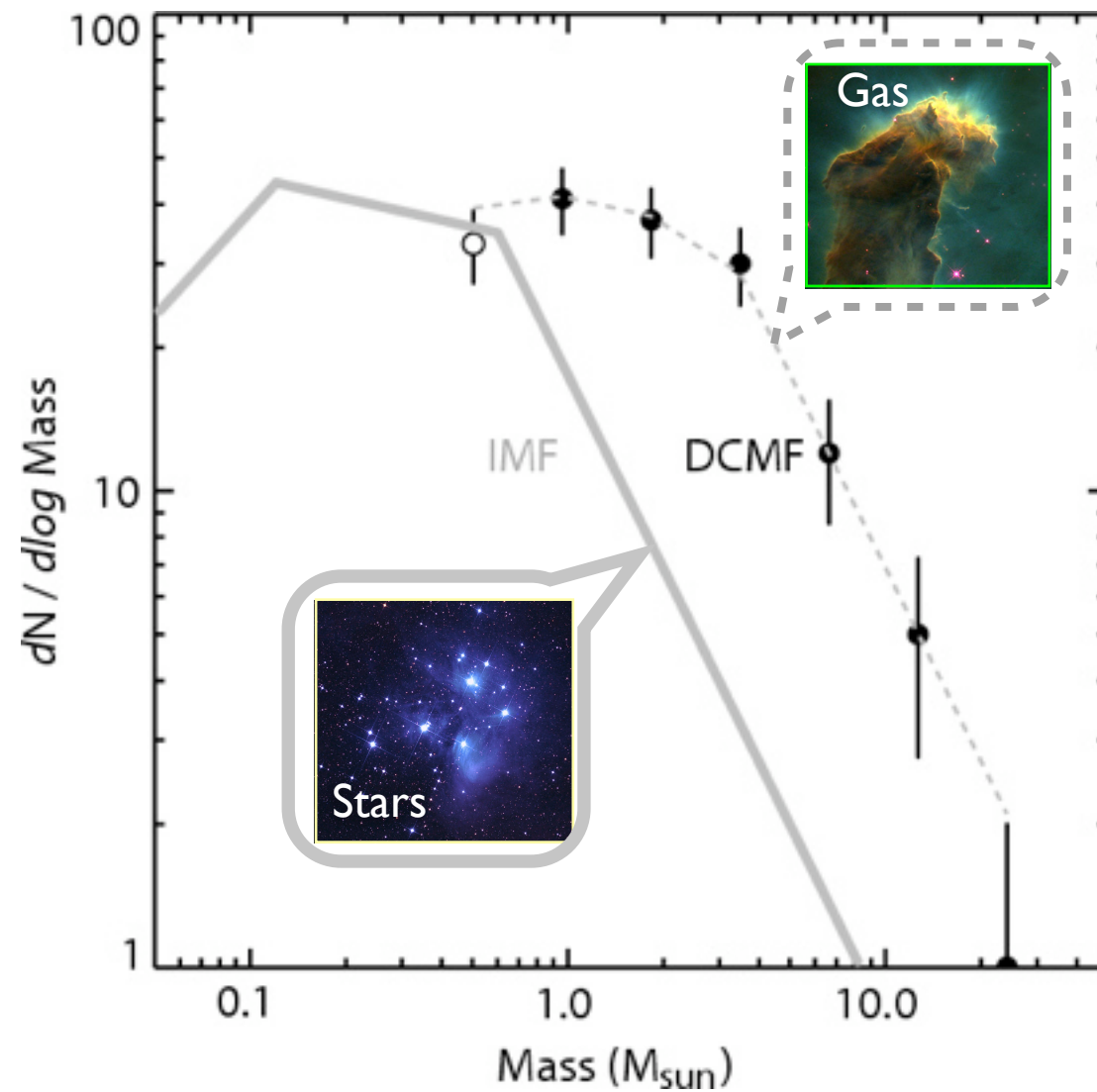
Dimensions: 40000. AU With Radiative Feedback Time: 0. yr



-1.0 -0.5 0.0 0.5 1.0 1.5 2.0
Log Column Density [g/cm^2]

Matthew Bate

cf. Padoan & Nordlund 2002



Alves, Lombardi & Lada 2007

LETTERS

A role for self-gravity at multiple length scales in the process of star formation

Allyssa A. Goodman^{1,2}, Erik W. Rosolowsky^{1,2}, Michelle A. Barkin¹, Jonathan S. Foster¹, Michael Hebb^{1,2}, Jim Kaufman^{1,2} & James I. Probst¹

Self-gravity plays a decisive role in the final stages of star formation, where dense cores (or self-gravitating molecular clouds) collapse to form star-planet disk systems. But self-gravity's role at earlier stages and on larger length scales, such as the formation of molecular cloud filaments that do not include self-gravity, remains unclear. We use a hierarchical approach to self-gravity to assess a range of distances, from the molecular cloud core to the entire galactic disk. We use a hierarchical approach to self-gravity to assess a range of distances, from the molecular cloud core to the entire galactic disk. We use a hierarchical approach to self-gravity to assess a range of distances, from the molecular cloud core to the entire galactic disk.



Figure 1. Three infrared images of the L1448 star-forming region with dendrogram overlays. The images show the spatial distribution of dust emission, and the dendrogram highlights hierarchical structures within the region.

LETTERS

“bi-jection”

“virial parameter”

The relationship between α_{vir} and β_{vir} is a “bi-jection” between a volume in parameter space and a volume of physical parameter space.



Figure 4. The relationship between virial parameter and another parameter. The plot shows a clear correlation between the two variables, illustrating the 'bi-jection' concept.

LETTERS

“turbulent power spectrum”

“synthetic observation”

Using 2D maps of column density, we have developed a structure-identification algorithm that extracts the hierarchical structure of a 2D (p-p) data cube into an easily visualized representation called a ‘dendrogram’.

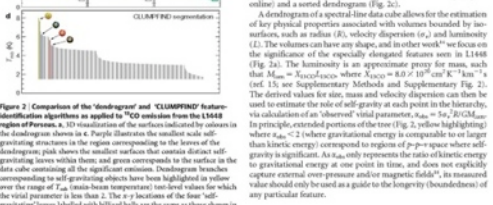


Figure 2. Comparison of the 'dendrogram' and 'CLUMPFIND' feature-identification algorithms. The figure shows two different ways of representing the same data, highlighting the differences in their hierarchical structures.

LETTERS

“depletion, opacity”

“taste-test”

combining the regions are associated with a self-gravitating lead in the star-forming region. We note that these associations suggest that self-gravitating leads are critical to the surface physics of star formation.

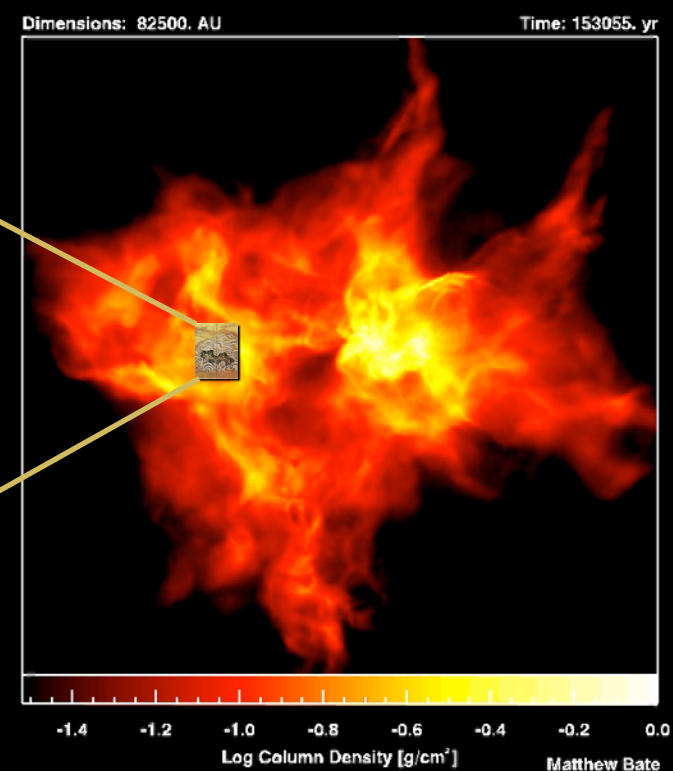
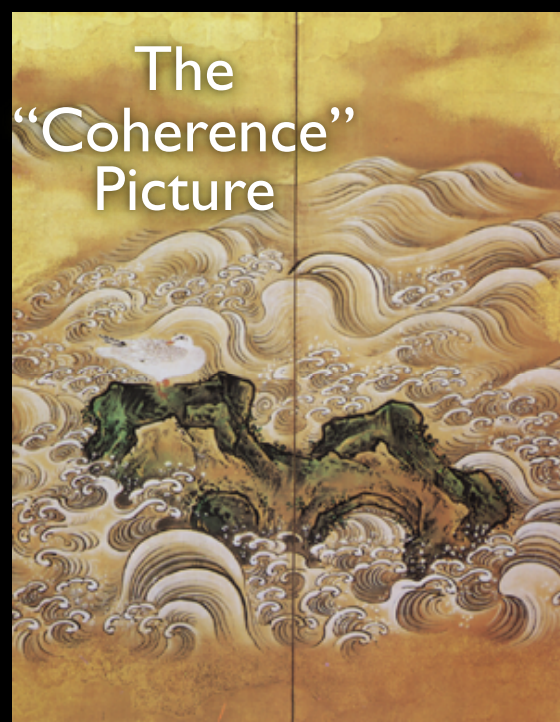
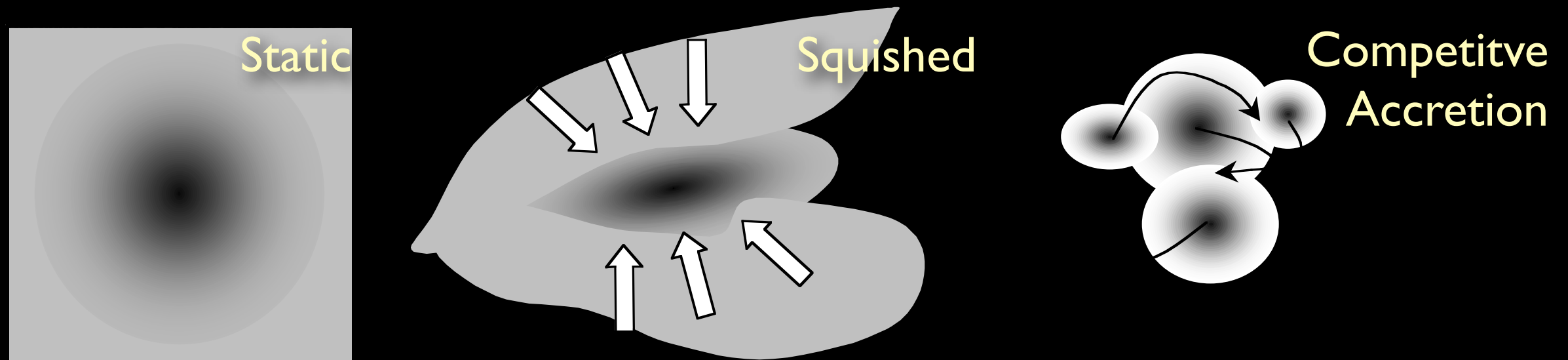


Figure 3. Schematic illustration of the dendrogram process. The diagram shows how a 1D data set is processed through various steps (Local max, Merge, etc.) to create a hierarchical tree structure.

“bi-jection”
“virial parameter”
“turbulent power spectrum”
“synthetic observation”
“depletion, opacity”
“taste-test”
caveats

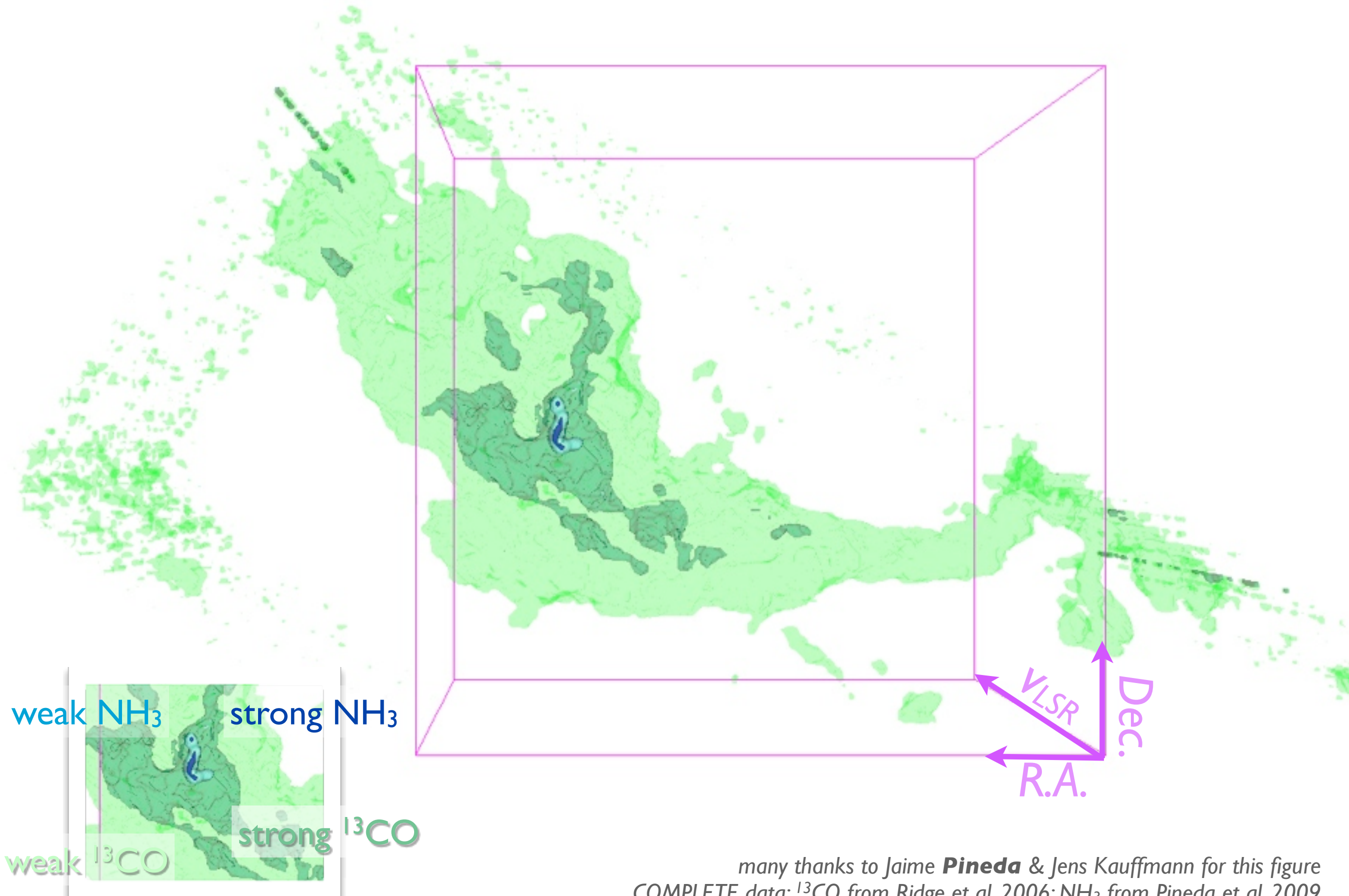
How calm, and how long-lasting are cores? (relevant motions/forces & the “virial parameter”)

Three main views at present...



The “*bijection*” problem...
this is $p-p-p$,
but we have
only $p-p-v$...

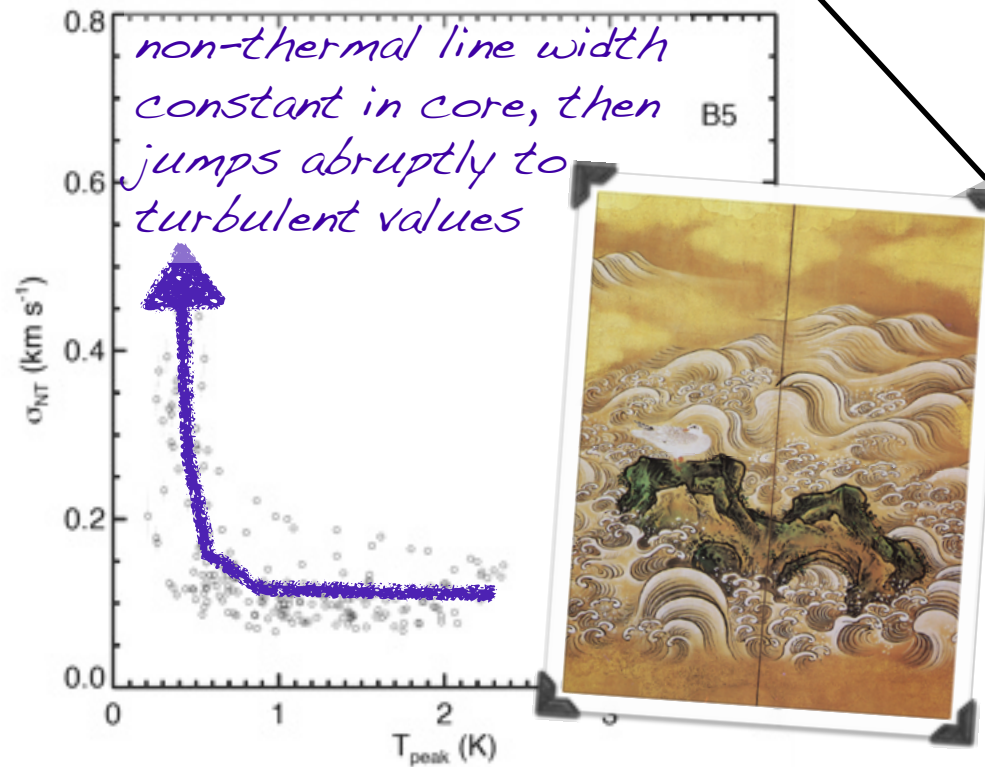
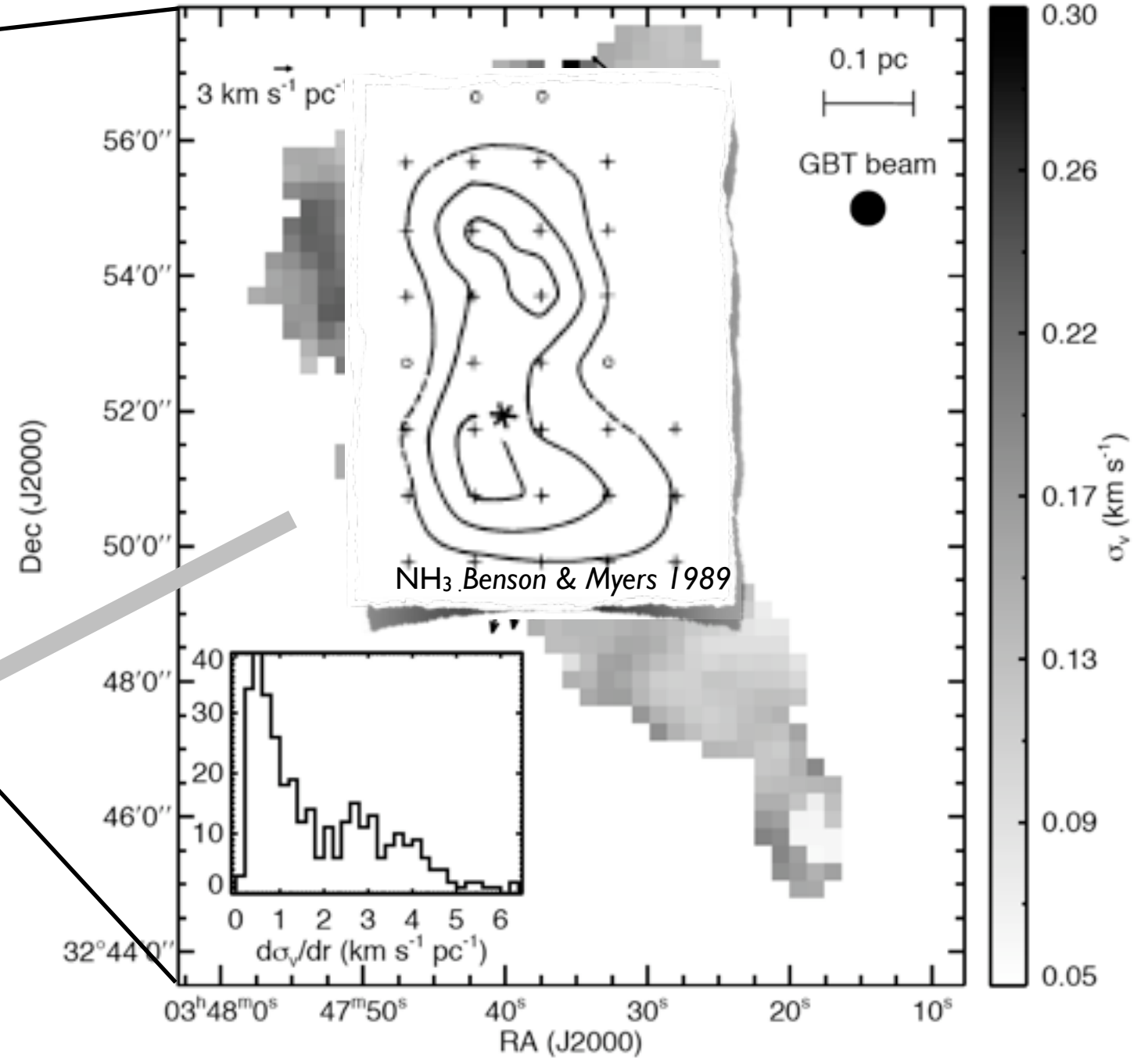
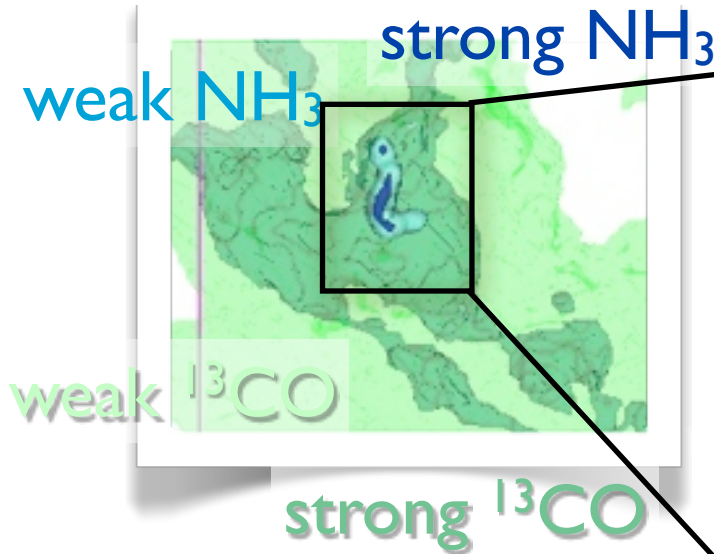
p - p - v structure of the B5 region in Perseus



many thanks to Jaime **Pineda** & Jens Kauffmann for this figure
COMPLETE data: ^{13}CO from Ridge et al. 2006; NH_3 from Pineda et al. 2009

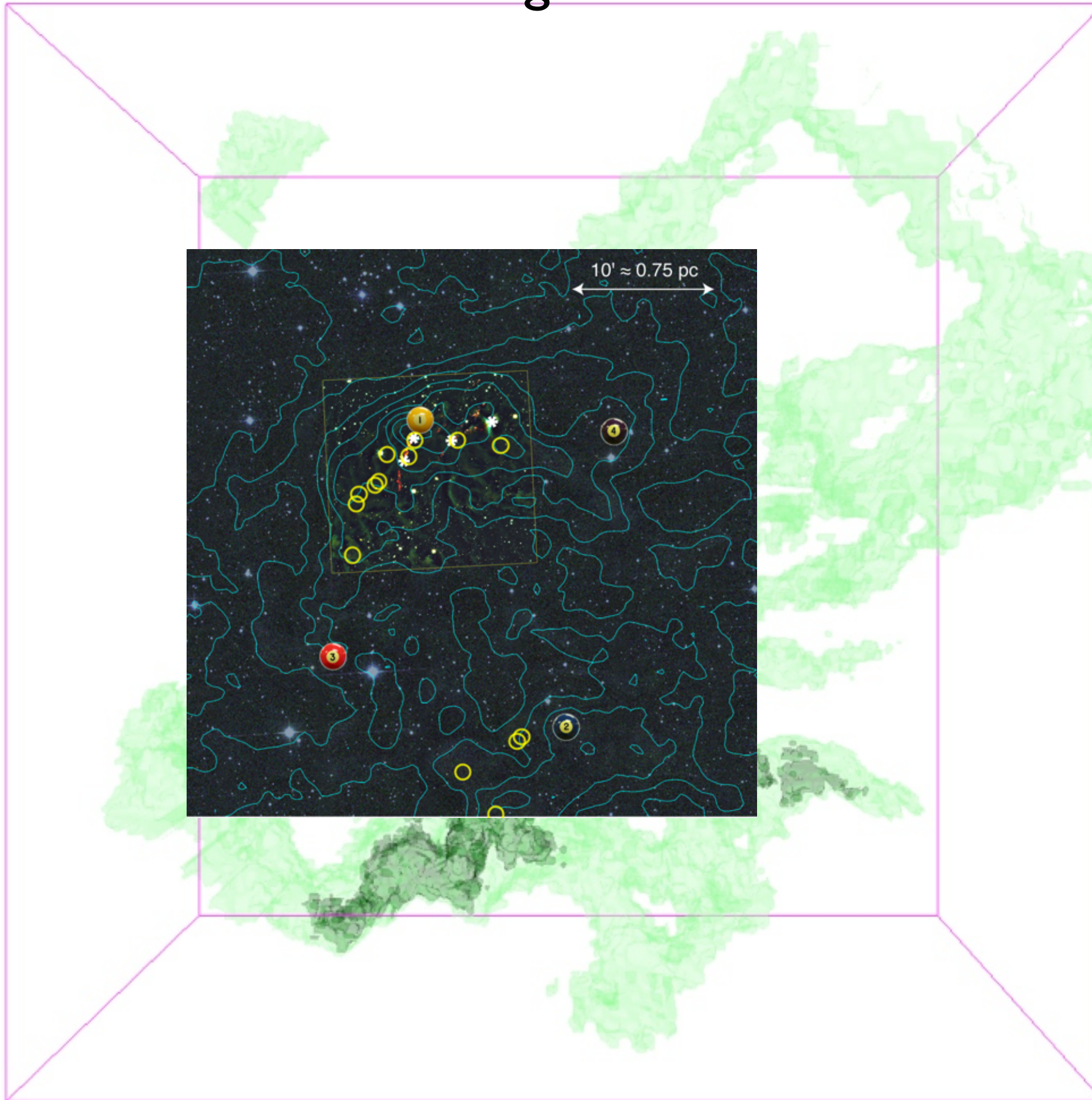
STRONG Evidence for Coherence in Dense Cores

greyscale shows NH_3 velocity dispersion, arrows show gradient in dispersion

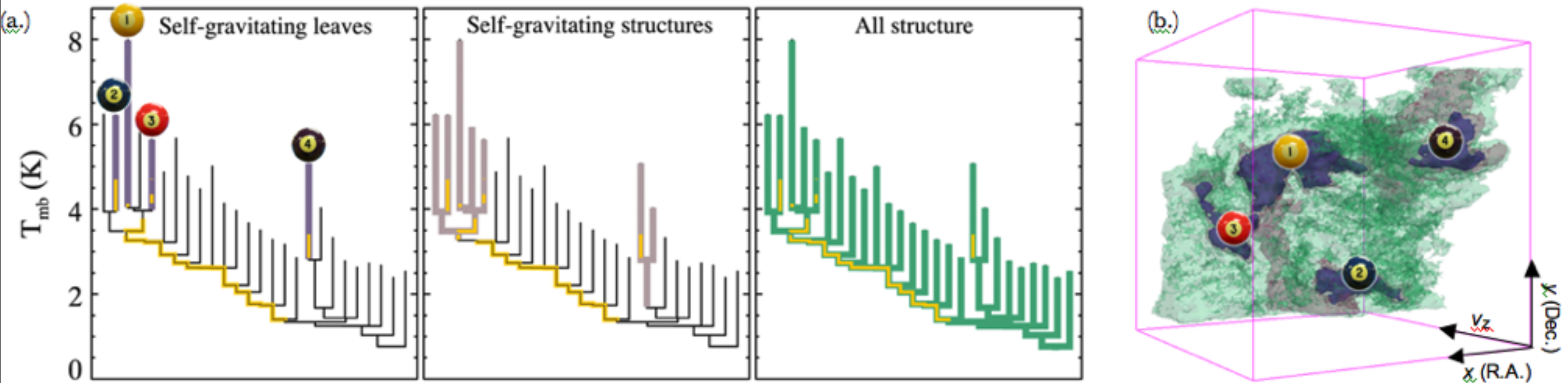


Brand-new GBT NH_3 observations of the B5 core,
work of Jaime Pineda

Returning to *L1448*..



Dendrograms & “Self-Gravity”



Yellow highlighting= “self-gravitating”

“Self-gravitating” here just means $\alpha_{vir} (=5\sigma_v^2 R/GM_{lum}) < 2$
(à la Bertoldi & McKee 1992)

*Rosolowsky et al. 2008 (ApJ) &
Goodman et al. 2009 (Nature)*

see PDF...

A role for self-gravity at multiple length scales in the process of star formation

Alyssa A. Goodman^{1,2}, Erik W. Rosolowsky^{1,2}, Michelle A. Barkin¹, Jonathan S. Foster¹, Michael Heide^{1,2}, Jim Kaufman^{1,2}, & James E. Probst¹

Self-gravity plays a decisive role in the final stages of star formation, where dense cores (or self-gravitating molecular clouds) collapse to form star-planet disk systems. But self-gravity acts on smaller scales than ionization length scales, such as 1 pc, to ionize star-forming molecular clouds. We investigate whether self-gravity plays a role in the ionization of star-forming regions. We use a 3D visualization of the ionization state of a star-forming region to show that self-gravity plays a role in the ionization of star-forming regions. We use a 3D visualization of the ionization state of a star-forming region to show that self-gravity plays a role in the ionization of star-forming regions. We use a 3D visualization of the ionization state of a star-forming region to show that self-gravity plays a role in the ionization of star-forming regions.



Figure 1. A 3D visualization of the ionization state of a star-forming region. The plot shows a complex, multi-colored structure representing the ionization state. The colors range from blue (low ionization) to red (high ionization). The structure is highly irregular and shows a clear hierarchical structure.

LETTERS

LETTERS

LETTERS

LETTERS



Figure 4. The fraction of self-gravitating volume as a function of scale in the 100 pc region. The fraction of self-gravitating volume increases with scale, reaching a plateau of approximately 0.5 at scales greater than 1 pc.

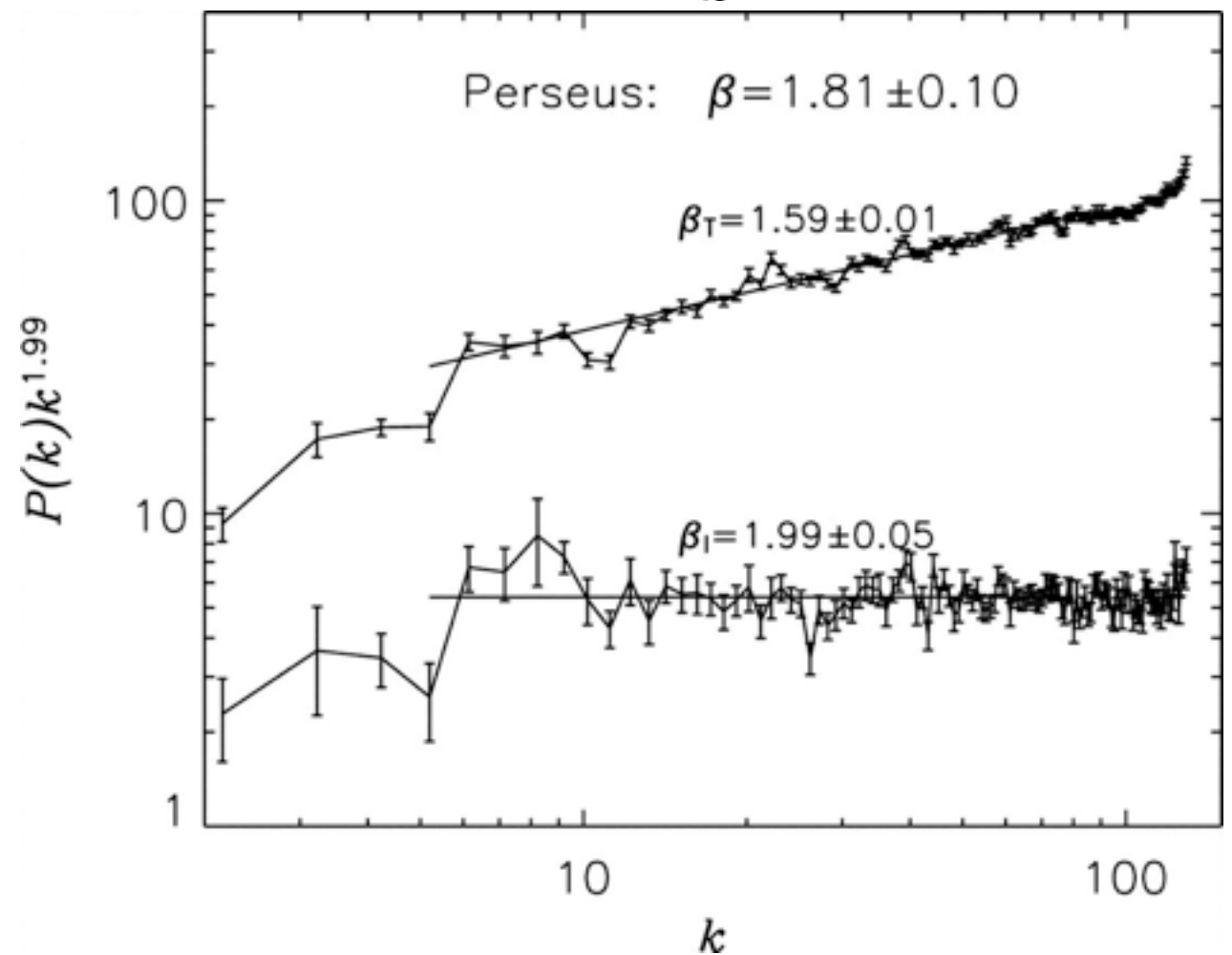
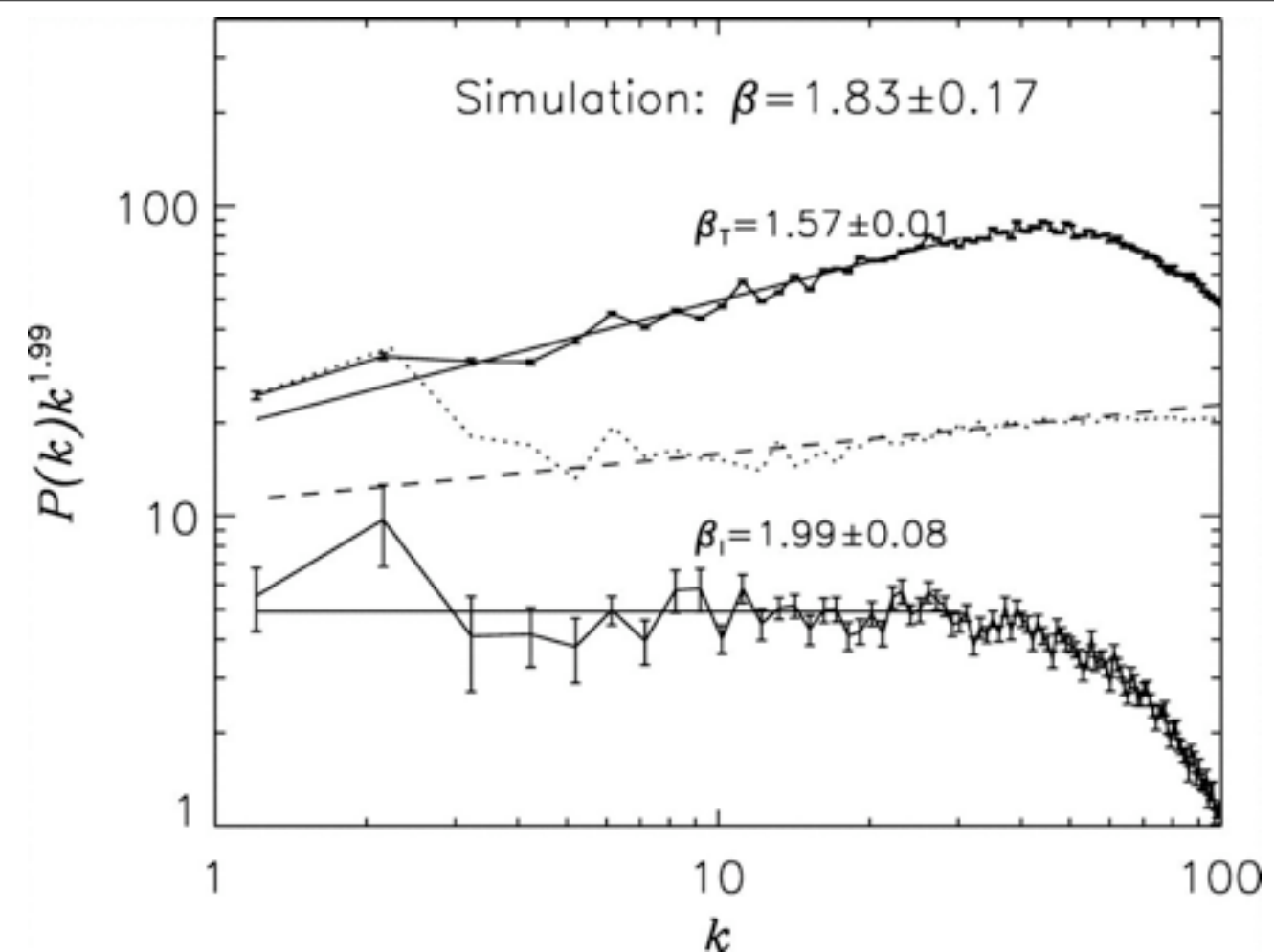
LETTERS

“turbulent power spectrum”
“synthetic observation”
“depletion, opacity”
“taste-test”
caveats

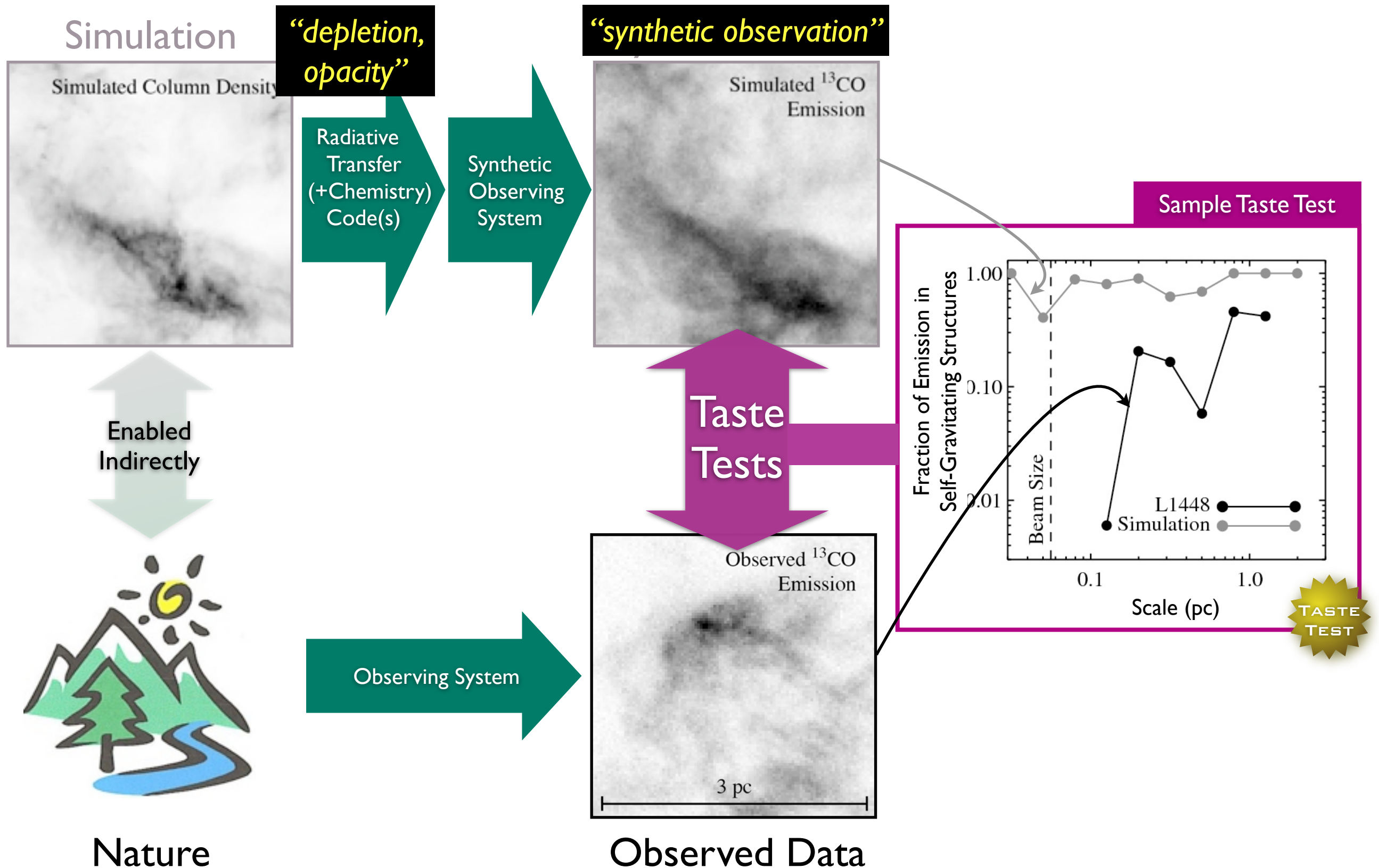
Choosing a relevant simulation to taste...

How about one with a
“*turbulent power spectrum*” shown
to match COMPLETE data?
from Padoan et al. 2006
(see Lazarian & Pogosyan 2000 for
methodology)

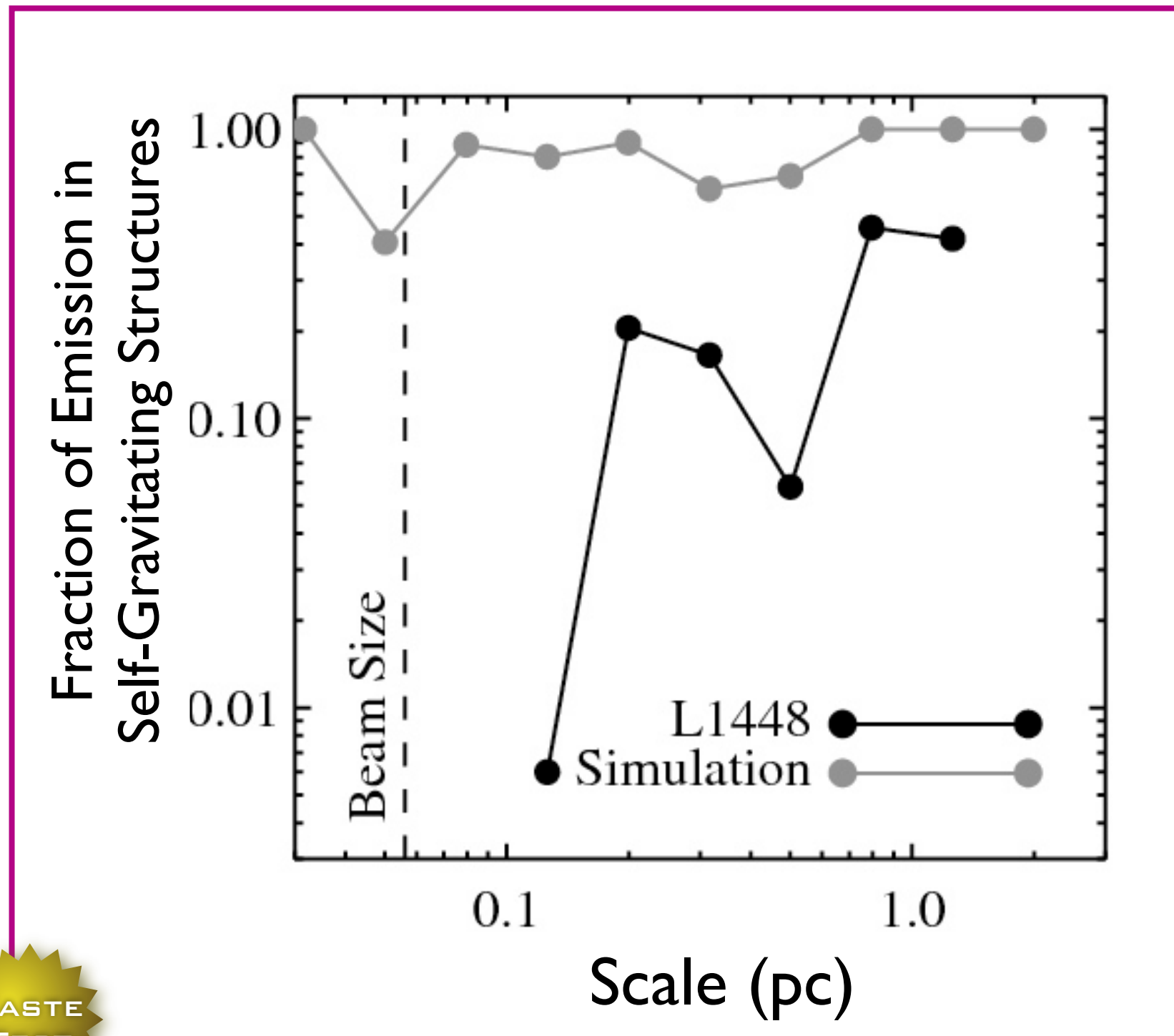
Note: This simulation does NOT include *gravity*,
magnetic fields, radiative effects, or explicit
heating & cooling—it is pure hydrodynamics.



The Taste-Testing Process

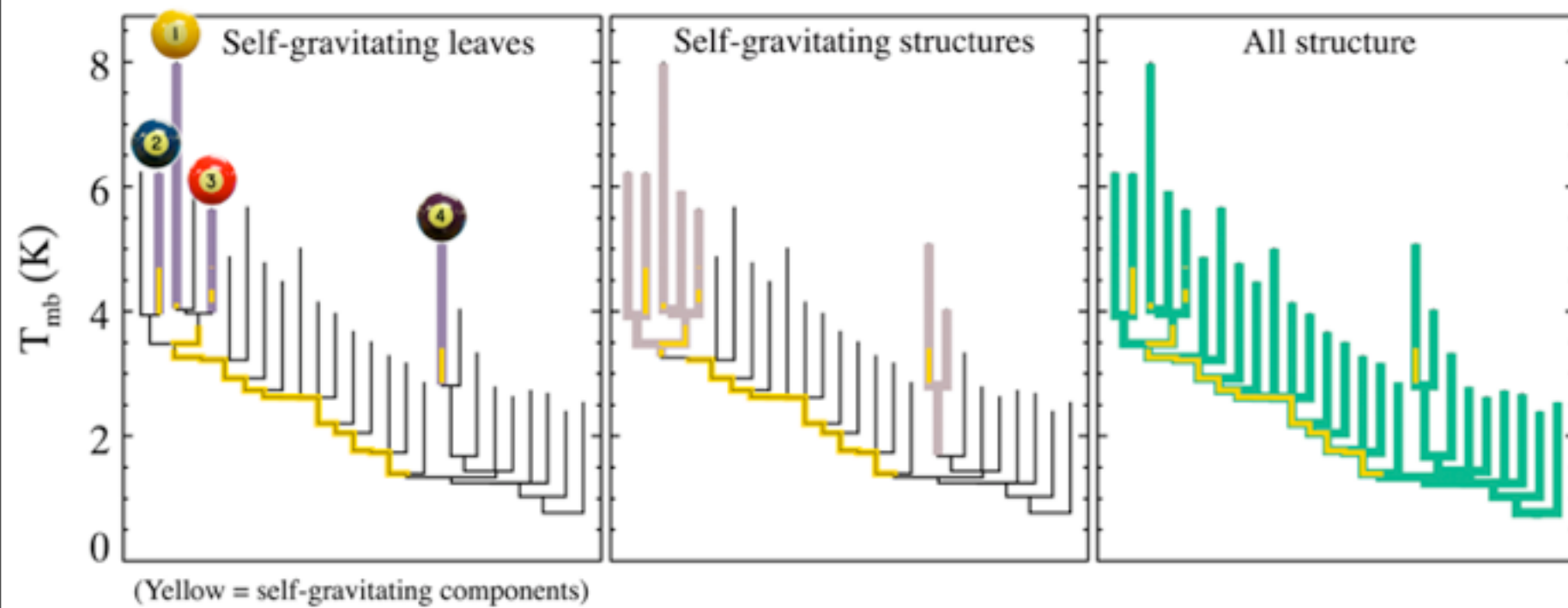


Taste-Testing Gravity

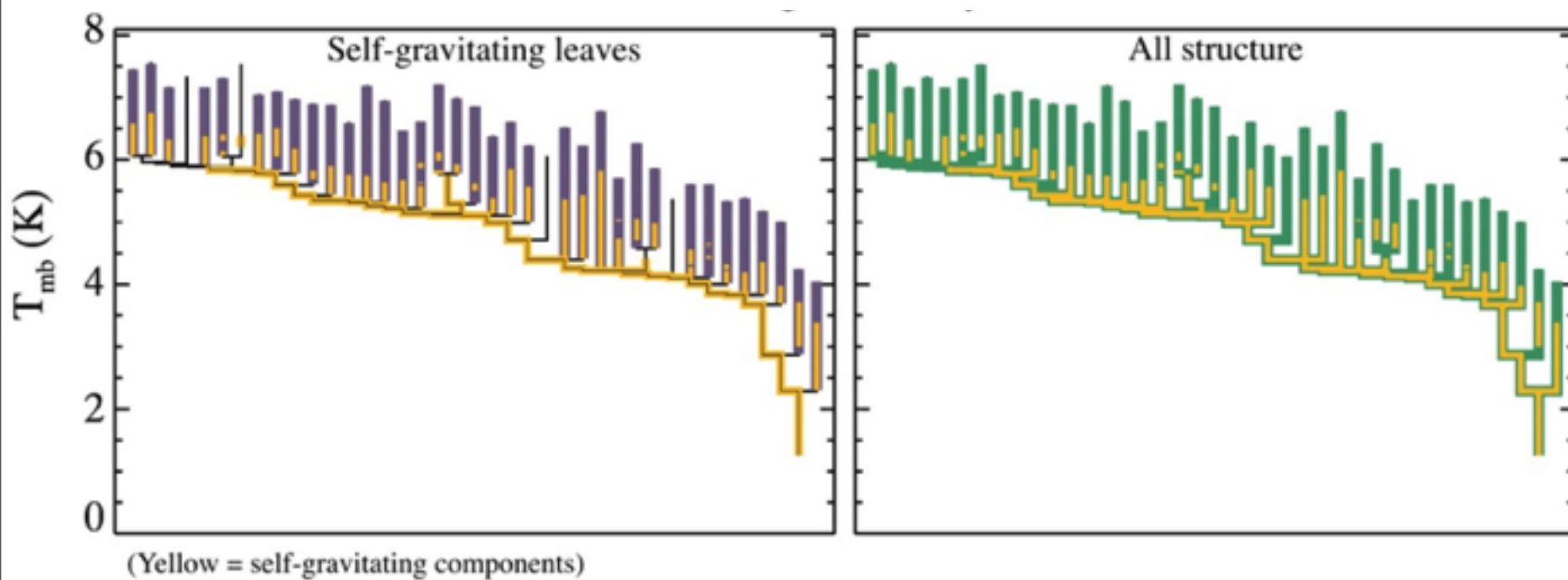


Gravity-free HD Simulations from Padoan et al. 2006;
L1448 analysis from Rosolowsky et al. 2008
both lines derived from ^{13}CO “observations”

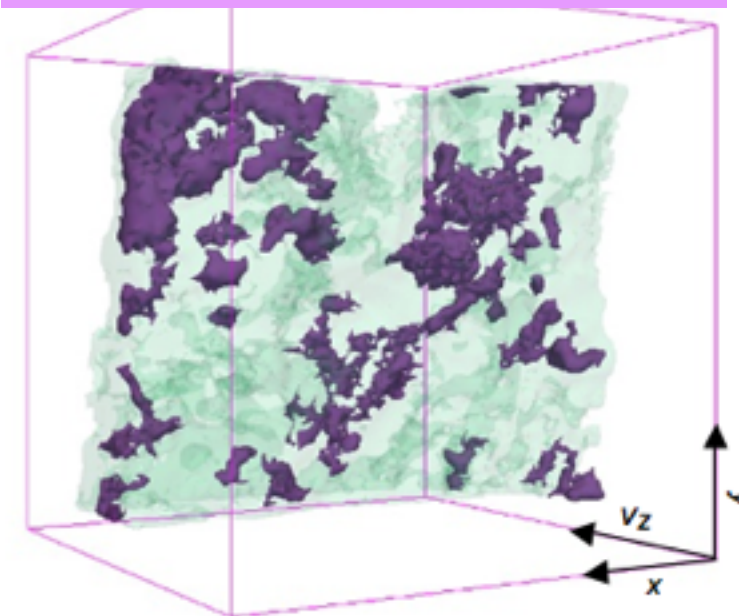
Real vs. Simulated ^{13}CO



Real



Simulated



LETTERS

A role for self-gravity at multiple length scales in the process of star formation

Allyssa A. Goodman^{1,2}, Erik W. Rosolowsky^{1,2}, Michelle A. Barkin¹, Jonathan S. Foster¹, Michael Hebb^{1,2}, Jim Kaufman^{1,2} & James E. Peavey¹

Self-gravity plays a decisive role in the final stages of star formation, where dense cores (or self-gravitating molecular clouds) collapse to form star-planet systems. But self-gravity acts at smaller scales than the larger length scales, such as 1 pc, in which most molecular cloud simulations that do not include self-gravity suggest that turbulent fragmentation alone is sufficient to create a mass distribution of dense cores that resembles, and only, the stellar initial mass function. Here we report a 'dendrogram' hierarchical tree-structure analysis that reveals that self-gravity plays a significant role over the full range of possible scales tested by ¹²CO observations in the L1448 molecular cloud, but not everywhere in the observed region. In particular, more than 90 per cent of the compact 'pre-stellar cores' traced by peaks of dust emission¹ are projected on the sky within one of the dendrogram's self-gravitating 'cores'. As these peaks mark the locations of already-forming stars, as well as protostars about to form, self-gravitating cores provide a critical condition for the formation of stars. Turbulent fragmentation contributes without self-gravity to the formation of protostellar cores, but self-gravity is essential for the formation of stars.



Figure 1. A 3D visualization of the L1448 star-forming region with a dendrogram overlaid. The dendrogram shows the hierarchical structure of the cloud, with branches representing self-gravitating cores. The cores are color-coded by mass and age, with red representing the most massive and youngest structures, and blue representing less massive and older structures. The dendrogram highlights the self-gravitating cores and their hierarchical relationships within the cloud.

LETTERS

The formation of self-gravitating cores in a turbulent field in the L1448 star-forming region

Allyssa A. Goodman^{1,2}, Erik W. Rosolowsky^{1,2}, Michelle A. Barkin¹, Jonathan S. Foster¹, Michael Hebb^{1,2}, Jim Kaufman^{1,2} & James E. Peavey¹

The formation of self-gravitating cores in a turbulent field in the L1448 star-forming region is investigated using a dendrogram analysis. The dendrogram reveals the hierarchical structure of the cloud, with branches representing self-gravitating cores. The cores are color-coded by mass and age, with red representing the most massive and youngest structures, and blue representing less massive and older structures. The dendrogram highlights the self-gravitating cores and their hierarchical relationships within the cloud. The analysis shows that self-gravity plays a significant role over the full range of possible scales tested by ¹²CO observations in the L1448 molecular cloud, but not everywhere in the observed region. In particular, more than 90 per cent of the compact 'pre-stellar cores' traced by peaks of dust emission¹ are projected on the sky within one of the dendrogram's self-gravitating 'cores'. As these peaks mark the locations of already-forming stars, as well as protostars about to form, self-gravitating cores provide a critical condition for the formation of stars. Turbulent fragmentation contributes without self-gravity to the formation of protostellar cores, but self-gravity is essential for the formation of stars.

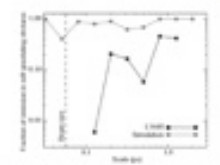


Figure 2. Comparison of the 'dendrogram' and 'CLUMPFIND' feature-identification algorithms. The dendrogram shows a hierarchical tree structure, while CLUMPFIND shows a set of rectangular boxes representing identified features. The dendrogram shows a more complex and detailed structure than CLUMPFIND, which tends to identify larger, more contiguous regions.

LETTERS

Using 2D maps of column density to identify self-gravitating cores in the L1448 star-forming region

Allyssa A. Goodman^{1,2}, Erik W. Rosolowsky^{1,2}, Michelle A. Barkin¹, Jonathan S. Foster¹, Michael Hebb^{1,2}, Jim Kaufman^{1,2} & James E. Peavey¹

Using 2D maps of column density to identify self-gravitating cores in the L1448 star-forming region. The dendrogram analysis shows that self-gravity plays a significant role over the full range of possible scales tested by ¹²CO observations in the L1448 molecular cloud, but not everywhere in the observed region. In particular, more than 90 per cent of the compact 'pre-stellar cores' traced by peaks of dust emission¹ are projected on the sky within one of the dendrogram's self-gravitating 'cores'. As these peaks mark the locations of already-forming stars, as well as protostars about to form, self-gravitating cores provide a critical condition for the formation of stars. Turbulent fragmentation contributes without self-gravity to the formation of protostellar cores, but self-gravity is essential for the formation of stars.

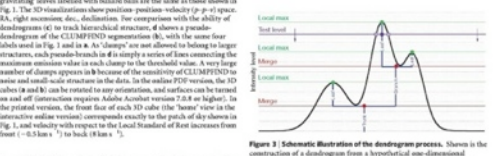


Figure 3. Schematic illustration of the dendrogram process. The dendrogram shows the hierarchical structure of the cloud, with branches representing self-gravitating cores. The cores are color-coded by mass and age, with red representing the most massive and youngest structures, and blue representing less massive and older structures. The dendrogram highlights the self-gravitating cores and their hierarchical relationships within the cloud.

LETTERS

Comparison of the 'dendrogram' and 'CLUMPFIND' feature-identification algorithms as applied to ¹²CO emission from the L1448 star-forming region

Allyssa A. Goodman^{1,2}, Erik W. Rosolowsky^{1,2}, Michelle A. Barkin¹, Jonathan S. Foster¹, Michael Hebb^{1,2}, Jim Kaufman^{1,2} & James E. Peavey¹

Comparison of the 'dendrogram' and 'CLUMPFIND' feature-identification algorithms as applied to ¹²CO emission from the L1448 star-forming region. The dendrogram analysis shows that self-gravity plays a significant role over the full range of possible scales tested by ¹²CO observations in the L1448 molecular cloud, but not everywhere in the observed region. In particular, more than 90 per cent of the compact 'pre-stellar cores' traced by peaks of dust emission¹ are projected on the sky within one of the dendrogram's self-gravitating 'cores'. As these peaks mark the locations of already-forming stars, as well as protostars about to form, self-gravitating cores provide a critical condition for the formation of stars. Turbulent fragmentation contributes without self-gravity to the formation of protostellar cores, but self-gravity is essential for the formation of stars.



Figure 4. Schematic illustration of the dendrogram process. The dendrogram shows the hierarchical structure of the cloud, with branches representing self-gravitating cores. The cores are color-coded by mass and age, with red representing the most massive and youngest structures, and blue representing less massive and older structures. The dendrogram highlights the self-gravitating cores and their hierarchical relationships within the cloud.

“turbulent power spectrum”
✓
“synthetic observation”
✓
“depletion, opacity”
✓
“taste-test”
✓
caveats

LETTERS

A role for self-gravity at multiple length scales in the process of star formation

Alyssa A. Goodman¹, Erik W. Rosolowsky², Michelle A. Barkin¹, Jonathan S. Foster³, Michael Hebb⁴, Jim Kaufman⁵ & James E. Probst⁶

Self-gravity plays a decisive role in the final stages of star formation, where dense cores (or clumps) rapidly contract and collapse to form star-planet disk systems. But self-gravity's role at earlier times and on larger length scales, such as 10³ parsecs, is unclear. Some molecular cloud simulations that do not include self-gravity suggest that turbulent fragmentation alone is sufficient to create a mass distribution of dense cores, that eventually, and only, the stellar initial mass function. Here we report a 'desmogger' hierarchical tree-diagram analysis that reveals that self-gravity plays a significant role over the full range of possible mass scales. In the CLUMPFIND decomposition of the L1448 region, the presence of self-gravity is particularly clear in the 10³ pc scale, but not in the 10² pc scale. The 10³ pc scale is the largest scale at which self-gravity is significant. This suggests that self-gravity is important at multiple length scales, but not at the largest scales. The 10³ pc scale is the largest scale at which self-gravity is significant. This suggests that self-gravity is important at multiple length scales, but not at the largest scales.

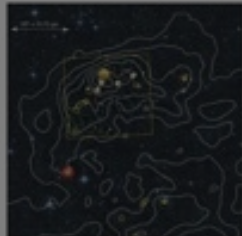


Figure 1. Hierarchical tree-diagram analysis of the L1448 star-forming region. The diagram shows the fragmentation of the gas into smaller-scale structures. The root node is at the top, and the branches lead to smaller-scale structures at the bottom. The nodes are labeled with mass and size, and the branches are color-coded to indicate different physical regimes.

LETTERS

A role for self-gravity at multiple length scales in the process of star formation

A role for self-gravity at multiple length scales in the process of star formation

Alyssa A. Goodman¹, Erik W. Rosolowsky², Michelle A. Barkin¹, Jonathan S. Foster³, Michael Hebb⁴, Jim Kaufman⁵ & James E. Probst⁶

Self-gravity plays a decisive role in the final stages of star formation, where dense cores (or clumps) rapidly contract and collapse to form star-planet disk systems. But self-gravity's role at earlier times and on larger length scales, such as 10³ parsecs, is unclear. Some molecular cloud simulations that do not include self-gravity suggest that turbulent fragmentation alone is sufficient to create a mass distribution of dense cores, that eventually, and only, the stellar initial mass function. Here we report a 'desmogger' hierarchical tree-diagram analysis that reveals that self-gravity plays a significant role over the full range of possible mass scales. In the CLUMPFIND decomposition of the L1448 region, the presence of self-gravity is particularly clear in the 10³ pc scale, but not in the 10² pc scale. The 10³ pc scale is the largest scale at which self-gravity is significant. This suggests that self-gravity is important at multiple length scales, but not at the largest scales.

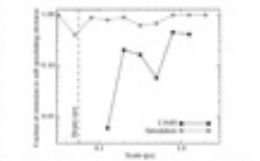


Figure 2. Comparison of the 'desmogger' and CLUMPFIND feature-identification algorithms as applied to CO emission from the L1448 region. (a) 'desmogger' results and (b) CLUMPFIND results. Both panels show hierarchical tree diagrams and associated data plots.

LETTERS

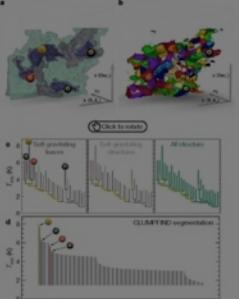


Figure 3. Schematic illustration of the desmogger process. The figure shows a 3D visualization of a gas cloud with a hierarchical tree diagram overlaid. The tree diagram shows the fragmentation of the gas into smaller-scale structures. The 3D visualization shows the spatial distribution of the gas and the location of the fragmentation nodes.

using 2D maps of column density. With this early 2D work as inspiration, we have developed a structure-identification algorithm that extracts the hierarchical structure of a 3D (p-p-v) data cube into an easily visualized representation called a 'desmogger'. Although well developed in other data-intensive fields^{1,2}, it is curious that the application of our methodology to the intergalactic medium has been rare, and almost exclusively within the area of galaxy evolution, where 'desmogger' has been used with increasing frequency^{3,4}. Figure 1 and its legend explain the construction of desmoggers schematically. The desmogger quantifies how and where local maxima of emission merge with each other, and its implementation is explained in Supplementary Methods. Critically, the desmogger is determined almost entirely by the data itself, and it has negligible sensitivity to algorithm parameters. To make graphical presentation possible on paper and 2D screens, we 'flatten' the desmoggers of 3D data (see Fig. 1 and its legend), by sorting their 'branches' by root mass, which discards hierarchical information on the z-axis while preserving all information about connectivity and hierarchical 'backbone' (full 3D labels in the figure and the reader match features between a 2D map (Fig. 1), an interactive 3D map (Fig. 2a online) and a sorted desmogger (Fig. 2c).

A desmogger of an optical line data cube allows for the extraction of key physical properties associated with volumes bounded by isosurfaces, such as radius (R), velocity dispersion (v), and luminosity (L). The volumes can have any shape, and 'fatter' nodes⁵ we focus on the significance of the especially elongated features seen in L1448 (Fig. 2a). The luminosity is an approximate proxy for mass, such that M_{star} ≈ X_{CO,0.2-0.3} L, where X_{CO,0.2-0.3} ≈ 0.07^{6,7} on K⁸ km⁻¹ s⁻¹ (ref. 1); see Supplementary Methods and Supplementary Fig. 2). The default values for size, mass and velocity dispersion can then be used to estimate the role of self-gravity in the hierarchy, via calculation of an 'observed' virial parameter, α_{obs} ≈ 2πGM_{star}/Rv². In principle, extended portions of the tree (Fig. 2c, yellow highlighting) where α_{obs} < 2 (where gravitational energy is comparable to or larger than kinetic energy) correspond to regions of p-p-v space where self-gravity is significant. As α_{obs} only represents the ratio of kinetic energy to gravitational energy at one point in time, and does not explicitly capture external over-pressure and/or magnetic fields⁹, its measured value should only be used as a guide to the longevity (back-to-backness) of any particular feature.

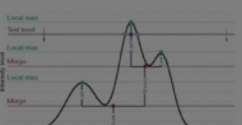


Figure 4. Comparison of the 'desmogger' and CLUMPFIND feature-identification algorithms as applied to CO emission from the L1448 region. (a) 'desmogger' results and (b) CLUMPFIND results. Both panels show hierarchical tree diagrams and associated data plots.

LETTERS

A role for self-gravity at multiple length scales in the process of star formation

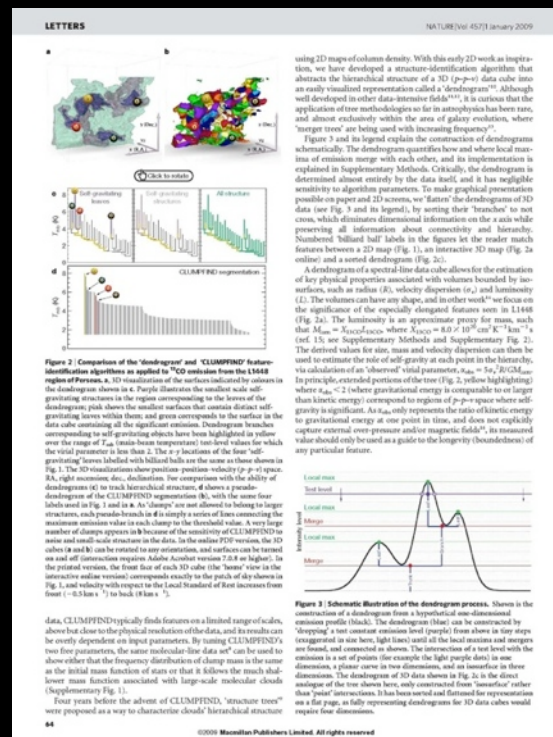
Alyssa A. Goodman¹, Erik W. Rosolowsky², Michelle A. Barkin¹, Jonathan S. Foster³, Michael Hebb⁴, Jim Kaufman⁵ & James E. Probst⁶

Self-gravity plays a decisive role in the final stages of star formation, where dense cores (or clumps) rapidly contract and collapse to form star-planet disk systems. But self-gravity's role at earlier times and on larger length scales, such as 10³ parsecs, is unclear. Some molecular cloud simulations that do not include self-gravity suggest that turbulent fragmentation alone is sufficient to create a mass distribution of dense cores, that eventually, and only, the stellar initial mass function. Here we report a 'desmogger' hierarchical tree-diagram analysis that reveals that self-gravity plays a significant role over the full range of possible mass scales. In the CLUMPFIND decomposition of the L1448 region, the presence of self-gravity is particularly clear in the 10³ pc scale, but not in the 10² pc scale. The 10³ pc scale is the largest scale at which self-gravity is significant. This suggests that self-gravity is important at multiple length scales, but not at the largest scales.

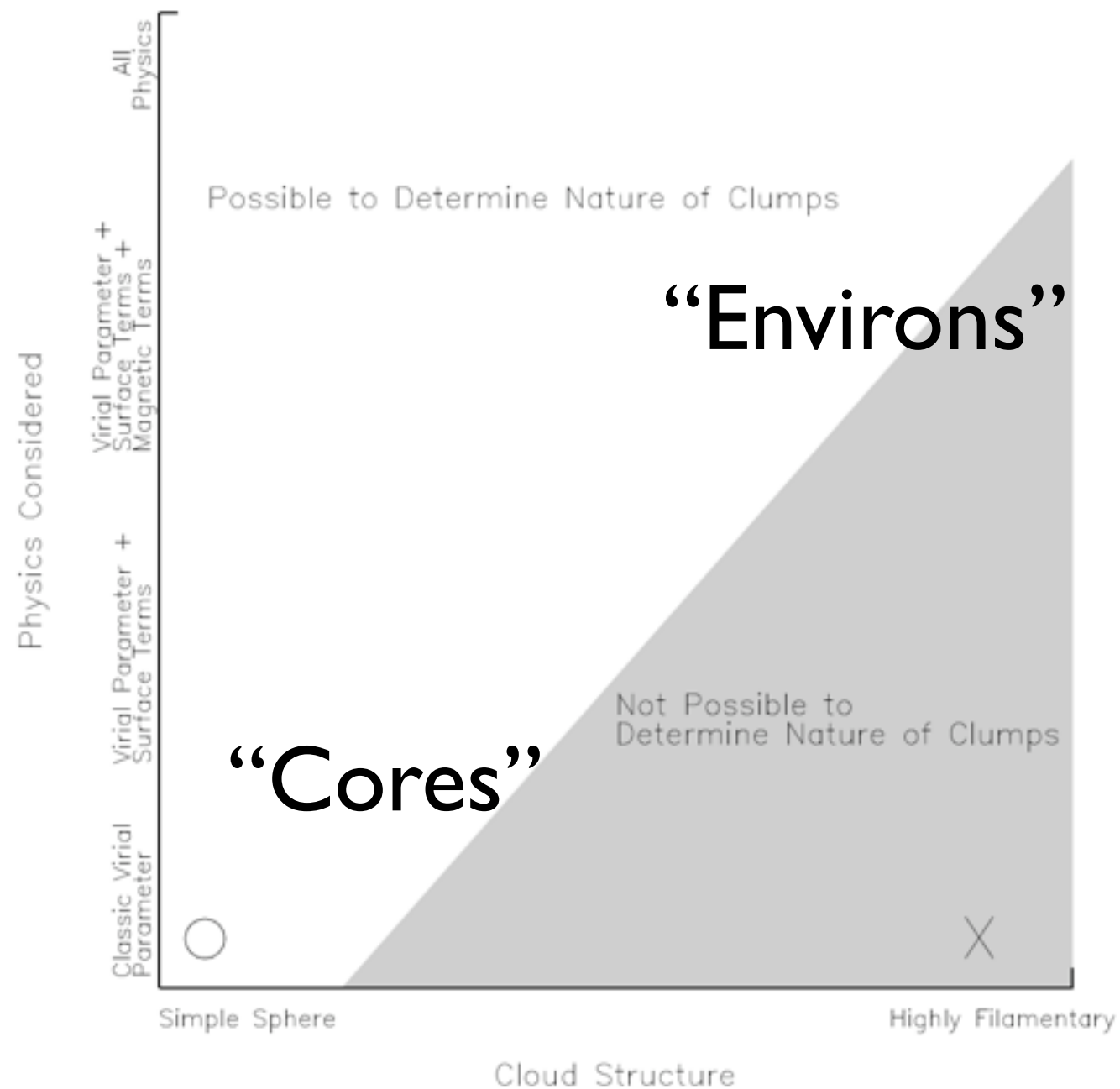


Figure 5. Hierarchical tree-diagram analysis of the L1448 star-forming region. The diagram shows the fragmentation of the gas into smaller-scale structures. The root node is at the top, and the branches lead to smaller-scale structures at the bottom. The nodes are labeled with mass and size, and the branches are color-coded to indicate different physical regimes.

Star formation takes place in self-gravitating “coccoons,” and some of those coccoons are bound to each other.



Caveats/Worries about p - p - v (bijection) ... and the virial parameter



from **Shetty**, Collins, Kauffmann, Goodman, Rosolowsky 2009;
see also recent work of Ostriker et al., Ballesteros-Paredes et al., Myers, and Smith, Clark & Bonnell

What (else) keeps me up at night now...

“Bi-jection” or “ $p-p-p$ to/from $p-p-v$ ” & the impact
of missing terms in **virial analysis** in each space
[Shetty, Collins, et al.]

Projection effects in analyzing **spatial & velocity
offsets**
[Kirk, Pineda, Offner, et al.]

When/how can we best **measure YSO velocities**
& what should they be?
[Covey, Offner, et al.]

How much excess column is there **beyond “log-
normal”**?
[Foster, Offner, et al.]

Effects of **Cloudshine** on **Deep NIR Point Source
Photometry** (e.g. JWST) [Foster!]

Can we **differentiate** simulations **with** known &
simple new “**taste tests**”
[Rosolowsky, Shetty, et al.]
...for example, how do **cores connect to** their
environment?
[Kauffmann, Myers, Pineda, Alves, Foster,
Rosolowsky, Offner, et al.]?

Can we do better than **Kennicutt-Schmidt**,
really?
[Cox, Narayanan, Shetty, Rosolowsky et al.]

Effects of **B-Star Winds** on Cloud Evolution
[Covey, Sharma, Valverde, Dupree, Borkin, Arce et al.]

Do **dendrograms** give a different **CMF**?
[Alves, Rosolowsky, Pineda et al.]

And, what about **magnetic fields**?!
[Li et al.]

...and WWT, IIC, 3D Data Desk, WGBH, VAO...and my family.

“turbulent fragmentation” “LI 448” “(magneto-)hydrodynamic simulation”

“Cloudshine”

“bi-jection”

“pre-stellar core”

“virial parameter”

“protostar”

“column density”

“integrated intensity”

“turbulent power spectrum”

“p-p-v cube”

“synthetic observation”

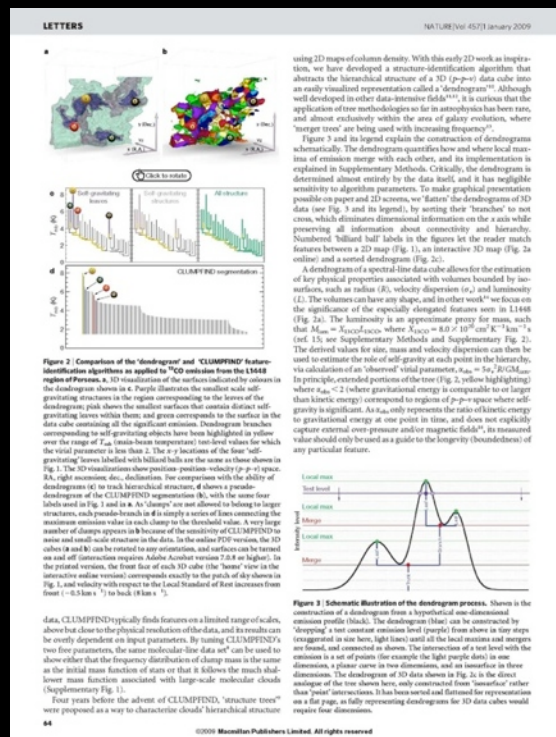
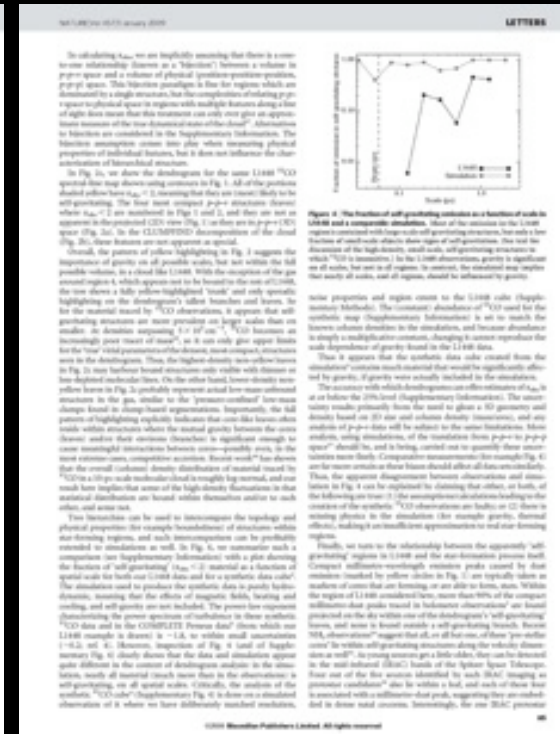
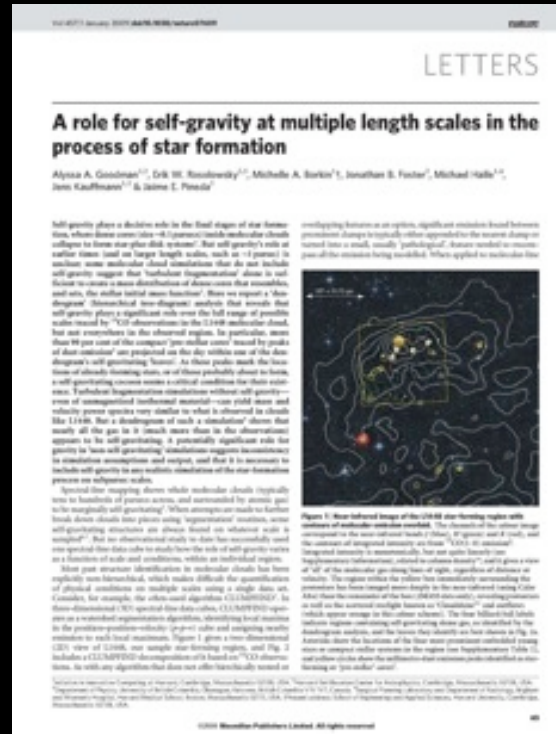
“segmentation”

“depletion, opacity”

“CLUMPFIND”

“taste-test”

“Dendrogram”



“COMPLETE”

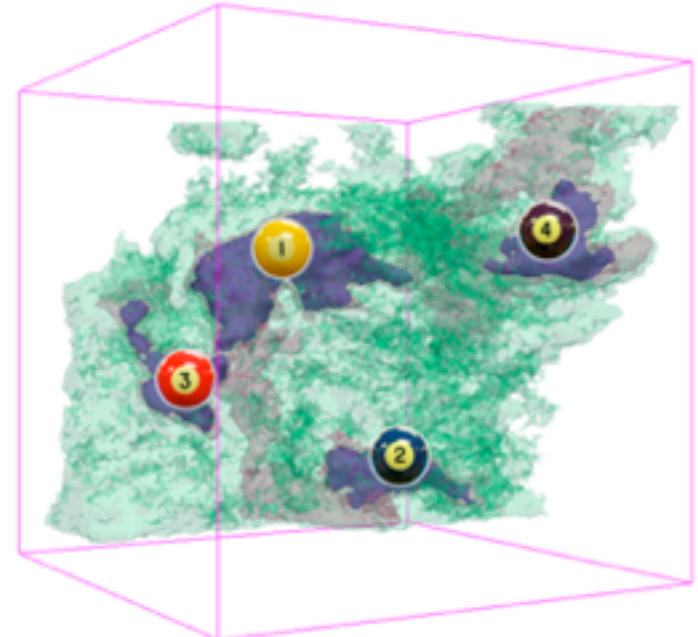
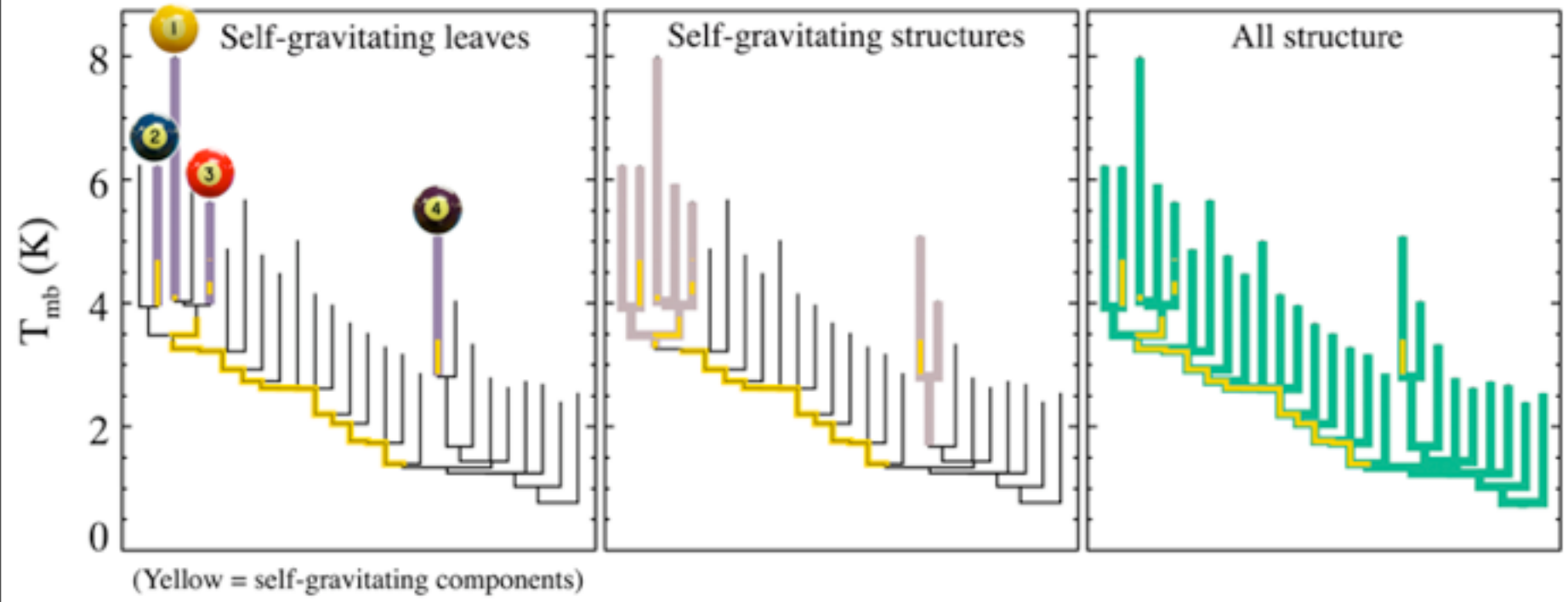
“3D PDF”

caveats

Extra Slides

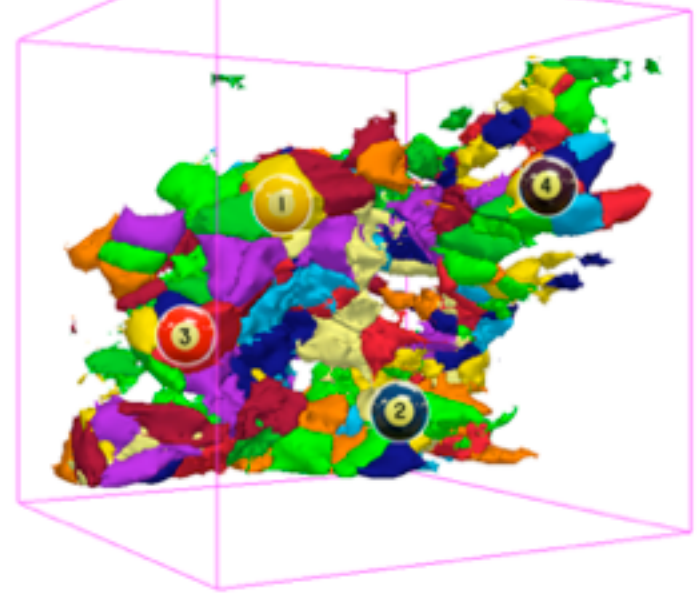
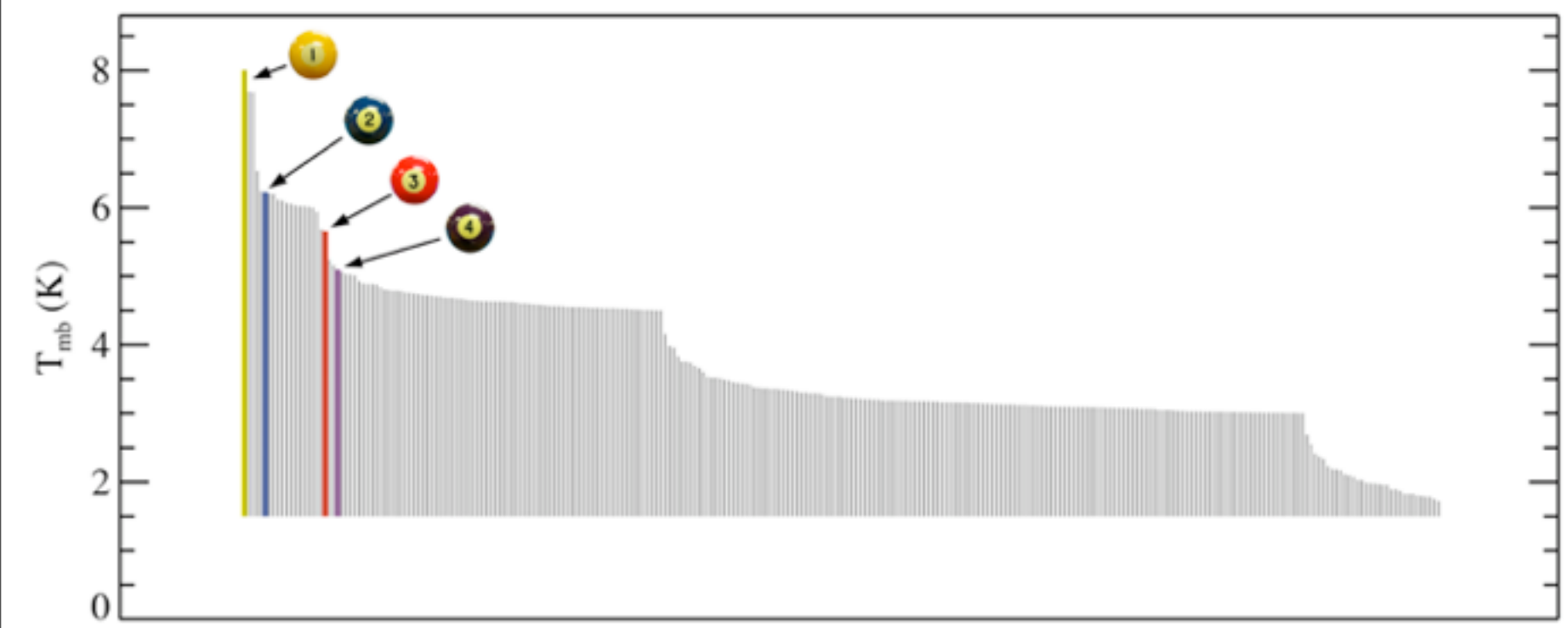
CLUMPFIND vs. Dendrograms: LI 448

Dendrograms



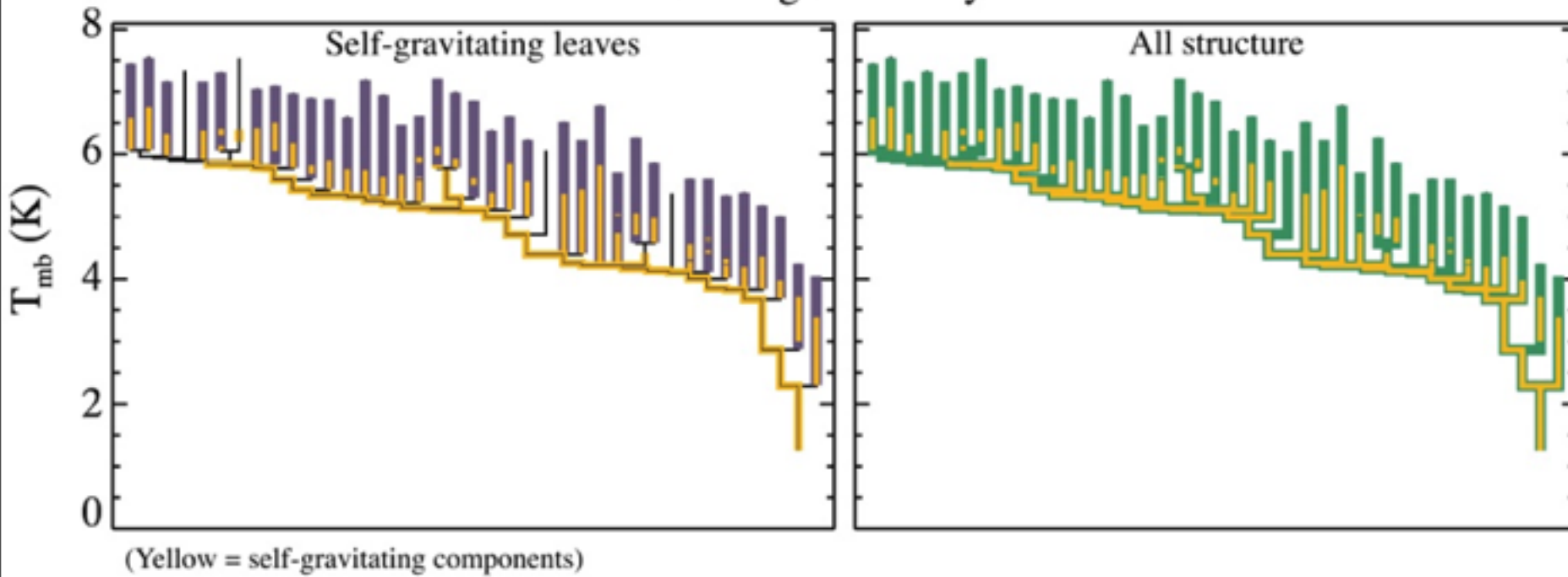
The online PDFs of these insets

“CLUMPFIND”

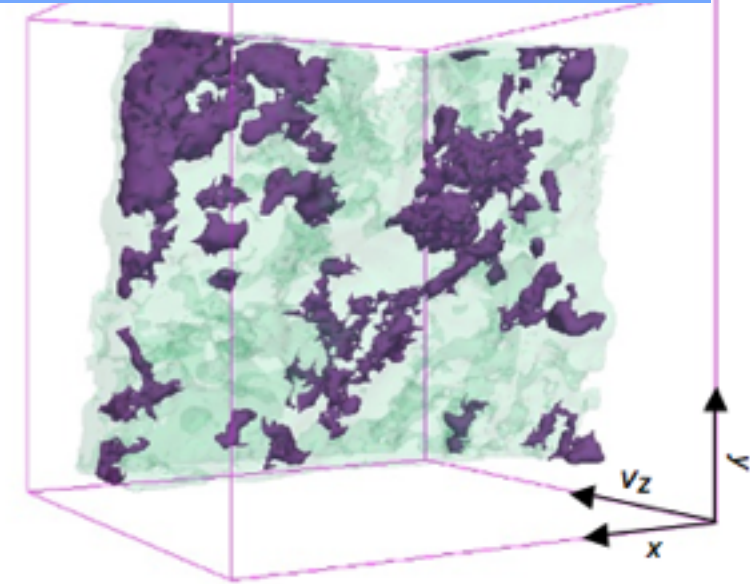


CLUMPFIND vs. Dendrograms: Synthetic Data

Dendrogram Analysis

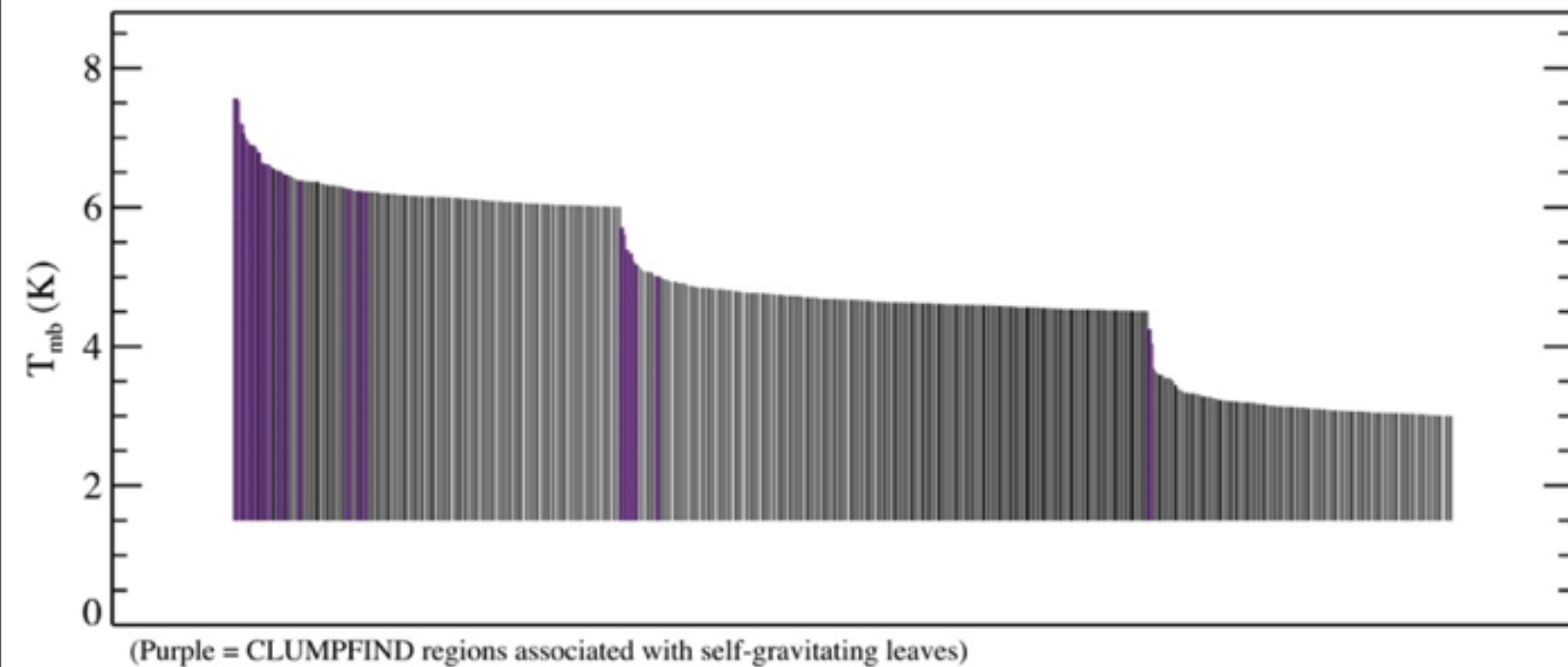


Dendrograms

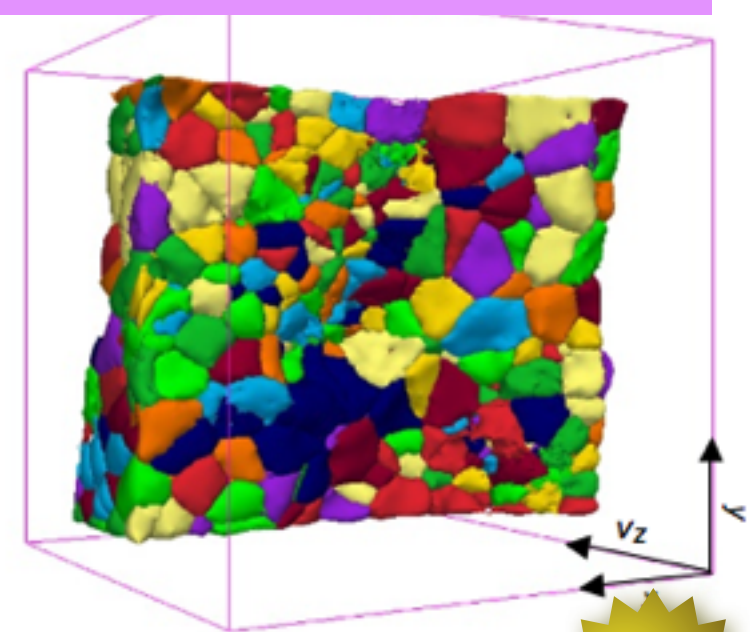


i The online PDFs of these insets are interactive, offer additional surfaces, and can be rotated and manipulated by

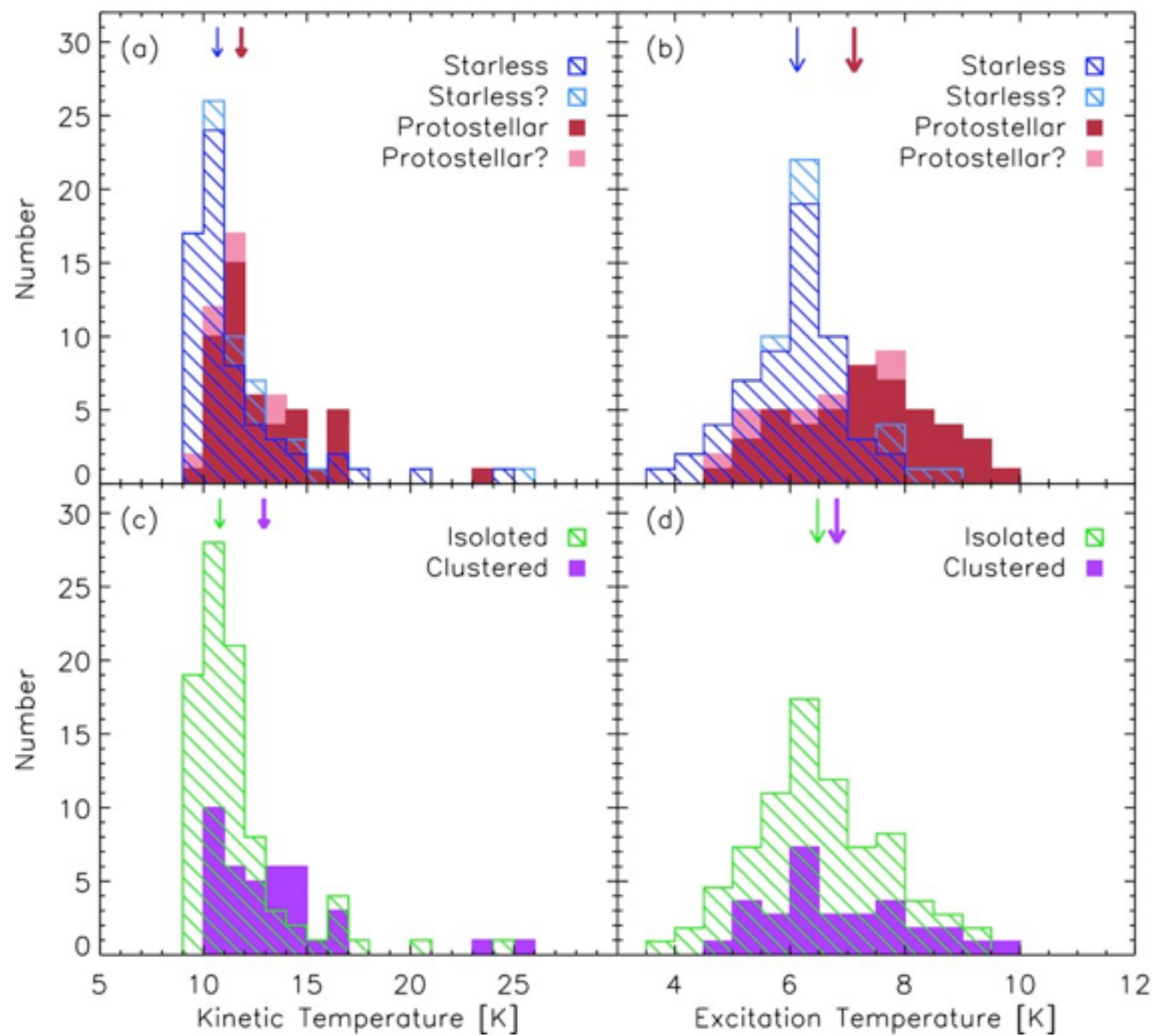
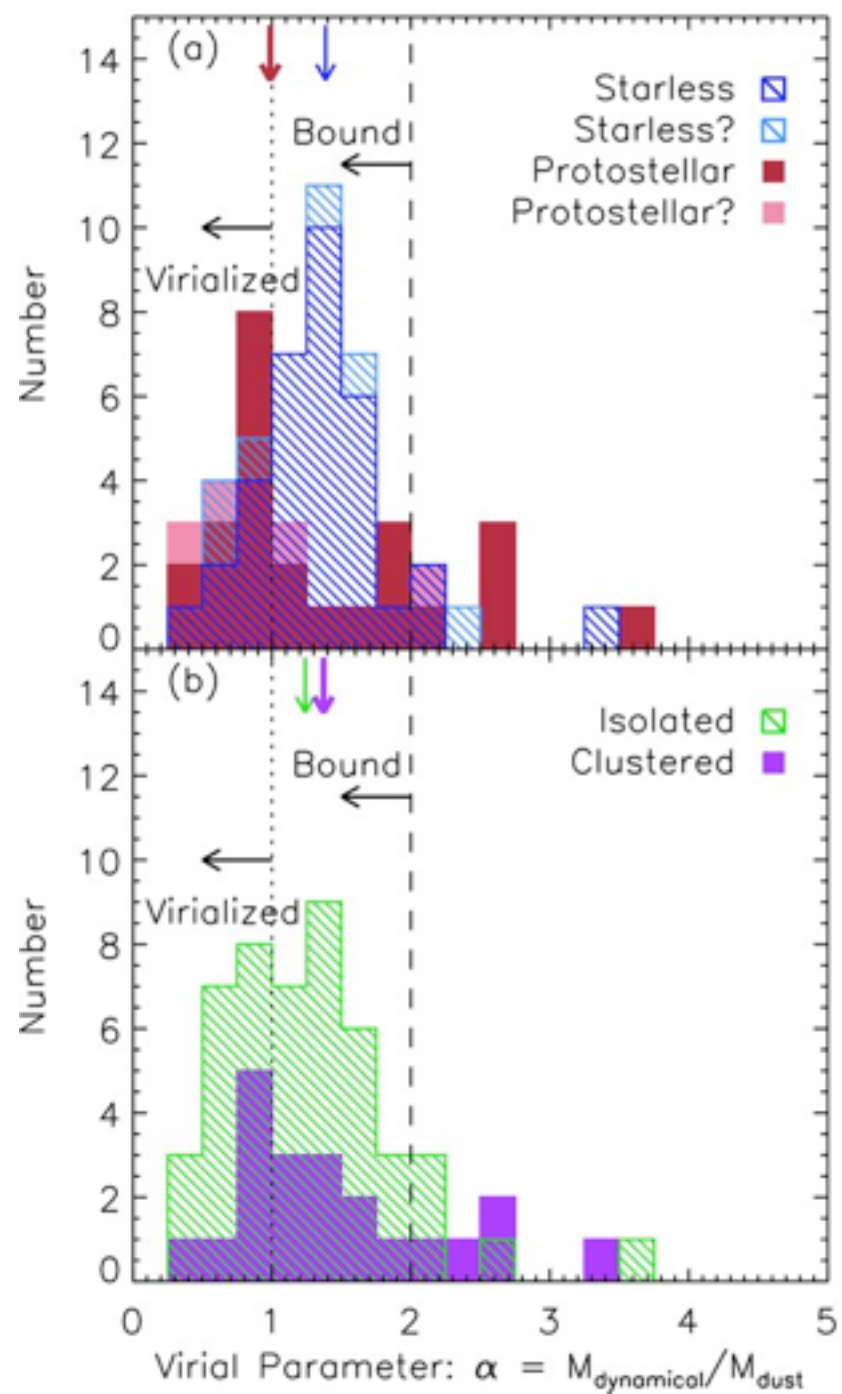
CLUMPFIND Analysis



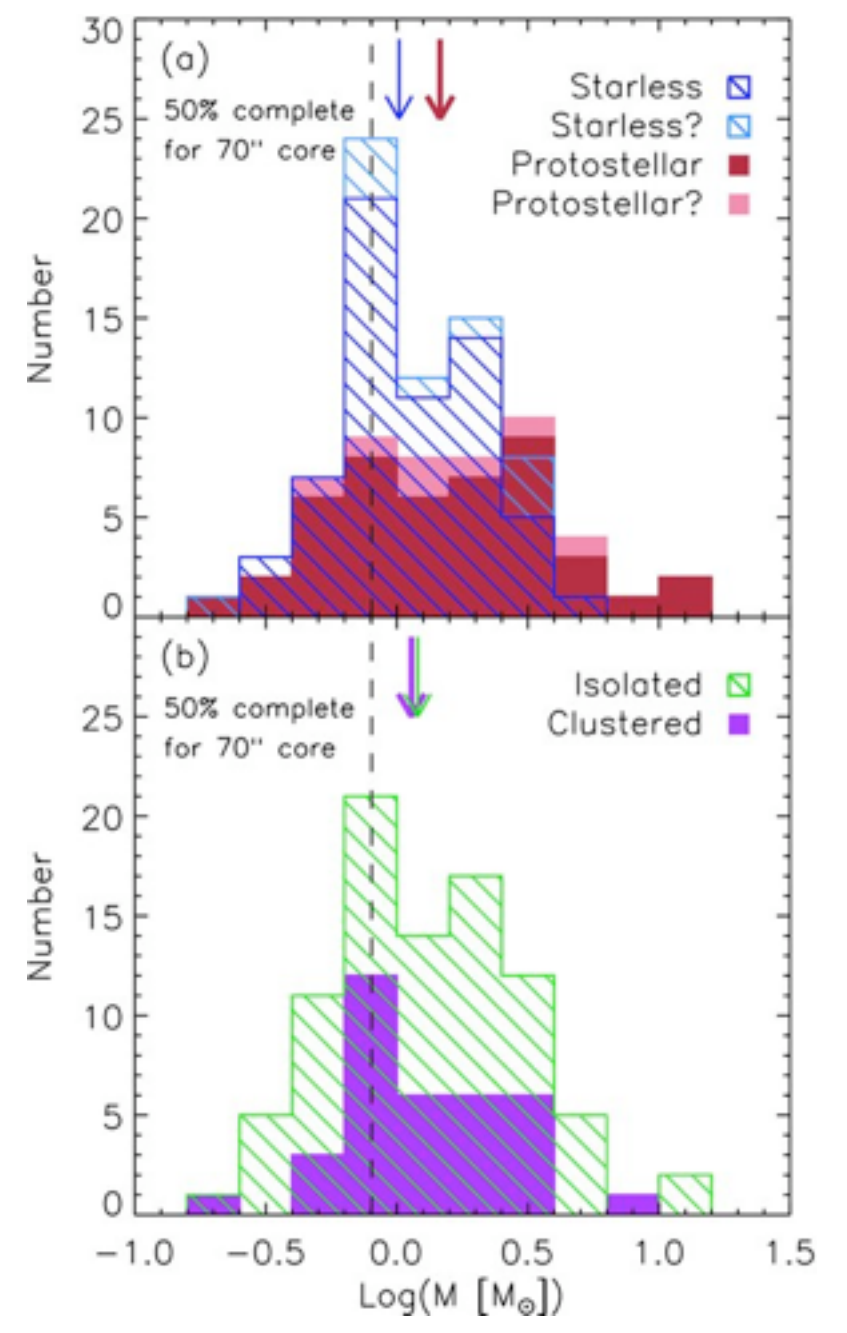
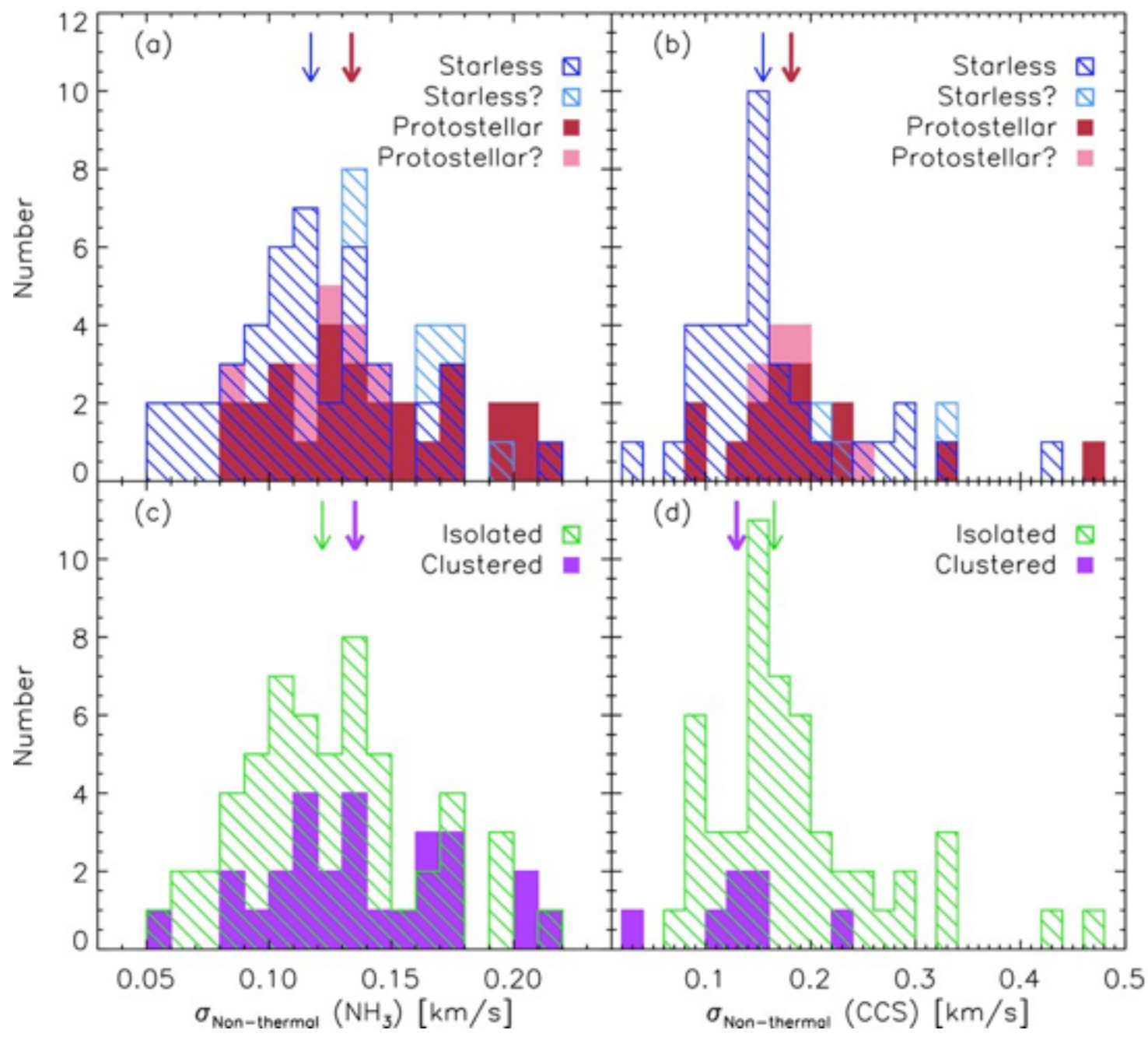
“CLUMPFIND”



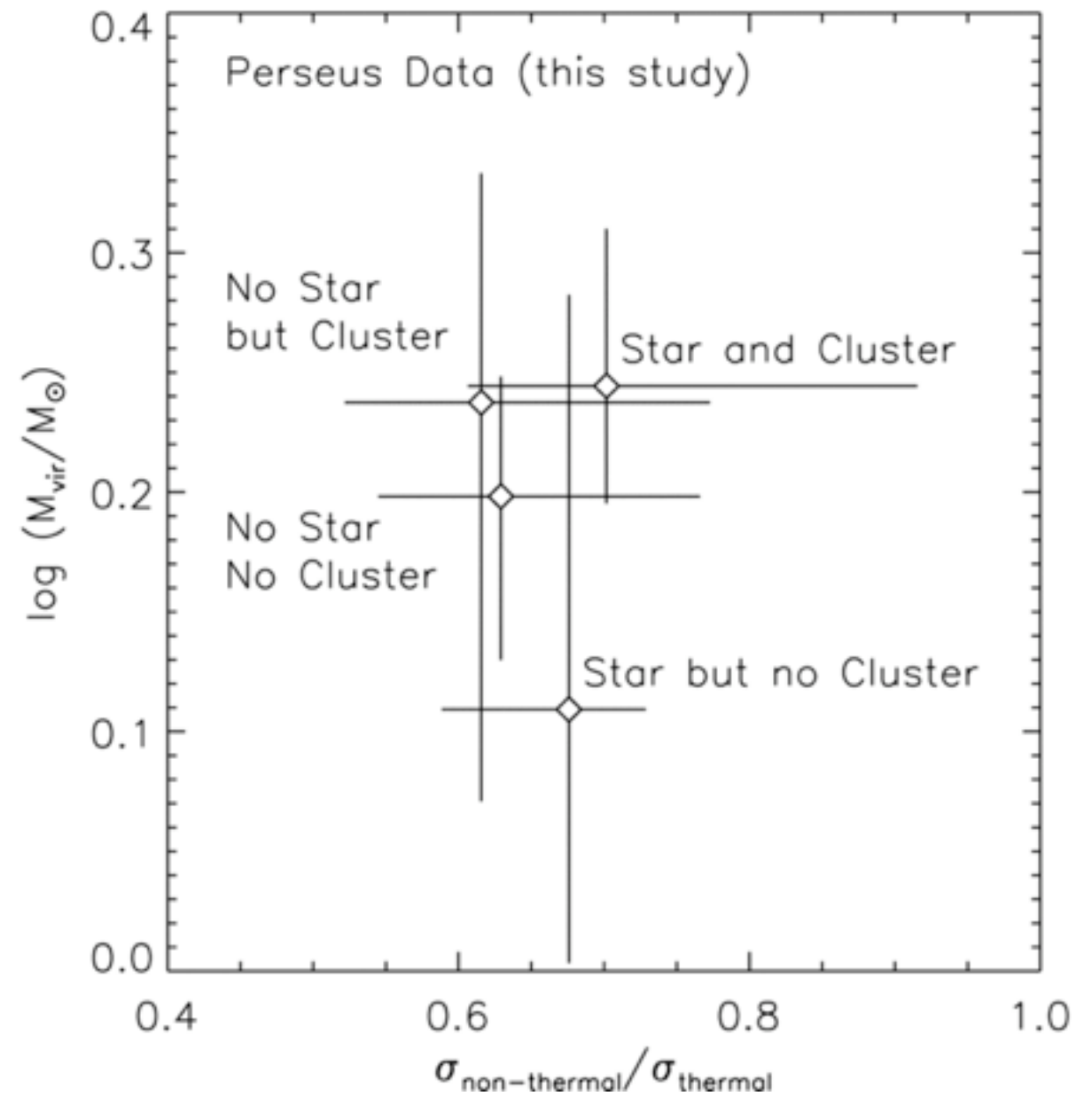
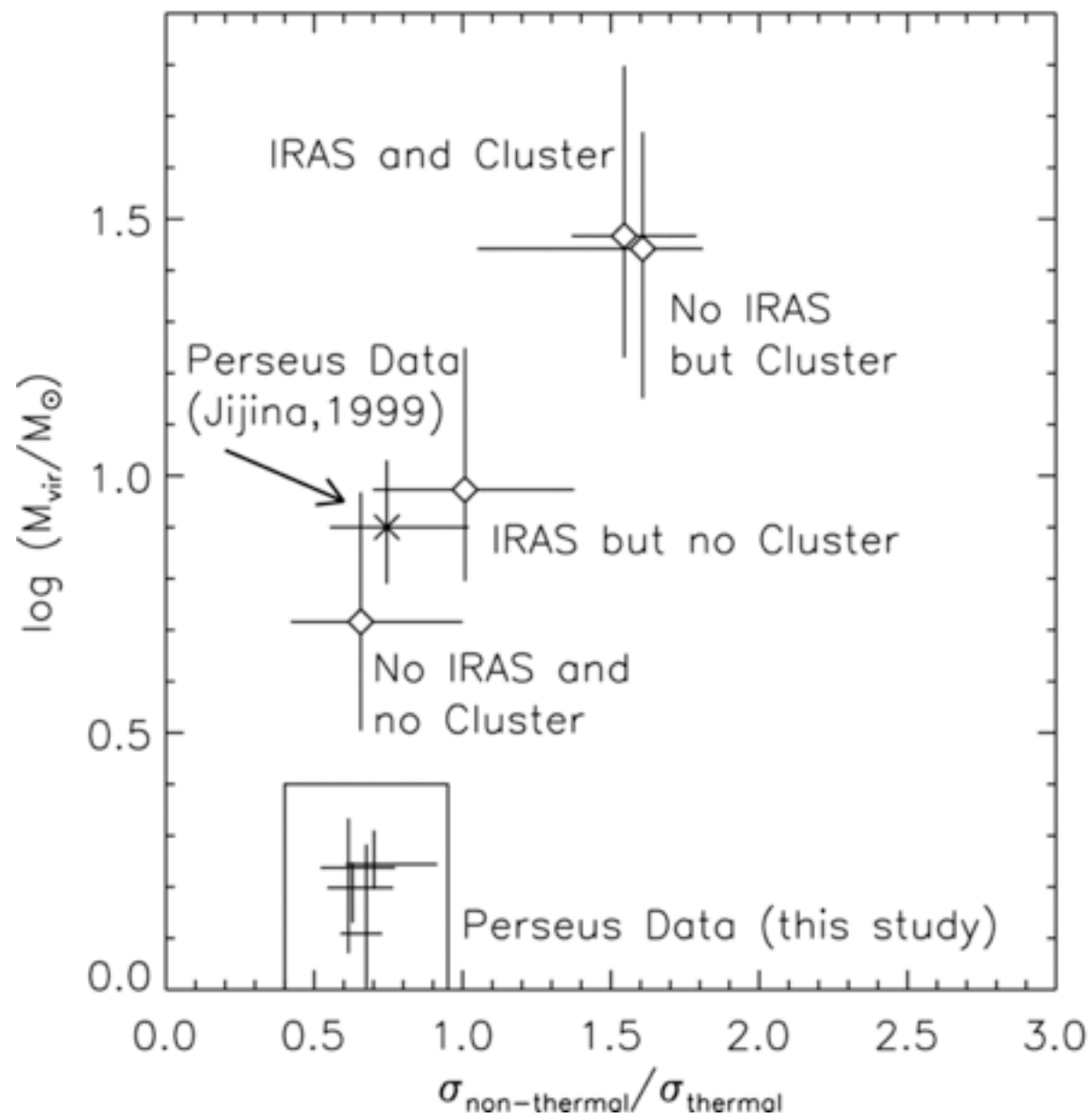
TASTE TEST



Foster et al. 2009



Foster et al. 2009



Foster et al. 2009

